MAX-PLANCK-INSTITUT
FÜR METEOROLOGIE

On the Spatio-Temporal Variability of Instability Waves in the Tropical Atlantic Ocean and their Impact on Mixing

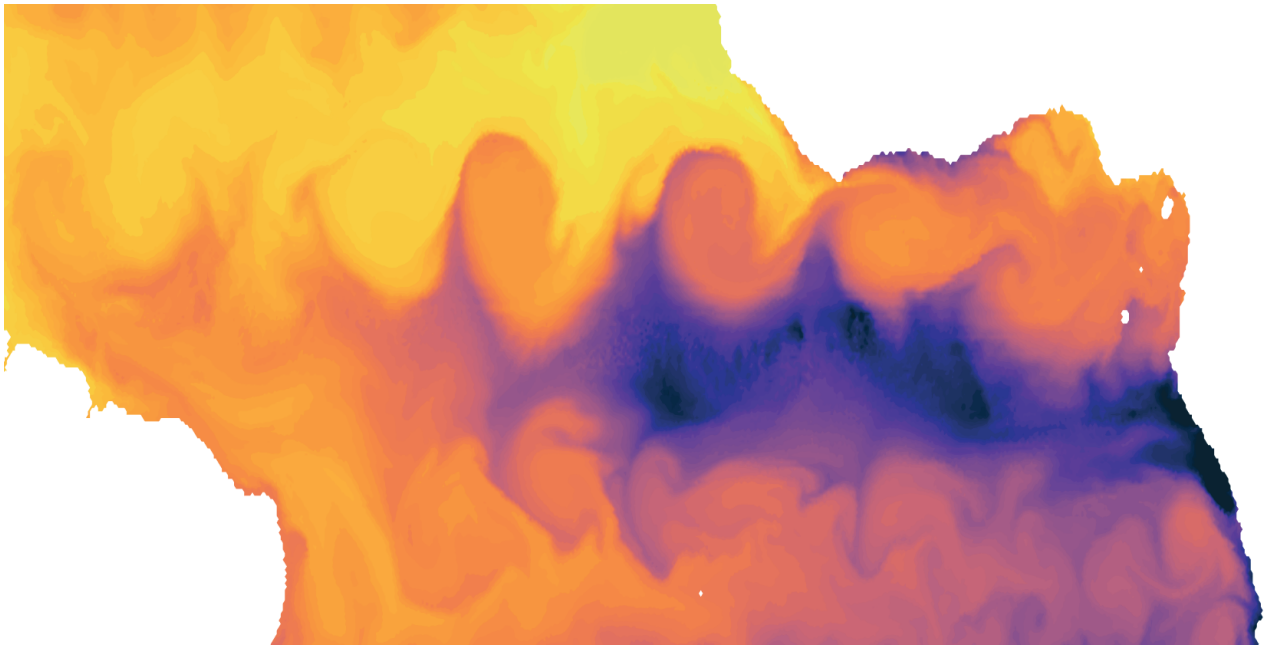

Mia Sophie Specht

Hamburg 2023

Berichte zur Erdsystemforschung
Reports on Earth System Science

267
2023

Hinweis

Die Berichte zur Erdsystemforschung werden vom Max-Planck-Institut für Meteorologie in Hamburg in unregelmäßiger Abfolge herausgegeben.

Sie enthalten wissenschaftliche und technische Beiträge, inklusive Dissertationen.

Die Beiträge geben nicht notwendigerweise die Auffassung des Instituts wieder.

Die "Berichte zur Erdsystemforschung" führen die vorherigen Reihen "Reports" und "Examensarbeiten" weiter.

Anschrift / Address

Max-Planck-Institut für Meteorologie
Bundesstrasse 53
20146 Hamburg
Deutschland

Tel./Phone: +49 (0)40 4 11 73 - 0
Fax: +49 (0)40 4 11 73 - 298

name.surname@mpimet.mpg.de
www.mpimet.mpg.de

Notice

The Reports on Earth System Science are published by the Max Planck Institute for Meteorology in Hamburg. They appear in irregular intervals.

They contain scientific and technical contributions, including PhD theses.

The Reports do not necessarily reflect the opinion of the Institute.

The "Reports on Earth System Science" continue the former "Reports" and "Examensarbeiten" of the Max Planck Institute.

Layout

Bettina Diallo and Norbert P. Noreiks
Communication

Copyright

Photos below: ©MPI-M
Photos on the back from left to right:
Christian Klepp, Jochem Marotzke,
Christian Klepp, Clotilde Dubois,
Christian Klepp, Katsumasa Tanaka

On the Spatio-Temporal Variability of Instability Waves in the Tropical Atlantic Ocean and their Impact on Mixing

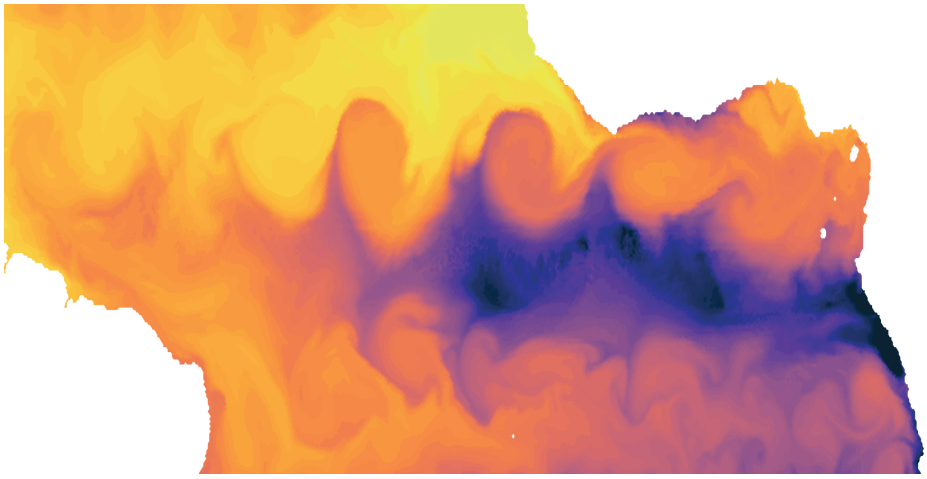

Mia Sophie Specht

Hamburg 2023

Mia Sophie Specht
aus Eutin, Deutschland

Max-Planck-Institut für Meteorologie
The International Max Planck Research School on Earth System Modelling
(IMPRS-ESM)
Bundesstrasse 53
20146 Hamburg

Tag der Disputation: 24. März 2023

Folgende Gutachter empfehlen die Annahme der Dissertation:
Dr. Johann Jungclaus
Prof. Dr. Jochem Marotzke

Vorsitzender des Promotionsausschusses:
Prof. Dr. Hermann Held

Dekan der MIN-Fakultät:
Prof. Dr.-Ing. Norbert Ritter

Titelgrafik: *Snapshot of simulated sea surface temperature, showing the characteristic tropical instability wave cold cusps.* Credit: Mia Sophie Specht

Berichte zur Erdsystemforschung / Max-Planck-Institut für Meteorologie 267
Reports on Earth System Science / Max Planck Institute for Meteorology 2023

ISSN 1614-1199 - doi: 10.17617/2.3508773

Mia Sophie Specht

On the Spatio-Temporal Variability of Instability Waves in the Tropical Atlantic Ocean and their Impact on Mixing

ABSTRACT

Tropical Instability Waves (TIWs) are large scale waves in the tropical upper oceans, which impact air-sea interactions, ocean biogeochemistry, the mixed layer heat budget as well as surface temperatures. While TIWs have been shown to modulate mixing, previous studies generally consider only few TIWs and thereby neglect their temporal variability. Furthermore, while TIWs close to the surface have been extensively studied, their vertical structure remains largely unknown. However, a recent study suggests that there also exist subsurface TIWs (subTIWs). Presently, subTIWs have been studied exclusively in the Pacific Ocean and their impact on mixing is yet to be shown.

I hypothesize that a lack of understanding of the spatio-temporal variability of instability waves in the Atlantic Ocean has led to previous disagreements on the impact of TIWs on mixing. Therefore, I examine instability waves in the Atlantic Ocean and their effect on mixing under the explicit consideration of their horizontal and vertical structure, as well as their temporal variability. To this end, I exploit long simulations from a global, high-resolution ocean model, which allow for the analysis of over 60 instability waves, thereby overcoming limitations present within previous studies that are based on only few wave events.

I demonstrate for the first time that mixing at TIW fronts in the Atlantic Ocean exhibits a strong seasonal cycle, with mixing occurring mainly in summer, regardless of whether TIWs are present earlier in the year or not. I argue that shear from TIWs alone is not sufficient to trigger mixing. Instead, additional background shear is required and is provided by increased shear between the mean zonal currents. This in turn is largely driven by the seasonality of the South Equatorial Current (SEC), which thus strongly contributes to the modulation of TIW related mixing. Further, I show the presence of subTIWs in the Atlantic Ocean for the first time, characterize their spatio-temporal variability and investigate their impact on mixing. I find that unlike TIWs, subTIWs frequently occur on both sides of the Equator. subTIWs induce a multi-layer shear structure, which suggests that subTIWs destabilize the mean flow and thereby cause mixing. This is strongest when TIWs and subTIWs act simultaneously.

My results show that the spatio-temporal variability of instability waves in the Atlantic Ocean largely influences their effect on ocean mixing. Therefore, I recommend the use of long data records to fully capture the spatio-temporal variability characterized herein. Furthermore, I suggest that future studies should consider not only TIWs, but also subTIWs due to their apparent interactions and effect on mixing.

ZUSAMMENFASSUNG

Tropische Instabilitätswellen (TIW) sind großskalige Wellen in den oberen Schichten der tropischen Ozeane, die sich auf die Ozean-Atmosphäre Wechselwirkung, die Biogeochemie, den Wärmehaushalt der turbulenten Grenzschicht im Ozean sowie die Temperatur der Meeresoberfläche auswirken. Zwar wurde bereits erwiesen, dass TIW die Vermischung im Ozean beeinflussen, doch berücksichtigen frühere Studien im Allgemeinen nur wenige TIW und vernachlässigen damit deren zeitliche Variabilität. Darüber hinaus wurden zwar oberflächennahe TIW vielfach untersucht, jedoch ist die vertikale Struktur weitgehend unbekannt. Eine neuere Studie weist jedoch darauf hin, dass es auch tiefere TIW (subTIW) gibt. Bisher wurden subTIW allerdings ausschließlich im Pazifischen Ozean untersucht und deren Auswirkung auf die Vermischung muss erst noch nachgewiesen werden.

Ich stelle die Hypothese auf, dass ein mangelndes Verständnis der räumlichen und zeitlichen Variabilität von Instabilitätswellen im Atlantischen Ozean zu früheren Unstimmigkeiten über den Einfluss von TIW auf die Vermischung geführt hat. Daher untersuche ich Instabilitätswellen im Atlantik und ihre Rolle für die Vermischung im Ozean unter ausdrücklicher Berücksichtigung ihrer horizontalen und vertikalen Struktur sowie ihrer zeitlichen Variabilität. Hierfür nutze ich lange Simulationen eines globalen, hochauflösenden Ozeanmodells, welche die Analyse von über 60 Instabilitätswellen ermöglichen und damit die Einschränkungen früherer Studien überwinden, die auf nur wenigen Wellenereignissen basieren.

Ich zeige zum ersten Mal, dass die Vermischung an TIW-Fronten im Atlantischen Ozean einen starken saisonalen Zyklus aufweist, wobei die Vermischung primär im Sommer auftritt, unabhängig davon, ob TIW bereits früher im Jahr auftreten oder nicht. Ich argumentiere, dass die Scherung von TIW allein nicht ausreicht, um Vermischung zu verursachen. Stattdessen ist zusätzliche Hintergrundscherung erforderlich, die durch erhöhte Scherung zwischen den mittleren zonalen Strömungen geliefert wird. Diese Scherung wiederum wird größtenteils durch die Saisonalität des Südäquatorialstroms (SEC) bestimmt, der somit stark zur Modulation der TIW-bedingten Vermischung beiträgt. Darüber hinaus zeige ich zum ersten Mal die Existenz von subTIW im Atlantik, charakterisiere ihre räumlich-zeitliche Variabilität und untersuche ihren Einfluss auf die Vermischung. Ich finde heraus, dass subTIW im Gegensatz zu TIW häufig auf beiden Seiten des Äquators auftreten. subTIW verursachen eine mehrschichtige Scherungsstruktur, die darauf hindeutet, dass subTIW die mittlere Strömung destabil-

isieren und dadurch Vermischung induzieren. Dies ist am stärksten, wenn TIW und subTIW gleichzeitig auftreten.

Meine Ergebnisse zeigen, dass die räumlich-zeitliche Variabilität von Instabilitätswellen im Atlantik deren Effekt auf die Vermischung des Ozeans maßgeblich beeinflusst. Daher empfehle ich die Analyse langer Datensätze, um die hier beschriebene räumlich-zeitliche Variabilität vollständig zu erfassen. Darüber hinaus schlage ich vor, dass zukünftige Studien nicht nur TIW, sondern auch subTIW aufgrund ihrer scheinbaren Wechselwirkungen und ihres Einflusses auf die Vermischung berücksichtigen sollten.

PUBLICATIONS RELATED TO THIS DISSERTATION

Parts of this dissertation are pre-published or in preparation for publication. Publications as first author are attached to this dissertation:

APPENDIX A

Specht, Mia Sophie, Johann Jungclaus, and Jürgen Bader. "Seasonality of Mixing at Tropical Instability Wave Fronts in the Atlantic Ocean." *In preperation for submission at Journal of Geophysical Research: Oceans*

APPENDIX B

Specht, Mia Sophie, Johann Jungclaus, and Jürgen Bader. "Identifying and Characterizing Subsurface Tropical Instability Waves in the Atlantic Ocean in Simulations and Observations." *Journal of Geophysical Research: Oceans* 126.10 (2021): e2020JC017013.

Further publications related to this dissertation as contributing author, which are not included as an appendix:

Hohenegger, Cathy, et al. "ICON-Sapphire: simulating the components of the Earth System and their interactions at kilometer and subkilometer scales." *Geoscientific Model Development Discussions* (2022): 1-42. APA

CONTENTS

LIST OF ACRONYMS

ACT	Atlantic cold tongue
AMM	Atlantic meridional mode
AZM	Atlantic zonal mode
ENSO	El Niño - Southern Oscillation
EOF	Empirical Orthogonal Function
EUC	Equatorial Undercurrent
ICON	Icosahedral Nonhydrostatic Weather and Climate Model
ICON-O	ICON-Ocean
ITCZ	Intertropical Convergence Zone
LEF	lead edge front
NECC	North Equatorial Countercurrent
PIRATA	Prediction and Research Moored Array in the Tropical Atlantic
SEC	South Equatorial Current
SST	Sea Surface Temperature
SUBTIW	subsurface Tropical Instability Wave
TACOS	Tropical Atlantic Current Observation Study
TEF	trail edge front
TIV	Tropical instability vortex
TIW	Tropical Instability Wave
TKE	turbulent kinetic energy
WES	wind-evaporation-sea surface temperature feedback

1 UNIFYING ESSAY

1.1 INTRODUCTION

In this dissertation, I describe my study of the spatio-temporal variability of instability waves in the tropical Atlantic Ocean and their impact on upper ocean mixing. To this end, I consider both the horizontal and vertical structure and the high temporal variability of the waves. I hypothesize that these two aspects, the spatial extent and the temporal variability of instability waves, could largely influence their impact on the upper ocean heat budget and surface temperature, and that therefore a lack of understanding of the spatio-temporal variability of instability waves may be responsible for discrepancies in past findings. I define the overarching research questions, that I answer within this dissertation as follows:

Overarching research questions

1. What is the characteristic spatial structure and temporal occurrence of instability waves in the tropical atlantic ocean, in particular in the vertical?
2. How is the influence of instability waves on upper ocean mixing in the tropical atlantic ocean altered by changes in the background conditions?

To answer these questions and to verify my hypothesis, I analyse over a decade of simulation output from a comprehensive, global, high-resolution ocean model. This allows for explicitly taking into account the high spatio-temporal variability and vertical structure of instability waves and thereby overcome limitations of previous studies that are based on only few wave events.

In this unifying essay I first introduce the background material, which lays the foundation for my research before guiding the reader through the main findings of two research papers, the result of my work on this dissertation. These are attached as Appendices A and B. Note that the attached papers are not sorted in order of their publication date but in a logical order in the context of my findings, following Tropical Instability Waves (TIWs) from surface to subsurface.

The first paper focuses on the analysis of the temporal variability of mixing related to instability waves close to the ocean surface, thereby providing an answer to the second overarching research question. In particular, Specht et al. (2023) investigate the seasonality of mixing at TIW fronts in the Atlantic Ocean, which has not previously been

considered. In contrast, the focus of the second paper (Specht et al., 2021b) is on investigating the spatial structure of TIWs, specifically under the consideration of the vertical extent of the waves, hence answering the first of the overarching research questions. This leads to the identification and characterization of subTIWs in the Atlantic Ocean for the first time in both simulations and observations. My findings advance the current understanding of the spatial structure of TIWs and the role of temporal variability in the impact of TIWs on upper ocean mixing in the tropical Atlantic Ocean.

Finally, I conclude this essay by discussing the importance of TIWs and subTIWs in the Atlantic Ocean, placing my findings in the broader context of research on instability waves and tropical ocean dynamics, and thereby highlight the novelty of my work.

1.1.1 *The Role of Tropical Oceans in the Climate System*

To understand why TIWs are of interest in the first place, it is necessary to first understand the crucial role tropical oceans play in the global climate system.

The incoming solar radiation is highest at the tropics, and is strong throughout the year. This leads to an excess of heat that must be redistributed both via ocean and atmosphere (Chang et al., 2006; Godfrey et al., 2001; Trenberth and Caron, 2001). Large amounts of this heat are taken up by the tropical oceans and transported polewards. The high Sea Surface Temperature (SST), which results from the strong solar radiation, favours ocean-atmosphere interaction by atmospheric deep convection (Carton et al., 1996; Chang et al., 2006; Godfrey et al., 2001). Modulation of the tropical SST is largely driven by the dominant winds in the tropics, the easterly trade winds. Along the Equator, these trade winds drive a poleward surface Ekman transport on both the north and south side of the Equator. This leads to a divergence at the ocean surface, which in turn drives upwelling of colder waters along the Equator. Similarly at the eastern boundaries of both tropical Pacific and Atlantic Oceans, winds force coastal upwelling of cold waters from below the thermocline, which leads to pronounced horizontal SST gradients (Moore and Philander, 1977).

The most widely known and extensively studied example of tropical air-sea interactions is the El Niño - Southern Oscillation (ENSO) in the Pacific. El Niño has far reaching influence on weather and climate not just over the adjacent continents, but worldwide (e.g. McPhaden et al., 2006; Trenberth et al., 1998). In addition, apart from ENSO a number of other modes of variability, both coupled and uncoupled, exists in all tropical oceans (Chang et al., 2006). Examples for these are the Atlantic zonal and meridional modes, which I will elaborate on more in Section 1.1.3. Despite being less well studied than ENSO, they are also important for the global distribution of heat, regional

and global climate. Hence, it is vital to gain a good understanding of the processes, which modulate tropical SST and heat uptake and to study how surface and deeper ocean interact.

Importance of the tropical Atlantic Ocean

While all tropical oceans are crucial parts of the climate system, in this dissertation I focus solely on TIWs in the Atlantic Ocean.

The tropical Atlantic Ocean is found to modulate the climate over the adjacent continents, particularly northeast Brazil, northwestern Africa, Central America, and the Caribbean regions, highlighting the importance of climate dynamics in the tropical Atlantic Ocean, and the need to better understand this part of the climate system (Muñoz et al., 2012). For example, studies show a high correlation between the meridional SST gradient in the tropical Atlantic Ocean and rainfall over northeast Brazil (e.g. Hormann and Brandt, 2007; Marshall et al., 2001; Wallace et al., 1998). This carries major societal implications due to the importance of rainfall for e.g. agriculture. The potential of tropical Atlantic SST to influence the regional climate over the adjacent continents makes the prediction of tropical Atlantic variability at seasonal and decadal timescales of great interest for industry, stakeholders and society as a whole (Cabos et al., 2019). Furthermore, the tropical Atlantic Ocean is proven to have a remote impact on the other tropical oceans (e.g. Ding et al., 2012; Kucharski et al., 2009). A comprehensive understanding of tropical Atlantic Ocean dynamics and variability across various time scales would allow for more accurate predictions of regional weather and climate, which is needed to mitigate or prevent possible damages connected to tropical Atlantic variability.

1.1.2 *Wind Driven Circulation in the Equatorial Atlantic Ocean*

Prevailing easterly trade winds drive the mean ocean circulation in the tropical Atlantic Ocean, which is largely governed by alternating zonal currents. These are crucial for the generation of TIWs. Therefore, in the following section I describe the features of the wind driven ocean circulation, which are most important in the context of TIWs, and their temporal variability.

Mean state

The trade winds directly force the westward South Equatorial Current (SEC) at the surface with two branches centred around 2°N and 4°S (see Figure 1.1). North of the SEC is the eastward flowing North Equatorial Countercurrent (NECC) between 3 and 10°N, which is forced seasonally by the wind stress curl (Philander, 2001; Sun et al., 2019). The prevailing easterly winds pile up warm surface waters at the western boundary of the basin and cause a sea surface depression at the eastern boundary (Philander, 2001; Talley, 2011). The resulting pressure gradient drives an intense eastward jet, centred in the subsurface, the so called Equatorial Undercurrent (EUC, Figure 1.1b). The

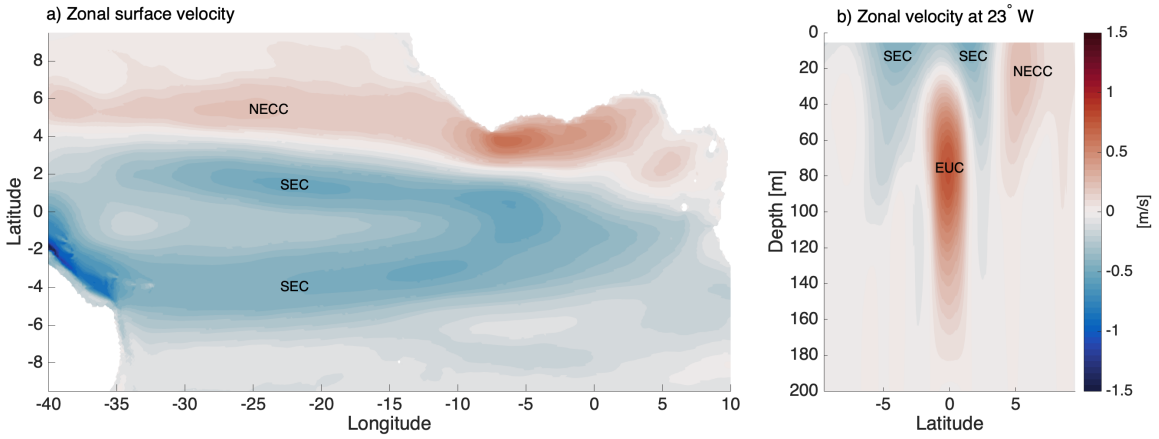

Figure 1.1: Mean zonal flow field in the tropical Atlantic Ocean, simulated in ICON-O over a 12 year period from January 2010 until December 2021. (a) Surface zonal velocities (b) Zonal velocities along 23°W.

EUC precisely marks the location of the Equator, where the Coriolis effect vanishes and the flow is driven by the pressure gradient force instead (Philander, 2001).

Variability

The trade winds follow a distinct seasonal cycle with a maximum between July and September (Philander, 2001). As a consequence, the SEC also intensifies in boreal summer. In addition, the SEC exhibits a second, weaker maximum in boreal winter, hence varying with a semi-annual cycle (Hummels et al., 2013; Richardson and McKee, 1984). In comparison, the EUC also exhibits a pronounced seasonal cycle. Unlike the SEC, where the semi-annual variability predominantly can be seen in terms of current strength, the seasonal variation of the EUC manifests as a modulation of both the EUC core depth, with a deepening in boreal summer (e.g. Brandt et al., 2008) and the current strength (Johns et al., 2014). The NECC also follows a seasonal cycle (Philander, 2001). During boreal winter, the region where the north-east and the south-east trade winds meet, the Intertropical Convergence Zone (ITCZ), shifts equatorward, which leads to relaxed winds along the Equator. During this time, the NECC practically disappears and the surface currents flow westward in the whole tropical Atlantic. When the winds intensify again in boreal spring and summer and the SEC intensifies, the NECC also reappears.

1.1.3 *Tropical Atlantic Sea Surface Temperature Variability*

In addition to the equatorial ocean circulation, SST also exhibits distinct temporal variability, which is a key component in the development of the characteristic TIW surface expression. The different modes of SST variability in the Atlantic Ocean and the drivers of such

variability are commonly described as Tropical Atlantic variability (TAV). Like the wind driven ocean circulation, TAV is dominated by a seasonal cycle (Xie and Carton, 2004), which is closely connected to the seasonality of the trade winds and as a result the ITCZ. While the seasonal cycle is the most pronounced ocean-atmosphere variability in the Atlantic basin (Ding et al., 2009; Muñoz et al., 2012), there is also distinct variability on interannual and longer time scales. In the following, I will give an overview of the most important modes of SST variability in the tropical Atlantic Ocean on different time scales.

Seasonal sst variability

Atlantic cold tongue

The most dominant feature of SST variability on seasonal time scales is the Atlantic cold tongue (Atlantic cold tongue (ACT)) in the eastern equatorial Atlantic. The evolution of the ACT is largely wind driven.

In boreal spring the trade winds are weak and the thermocline is deepest in the eastern basin, leading to less upwelling along the west African coast. This results in an SST maximum in the eastern equatorial Atlantic during boreal spring. At the same time the incoming solar radiation is at its maximum, which favours further ocean surface warming (Xie and Carton, 2004). In boreal summer the trade winds intensify, leading to an increased zonal surface pressure gradient and an uplifting of the thermocline in the east. Consequently, more cold water from the deeper ocean is brought to the surface, which leads to an SST cooling in the eastern equatorial Atlantic. In July, the SST most commonly reaches its minimum along the African coast due to strong upwelling, which extends northwards to the Gulf of Guinea shortly thereafter. This seasonal cooling phenomenon, which is most pronounced in July and August (Xie and Carton, 2004) characterizes the ACT.

The large temperature gradient between the cold ACT SST and the warm land surface further enhances the trade winds (Cabos et al., 2019). Furthermore, variations of the SST in the ACT region have a pronounced impact on precipitation over western Africa and can also modulate the onset of the West African monsoon (Brandt et al., 2011; Rodríguez-Fonseca et al., 2015). As such, a clear understanding of ACT dynamics and variability are of profound societal importance.

Interannual sst variability

Atlantic zonal mode

Interannual variability in the Atlantic Ocean is dominated by two leading modes of variability, the Atlantic zonal mode (AZM) and the Atlantic meridional mode (AMM, e.g. Chiang and Vimont, 2004; Murtugudde et al., 2001; Ruiz-Barradas et al., 2000; Zebiak, 1993). The former is often referred to as the Atlantic Niño due to a SST pattern similar to that of El Niño in the Pacific Ocean (Zebiak, 1993). The AZM is most commonly defined as the first mode of the Empirical Orthogonal Function (EOF), calculated from interannual SST anoma-

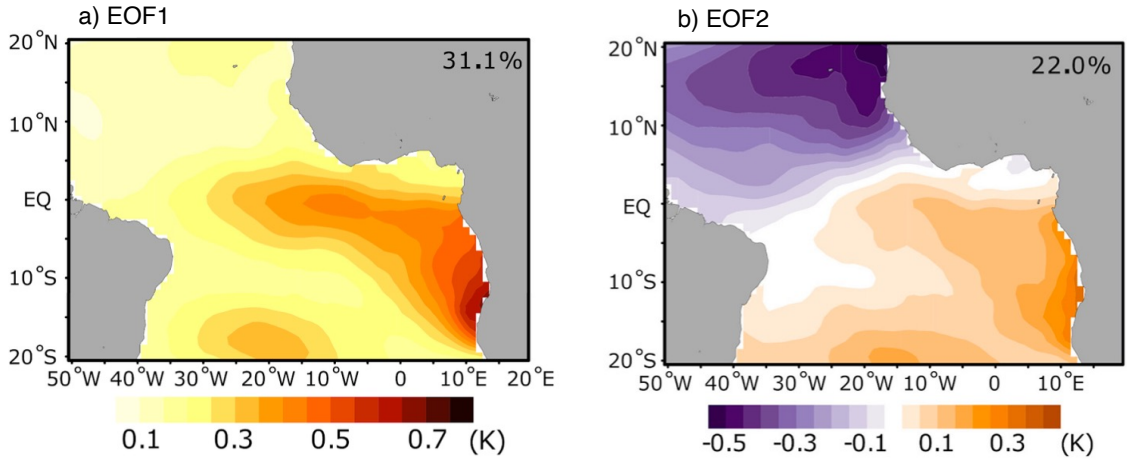

Figure 1.2: Empirical Orthogonal Function (EOF) 1st mode (a) and 2nd mode (b) for 12-monthly SST anomaly (1979–2015) obtained from TropFlux from Cabos et al. (2019), ©CC BY (http://creativecommons.org/licenses/by/4.0/).

lies (e.g. Cabos et al., 2019; Lübbecke et al., 2018). The pattern can be described as an L-shape, extending from the southwest coast of Africa towards South America, illustrated in Figure 1.2a (Cabos et al., 2019). The AZM is most pronounced in boreal summer and as such often occurs at the same time as the ACT. The AZM oscillates from warm to cold phases on a time scale of a few years (Cabos et al., 2019). The different phases of the AZM feature similar SST characteristics to the El Niño/La Niña phases in the Pacific Ocean, with the warm phases of the AZM in the Atlantic being comparable to El Niño and the cold phases being comparable to La Niña. A further similarity between the AZM and El Niño/La Niña is that they are both generated by the Bjerknes Feedback (Bjerknes, 1969), which describes a feedback between SST and surface winds.

Atlantic meridional mode

The second most dominant mode of variability in the tropical Atlantic Ocean is the AMM, which is defined as the second EOF of interannual SST anomalies. The AMM is characterized by an inter-hemispheric dipole structure with opposing SST anomalies in the northern and southern tropical Atlantic (e.g. Hastenrath, 1978; Murtugudde et al., 2001; Servain et al., 2000), which is shown in Figure 1.2b (Cabos et al., 2019). During its negative phase, SST anomalies are negative in the northern hemisphere and positive in the southern hemisphere. The opposite is true for the positive AMM phase. The AMM is most pronounced in boreal spring (April to May) and generated through the wind-evaporation-sea surface temperature feedback (WES, Cabos et al., 2019). Associated with the two centres of positive and negative SST anomaly are sea level pressure (SLP) anomalies. These different pressure fields produce a meridional pressure gradient and drive anomalous meridional surface winds. During the negative

AMM phase the generated surface wind anomalies north of the Equator increase the prevailing easterly trade winds, while south of the Equator they decrease the trade winds. Consequently, these changes drive latent heat fluxes and impact SST.

1.1.4 *Tropical Instability Waves*

While the seasonal cycle and interannual to decadal variability are the dominant modes of temperature and velocity variability in the tropical Atlantic Ocean (e.g. Ding et al., 2009; Prodhomme et al., 2019), there is also considerable intraseasonal variability tightly linked to the equatorial zonal flow field and modes of SST variability. Düing et al. (1975) were the first to find that the tropical Atlantic Ocean is traversed by intraseasonal waves, so called TIWs. Since then, TIWs have been extensively studied in both models and observations.

TIW *characteristics*

TIWs have been observed in the tropical Pacific and Atlantic Ocean with varying periods of about 15 to 60 days and a wavelength of 600 to 1200 km (e.g. de Decco et al., 2018; Jochum et al., 2004). They propagate westwards with a phase speed of 0.2 to 0.6 m/s (Jochum and Murtugudde, 2006). In the Atlantic Ocean, TIWs generally start to occur in May (Jochum and Malanotte-Rizzoli, 2004) as a response to the intensification of the southeasterly trades in boreal spring (von Schuckmann et al., 2008). The TIWs last until September and show strongest variability between July and September with a maximum in August. As such, TIWs can be considered a seasonal feature. Nonetheless, they can occur all year round and also exhibit pronounced interannual variability with several years of low TIW activity followed by periods of higher TIW activity (Caltabiano et al., 2005; Perez et al., 2012). Perez et al. (2012) and Wu and Bowman (2007) suggest that SST variability on interannual time scales such as the AZM is one reason for the interannual modulation of TIW. Despite their seasonal occurrence, the TIW strength is not seasonally modulated but rather appears to be stochastic (von Schuckmann et al., 2008).

TIWs are mainly confined to the upper ocean, namely the thermocline. However, their signal can reach down to greater depths of up to 800 m (Boebel et al., 1999). At the surface, TIWs are visible in pronounced SST patterns as seen in Figure 1.3. They form cusps of cold water, which transport cold, freshly upwelled water from the Equator polewards, while pushing warmer water equatorward (Jochum and Murtugudde, 2006). These cusps are characterized by sharp fronts with strong lateral temperature gradients (Warner et al., 2018). In general, TIWs are more pronounced in the northern hemisphere, however less energetic and well defined TIWs can also be found in the southern hemisphere (von Schuckmann et al., 2008).

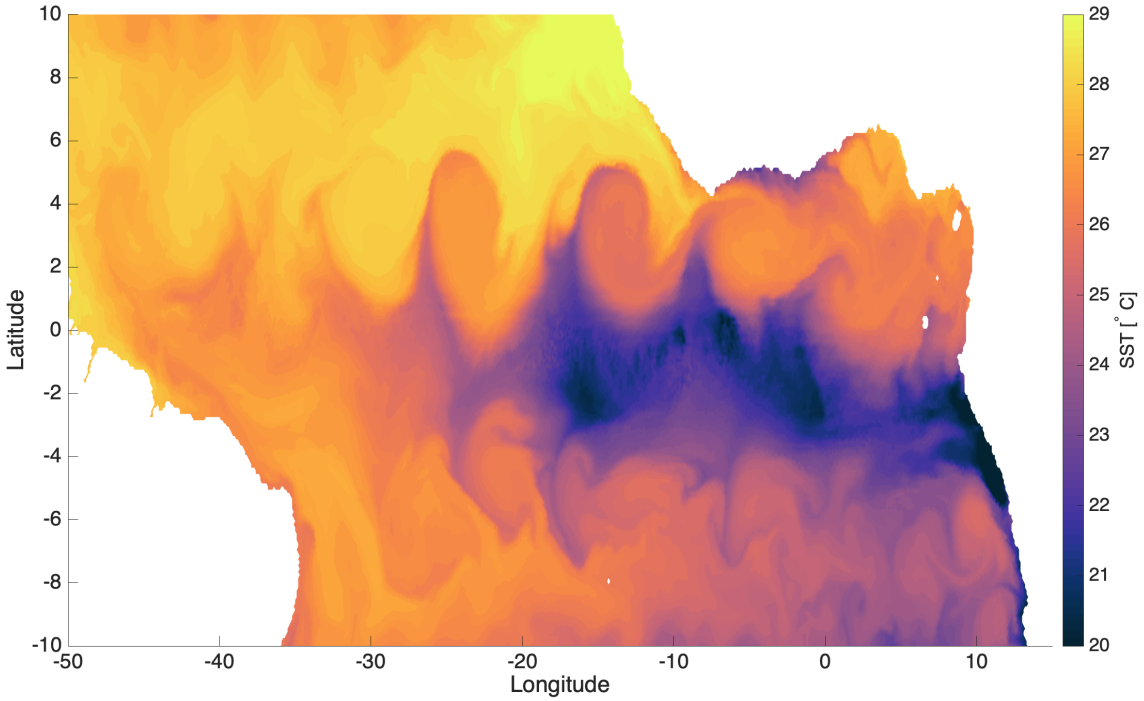

Figure 1.3: Snapshot of SST on 01.07.2011 simulated with ICON-O, showing characteristic TIW cold cusps in the Atlantic Ocean.

Generation mechanisms

TIWs draw their energy from the zonal mean flow via horizontal and vertical shear instabilities. These instabilities are mainly either barotropic or baroclinic. Other instabilities, like Kelvin-Helmholtz-Instabilities, are also thought to play a minor role in the generation of TIWs (Proehl, 1998). North of the Equator, the main source of TIW energy is the barotropic conversion of the zonal flow, namely instabilities and anticyclonic shear within the SEC as well as between the SEC and the EUC (Grodsky et al., 2005; Jochum et al., 2004; Proehl, 1998; von Schuckmann et al., 2008; Weisberg and Weingartner, 1988). Figure 1.4 shows a schematic of a typical TIW and the location of the prevailing mean currents. In Figure 1.4b the areas of high shear between the mean currents is also indicated. South of the Equator, the barotropic instability production rate is significantly lower than in the northern hemisphere. In comparison, the baroclinic production term is of similar magnitude in both hemispheres. This suggests differences in the generation of TIWs in northern and southern hemisphere (von Schuckmann et al., 2008).

Differences of TIWs *in Atlantic and Pacific Ocean*

Due to the similarities in the dynamic background conditions in the Pacific and Atlantic Ocean, the generation mechanisms and characteristics of TIWs in both oceans are largely comparable. However, there are also distinct differences between TIWs in Pacific and Atlantic

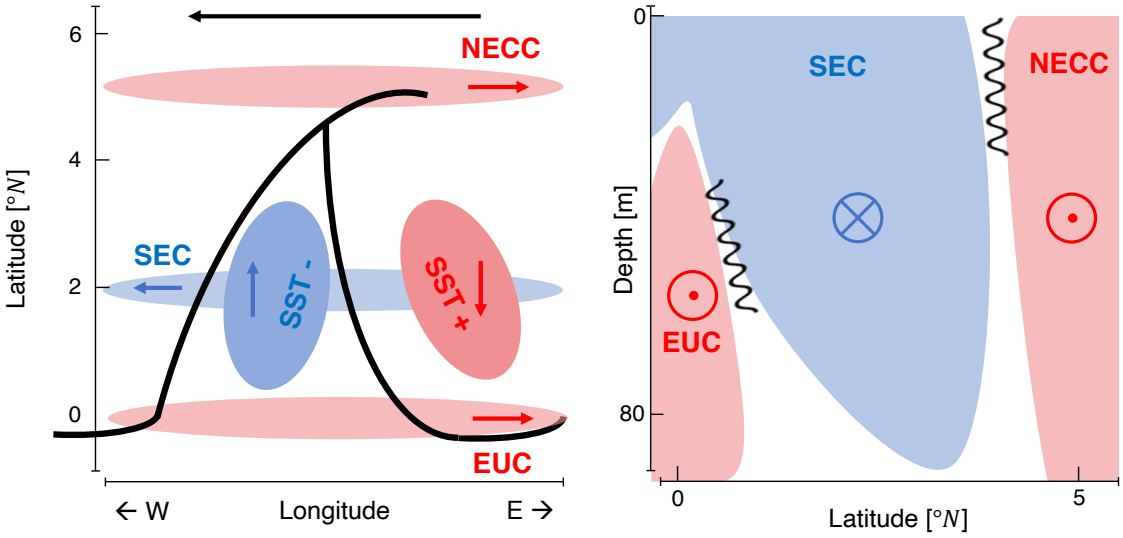

Figure 1.4: (a) Schematic of a TIW in the Atlantic Ocean. Black contour line shows the outline of a characteristic TIW, black arrow indicates the propagation direction. The centres of the dominant currents are displayed as coloured patches and coloured arrows indicate their direction. NECC: North Equatorial Counter Current, SEC: South Equatorial Current, EUC: Equatorial Undercurrent. NECC and SEC are surface currents, while the EUC is a subsurface current. Temperature anomalies associated with the TIW are also shown as coloured patches. Arrows indicate northward/southward transport of cold/warm water. (b) Schematic of the zonal mean currents in the central tropical Atlantic. Cross indicates a westward flow, dots indicate an eastward flow. Wavy lines indicate areas of high shear between the currents.

Oceans, which are worth pointing out. Considering the size of the waves and the basin size of the tropical Atlantic Ocean, there is space for approximately 2 to 3 TIWs at a time. Given that their periods are around 1 to 1.5 months on average, approximately 3 TIW oscillations can appear during boreal summer. In comparison, TIWs in the Pacific Ocean are found to have shorter periods of approximately 3 weeks and TIWs can also persist for a longer time throughout the year. Further, the basin size of the Pacific Ocean is significantly larger than the Atlantic Ocean by a factor of almost 2.5. Therefore, in the Pacific Ocean waves can cover a larger area and much longer TIW wave trains can be observed, persisting for large parts of the year (Philander, 2001).

1.1.4.1 *The importance of TIWs*

There are several aspects of TIW characteristics, which make them important for atmosphere, ocean interior, ocean biology, and ultimately for society.

Temperature fronts

One of those aspects are the surface temperature fronts, which accompany the TIW cold cusps. Sharp temperature fronts are of great relevance for the interaction and exchange between the ocean and the

overlying atmosphere, as well as the surface ocean with the ocean interior (Ferrari, 2011). The isopycnals at the fronts are strongly sloped, which enhances vertical velocities. Vertical velocity at sharp temperature fronts can be around one order of magnitude higher than in non-frontal regions (Thomas et al., 2008). As a result, carbon and heat is more likely to be transported into the ocean interior or vice versa at sharp temperature fronts. In addition, nutrient rich water from the deep ocean can be brought towards the surface by upwelling with implications for the biological production (Lévy et al., 2012; Sherman et al., 2022).

Air-Sea interaction in the presence of TIWs

Another consequence from the undulating SST fronts caused by the TIWs is that they lead to wind stress perturbations and thereby induce intraseasonal variability in the overlying wind field (Seo et al., 2007). These changes in the local wind field in turn generate additional wind stress and divergence. Furthermore, wind and SST are tightly coupled. For this reason, both latent and sensible heat flux are increased over the warm patch of TIWs (Hashizume et al., 2002; Seo et al., 2007), which can dampen the growth of TIWs. TIWs can also affect near surface wind on short time and space scales through air-sea coupling and thereby influence the location of the ITCZ. However, to date there is only limited research on air-sea interactions, mostly based on satellite observations and regional coupled models. Due to the small scale structure of the TIW temperature fronts, high-resolution coupled models are needed to further investigate such phenomena in the presence of TIWs.

Oceanic impact

Currently, the most important role of TIWs is their effect on the mixed layer heat budget and tropical SST. TIWs transport heat that is accumulated in the off-equatorial mixed layer towards the Equator, where it is removed by entrainment while pushing cold, freshly upwelled water from the Equator polewards (Jochum and Murtugudde, 2006, see Figure 1.4a). Hence, mixing and advection related to TIWs lead to a redistribution of heat with implications for the mixed layer heat budget in the tropical oceans (e.g. Foltz et al., 2020; Hummels et al., 2013; Inoue et al., 2019; Jochum and Murtugudde, 2006). Other studies also suggest that TIWs do not mainly mix temperature across the SST fronts but rather increase ocean-atmosphere heat flux and act as a vertical heat pump (Jochum and Murtugudde, 2006). TIWs are also suggested to play a role in the seasonal modulation of the cold tongue intensity. They cause cold tongue water to mix with warmer water from the off-equatorial regions and thereby prevent further cooling of the ACT SST (Perez et al., 2012). Furthermore, TIWs and intraseasonal waves that can be generated by TIWs, vertically propagate energy downward. This may contribute to the excitement and maintenance of the deep equatorial circulation (Ascani et al., 2010, 2015; Bastin et al., 2020; Greatbatch et al., 2018; Körner et al., 2022; Tuchen et al., 2018). Hence, TIWs are not only of interest in the upper

ocean but are also connected to deeper ocean dynamics.

Impact on ocean biology and biogechemistry

While in this dissertation, I exclusively focus on the physical oceanographic aspects of TIWs, it should not remain unmentioned that TIWs also play an important role in modulating the biology and biogeochemistry of the upper ocean in the tropics (Shi and Wang, 2021). An increased productivity and chlorophyll–a (Chl-a) concentration associated with TIW activity can be observed in both Pacific Ocean (Legeckis et al., 2004; Strutton et al., 2001) and Atlantic Ocean (Sherman et al., 2022). In fact, TIWs can be detected as chlorophyll fronts from space (Menkes et al., 2002). Based on observations from 2020 in the Pacific Ocean, Shi and Wang (2021) find that TIWs cause changes in salinity and nutrient concentration at the surface. This in turn leads to Chl-a variability in the Pacific Ocean from late May until the end of the year. However, the role of TIWs in the nutrient budget is still unclear (Sherman et al., 2022). A study by Evans et al. (2009) argues that TIWs drive a subduction of nutrient-poor waters north of the Equator, which is subsequently advected equatorward. This would lead to a reduced availability of nutrients at the Equator. However, as I will further elaborate on in the first part of this thesis (Appendix A), TIWs are associated with strong frontal mixing. This can lead to an upward supply of nutrients close to the Equator (Sherman et al., 2022). Furthermore, Eddebbar et al. (2021) report that in the tropical Pacific Ocean, Tropical instability vortices (TIVs), which are associated with TIWs (Flament et al., 1996; Kennan and Flament, 2000), drive a seasonal modulation of the oxygen minimum zone structure and impact the seasonality of ecosystem habitable space (Eddebbar et al., 2021).

1.1.4.2 *Discrepancies in current TIW research*

Despite large efforts to fully explain the role of TIWs in upper ocean dynamics, current findings on the impact of TIWs on mixed layer heat budget and SST are inconclusive. Several studies have attempted to assess the role of TIWs in the cooling or warming of surface waters, and to quantify the relative role of advection and vertical mixing. However, there remain discrepancies in the findings. While some studies suggest a surface warming induced by TIWs of up to 0.4°C in the Pacific (Maillard et al., 2022) and 0.35°C in the Atlantic Ocean (Grodsky et al., 2005), others report a TIW induced surface cooling in both Pacific (Moum et al., 2009) and Atlantic Ocean (Hummels et al., 2013). Some studies also argue that the effects of TIW related mixing and advection compensate each other, resulting in an overall weak contribution of TIWs to the mixed layer heat budget and SST (Jochum et al., 2004).

I hypothesize that these different findings arise as a result of the small number of TIW events most studies consider. In particular, stud-

ies based on observations strongly rely on the analysis of single events at specific locations. However, TIWs exhibit large spatio-temporal variability, which suggests that for more conclusive results, studies should be based on data which capture a larger number of TIWs. In fact, a recent study by Moum et al. (2022) suggests that they may have overestimated the effect of TIWs on surface cooling in the Pacific in previous work (Moum et al., 2009). The findings in Moum et al. (2009) were founded on observations of one particularly strong TIW, which can not be assumed to be representative for the impact of TIWs in general. Furthermore, it is suggested that in studies based on simulations, the findings on the effect of TIWs may depend on the choice of model and mixing parameterization scheme (Holmes and Thomas, 2015).

Realising that much of the discrepancies surrounding current TIW research stem from a general disregard of spatio-temporal variability, I was motivated to conduct the work described within this thesis. I aim to quantify the importance of TIW spatio-temporal variability in regards to mixing, by exploiting high-resolution global ocean model simulations, which allow for the study of over 60 TIWs, covering the entire tropical Atlantic basin over all seasons. While it is a major motivation for my work that no final agreement currently exists in the literature, on whether TIWs ultimately lead to cooling or warming, it should be noted that it is not the aim of my dissertation to offer a final conclusion to this point. Instead, I explore the factors and processes that might have lead to these discrepancies and provide suggestions on how they could be overcome in the future. The specific research questions I pose and my key findings are summarized in Sections 1.3 and 1.4.

1.2 MODELLING FRAMEWORK

Lack of observations

The overarching goal of my dissertation is to study the spatio-temporal variability of instability waves in the tropical Atlantic Ocean and their impact on upper ocean mixing. However, to date there exists no observational network sufficiently large to cover both the spatial and temporal extent of TIWs. The only observational platform that provides data in both space and time are satellite observations. However, these do not allow for the assessment of the vertical structure of TIWs. Instead, information on the vertical structure of TIWs obtained from observations relies on moorings and shipboard sections, which have insufficient spatio-temporal resolutions. Due to these shortcomings of available observational data, in regards to their spatial resolution, model simulations are the best option for studying the vertical extent and characteristics of TIWs.

High-resolution simulations from ICON-O

For this reason, in my dissertation I exploit high-resolution simulations of the ocean component from the comprehensive and global Icosahedral Nonhydrostatic Weather and Climate Model (ICON), unstructered-grid general circulation model of the Max Planck Institute for Meteorology. The model configuration I employ has a spatial resolution of $\sim$10 km and 128 vertical levels in the ocean with increased level spacing in the upper 100 m of $\sim$10 m (Korn et al., 2022). Such high resolution in both the horizontal and vertical is necessary to sufficiently resolve the sharp frontal features of TIWs. The simulations cover a period between 12 and 16 years with daily mean model output. For both simulations the model first underwent 25 years of spin-up, during which it was forced by daily OMIP (Ocean Model Intercomparison Project) data (Röske, 2006), and which was initialized with temperature and salinity fields from the Polar Science Center Hydrographic Climatology (PHC) (Steele et al., 2001). Following the spin-up is a simulation period from 1948 to 1978, which is forced by 6-hourly NCEP data (Kalnay et al., 1996). Then, from January 1979 onwards the ocean is forced by hourly ERA5 reanalysis data (Hersbach et al., 2020).

While the majority of the work for this dissertation was done using an uncoupled, ocean-only model configuration, ICON-Ocean (ICON-O) is just one part of a fully coupled model framework. Whereas the atmospheric component follows a non-hydrostatic approach and lends this term to the model's name (Giorgetta et al., 2018; Zängl et al., 2015), the ocean component resolves hydrostatic equations.

The decision to work with ICON-O simulations in order to study TIWs was made for two reasons. First, the long simulation period and large spatial domain allow for overcoming the previously mentioned shortcomings that arise when only few TIW events are considered at limited locations. I hypothesize that these shortcomings have likely

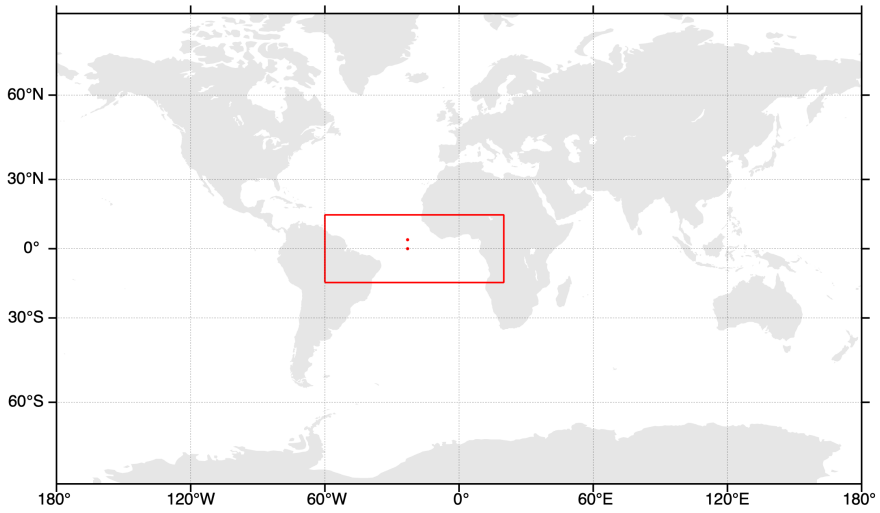

Figure 1.5: Map indicating the study area (red box) and the location of two moorings at 23°W, 0°N and 23°W, 4°N used in this study (red dots).

contributed to the discrepancies present in previous findings. Second, due to the coupled nature of the ICON framework, there is an opportunity to directly build on my results from exploring TIWs in the ocean-only setup, and analyse air-sea interactions in the presence of TIWs in a coupled model setup as a next step. However, the coupled simulations were not yet mature enough within the time frame of my thesis to advance this study by including air-sea interactions.

Study area

Despite the global model setup, in this dissertation I focus solely on TIWs in the tropical Atlantic Ocean. I limit the research area to 15°S to 15°N and 60°W to 20°E, indicated by the red box in Figure 1.5. This area is sufficiently large to cover the full spatial extent of TIWs in the Atlantic Ocean. In the second part of my thesis I also use data from two moorings to further support my findings. The moorings are located at 23°W, 0°N and 23°W, 4°N, which is shown as red dots in Figure 1.5.

After introducing the overall aim of this study and describing my strategy to reach this goal I will summarize each of the papers that result from this dissertation separately in the following sections. In each of the papers I specify research questions that I answer within with the aim to provide answers to my overarching research questions. For more details on the single studies I refer the reader to the full papers in Appendix A and B.

1.3 PAPER I: SEASONALITY OF MIXING AT TROPICAL INSTABILITY WAVE FRONTS IN THE ATLANTIC OCEAN

Motivation

It is well known that TIWs underlay strong spatio-temporal variability, in particular seasonality but also enhanced year-to-year variability. The modulation of mixing related to TIWs and their impact on mixed layer heat budget and SST have been studied rather extensively over the past years in both model and observations. However, the focus of these studies has been on understanding the processes and dynamics, which drive TIW related variations of shear and turbulence. While such process understanding of how TIWs modulate mixing is doubtlessly important, these process based studies have neglected the impact of temporal variability on TIW related mixing. In the first part of my thesis, I aim to fill this gap by exploring the question: Does mixing occur at all TIWs or is TIW related mixing influenced by processes on other time scales? In the next step, I investigate the drivers of TIW related mixing temporal variability based on my results. I state the following guiding research questions, which I answer in detail in the first paper related to this dissertation:

Research questions

1. DOES MIXING OCCUR AT ALL TIWS OR IS TIW RELATED MIXING ALSO INFLUENCED BY PROCESSES ON OTHER TIME SCALES?
2. WHAT CAUSES TEMPORAL VARIABILITY OF TIW RELATED MIXING?

As such, in this first part of my dissertation I answer the second overarching research question: HOW IS THE INFLUENCE OF INSTABILITY WAVES ON UPPER OCEAN MIXING IN THE TROPICAL ATLANTIC OCEAN ALTERED BY CHANGES IN THE BACKGROUND CONDITIONS? Furthermore, I aim to verify my hypothesis that the effect of TIWs on the mixed layer heat budget and SST is not well constrained in previous literature because only a few TIW events were considered.

Data and Methods

To answer the questions, I analyse 12 years of daily output from the global, comprehensive ICON-O model with a high spatial resolution of 10 km and 128 vertical levels between 2010 and 2021 (see Section 1.2). Such high spatial resolution is needed to sufficiently resolve TIW frontal dynamics. The configuration of the analysed simulation is comparable to that described in Korn et al. (2022) with the novel addition of an explicit online calculation of the separate heat budget terms. I focus on TIWs in the Atlantic Ocean, north of the Equator where the surface expression and therefore the temperature fronts are pronounced most strongly. Such a comprehensive simulation of over a decade offers the opportunity to evaluate about 60 TIWs across the width of the entire tropical Atlantic basin. To investigate the temporal variability of TIW related mixing, I analyse different proxies

for mixing such as the simulated vertical momentum diffusion, vertical shear squared $S^2 = \frac{du}{dz}^2 + \frac{dv}{dz}^2$ and the reduced shear squared $S_{red} = S^2 - 4N^2$, which puts shear (S^2) and stability (N^2) into relation. Here, N^2 is the Brunt-Väisälä-Frequency $N^2 = -\frac{g}{\rho}\frac{d\rho}{dz}$ with the gravitational acceleration $g = 9.81ms^{-2}$ and the potential density ρ. S_{red} relates to the Richardson Number Ri, such that $S_{red} > 0$ corresponds to $Ri < 0.25$, a common critical threshold, which indicates that the flow is unstable and mixing can occur (Howard, 1961; Miles, 1961). While the vertical momentum diffusion is a model parameter and is calculated online, S^2 and S_{red} are calculated offline based on output of daily mean values from the 2D velocity field and the vertical density gradient. Both S^2 and S_{red} are frequently used parameters for studying ocean mixing and can also be derived from observations. As such, the analysis of S^2 and S_{red} offers the potential for comparison of results based on simulations and observations.

Results

Firstly, I present evidence that deep reaching mixing at the trail edge front (TEF) of TIWs also occurs in the Atlantic Ocean, which follows the findings of previous studies from Lien et al. (2008), Holmes and Thomas (2015) and Cherian et al. (2021) in the Pacific Ocean. I demonstrate for the first time that such deep reaching mixing in the Atlantic Ocean underlies a pronounced seasonal cycle. The deep reaching mixing is strongly confined to the TEF of the TIW and generally starts in June/July before it subsides approximately three months later. While this mixing period often coincides with strong TIW activity, the onset of mixing appears to be independent of whether or not TIWs appear earlier in the year. As such, mixing does not occur at the TEF of all TIWs. Instead, even if there is pronounced TIW occurrence before boreal summer, frontal mixing does not occur before June. This suggests that the modulation of vertical shear by TIWs alone is not sufficient to trigger mixing. Instead, additional shear is needed to raise shear above a certain threshold and generate mixing. The apparent seasonality of the frontal mixing suggests that the process that provides the needed additional shear also follows a strong seasonal cycle. I find that this added shear stems from the seasonally modulated shear between the opposing mean zonal currents, EUC and SEC, which in turn is largely driven by the seasonally varying strength of the SEC.

Furthermore, I evaluate the simulated heat budget terms at the TIW fronts separately. I find that the deep reaching mixing leads to a local increase in temperature between the mixed layer depth and the thermocline. However, the impact of TIW related mixing on the mixed layer heat budget and SST are small. In addition, the impact of mixing on the temperature below the mixed layer depth is strongly confined to the TEF of the wave. Only there does temperature tendency due to mixing reach a comparable magnitude to the temperature tendency due to advection. In comparison, when considering the other parts

of the TIW, horizontal and vertical advection are the predominant terms that modulate the heat budget and substantially exceed the temperature effect of mixing both below and above the mixed layer depth. The key findings can be summed up as follows:

Key findings

1. DEEP REACHING MIXING AT THE TEF OF TIWS IN THE ATLANTIC OCEAN EXHIBITS A STRONG SEASONAL CYCLE.
2. SEASONALLY INCREASED SHEAR OF THE MEAN ZONAL CIRCULATION PROVIDES THE ADDITIONAL SHEAR THAT IS NECESSARY TO ELEVATE THE SHEAR AT TIW FRONTS ABOVE A CRITICAL THRESHOLD AND ALLOWS FOR DEEP REACHING MIXING TO OCCUR.
3. THE EFFECT OF MIXING AT TIW FRONTS FOR THE MIXED LAYER HEAT BUDGET AND SST IS SMALL.

Conclusion

In conclusion, I argue that seasonal mixing at TIW fronts results from a superposition of TIW related shear and elevated background shear of the mean zonal circulation. The SEC plays a major role in the seasonal increase of this background shear. As such, the SEC is a key component in the generation and modulation of deep reaching mixing at TIW fronts.

While frontal mixing leads to a local increase in temperature between mixed layer depth and thermocline, the overall effect of such mixing on mixed layer heat budget and SST is small. Furthermore, deep reaching mixing only occurs in boreal summer and only within a confined location, the TEF. As a result, studies that examine few TIWs or consider only single locations potentially overlook or overestimate the impact of TIWs on upper ocean cooling or warming. For a better understanding of the role of TIWs in equatorial mixing dynamics and their effect on upper ocean temperature, it is crucial to take spatio-temporal variability, and in particular seasonality, of both TIWs and the background state into account in future studies.

1.4 PAPER II: IDENTIFYING AND CHARACTERIZING SUBSURFACE TROPICAL INSTABILITY WAVES IN THE ATLANTIC OCEAN IN SIMULATIONS AND OBSERVATIONS

Introducing Subsurface Tropical Instability Waves

For the second part of my thesis I focus on investigating the spatial structure of TIWs. In particular, I consider the vertical extent and structure of the waves. To do so, I explore TIWs in the subsurface, down to the depth of the thermocline ($\sim$ 80-100 m). While many studies have undertaken research to better understand the role of TIWs close to the surface, the vertical structure of TIWs remains largely unknown. Despite TIWs being most energetic at the surface (Jochum et al., 2004) early studies found TIW signals down to 800 m depth (Boebel et al., 1999). A more recent study by Liu et al. (2019a) based on observations in the Pacific Ocean finds that TIWs can have complex vertical velocity structures, interacting with the zonal mean flow and thus affecting vertical mixing. Liu et al. (2019a) coin the term subsurface mode tropical instability waves (subTIWs), which can be distinguished from the commonly known surface-intensified TIWs. They state that the vertical shear from subTIWs can interact nonlinearly with the background shear of the zonal mean flow, namely the EUC, and change the total shear above the EUC core. Liu et al. (2019a) and Liu et al. (2020) conclude that subTIWs may play an important role in vertical heat transport and mixing.

Motivation

However, analysis of the only recently described subTIWs is based entirely on one single spot mooring in the Pacific Ocean at $0°N, 140°W$, which does not allow for determining the horizontal structure or temporal evolution of subTIWs. Further, the results are restricted to the Pacific Ocean. While the similarities of TIW characteristics in the Pacific and Atlantic Ocean suggest that subTIWs also occur in the Atlantic, their existence there is yet to be proven. In the second paper I tackle this problem and show that subTIWs are present in the tropical Atlantic Ocean as well. Furthermore, I extend the study by Liu et al. (2019a) by investigating the spatio-temporal variability of subTIWs in the Atlantic Ocean and relating their importance to TIWs at the surface. The main research questions, which I answer in the second part of this dissertation, are as follows:

Research questions

1. DO SUBTIWS ALSO EXIST IN THE ATLANTIC OCEAN?
2. WHAT IS THE SPATIO-TEMPORAL VARIABILITY OF SUBTIWS IN THE ATLANTIC OCEAN?
3. HOW IMPORTANT ARE SUBTIWS IN RELATION AND IN COMPARISON TO TIWS?

Investigating both time and space characteristics of subTIWs broadens the understanding of the vertical structure of instability waves, and

provides an answer to my first overarching research question: WHAT IS THE CHARACTERISTIC SPATIAL STRUCTURE AND TEMPORAL OCCURRENCE OF INSTABILITY WAVES IN THE TROPICAL ATLANTIC OCEAN, IN PARTICULAR IN THE VERTICAL?

Data

To present evidence for the first time that subTIWs do exist in the Atlantic Ocean, I use both observations and simulations. The observations are derived from two PIRATA moorings at 4°N, 23°W and 0°N, 23°W (Bourlès et al., 2019). At 4°N, 23°W a unique data set of hourly upper ocean velocity and shear measurements is available for 1 year from March 2017 to March 2018 (Perez et al., 2019). The mooring at 0°N, 23°W provides hourly velocity measurements in the upper 210 m from 2001 until 2015 (Bourlès et al., 2019). However, due to large data gaps prior to 2008, I only consider measurements after this period in my analysis. For the analysis of the spatio-temporal variability of subTIWs, I use 16 years (2003 to 2019) of daily mean temperature and velocity output from a global, comprehensive ICON-O simulation with a high spatial resolution of 10 km. This model configuration is comparable to that used in the first paper attached to this dissertation (Appendix A, Specht et al., 2023) but without the online heat budget diagnostic. This model configuration is shown to realistically reproduce TIWs (Specht et al., 2023). Compared to the sparse observations, in particular in the spatial domain, such a long simulation of more than one decade has the advantage to deliver results which are statistically more robust. By analysing the model output, I assess subTIW variability on different timescales, varying from intraseasonal variability over seasonal variability to year-to-year variability. Furthermore, I describe the spatial characteristics of the waves and their impact on vertical mixing in different areas of the tropical Atlantic Ocean, which is not plausible with mooring data alone. Lastly, I evaluate the importance of subTIWs compared to TIWs and the effect of a simultaneous occurrence of both TIWs and subTIWs.

How to identify subTIWs?

To investigate subTIWs in the Atlantic Ocean, I firstly identify the regions of strong instability wave occurrence. For that, I adapt the methods used by de Decco et al. (2018) to isolate TIWs through filtering. I apply a 2D gaussian filter to the simulated temperature field with a temporal filter bandwidth of 15 to 60 days and a spatial filtering bandwidth of 4 to 20°longitude. Previous studies (e.g. de Decco et al., 2018) argue that those filtering windows are appropriate to isolate TIWs in the Atlantic Ocean. I chose the filtering windows under the assumption that subTIWs lay within the same range as TIWs. Next, I modify the approach applied in Perez et al. (2019) to find strong instability wave events. I calculate the standard deviation of the previously filtered temperature field in a 4-month moving average window for each grid point and model layer within the the thermocline. I take

the 90th percentile of the domain wide filtered temperature standard deviation as a threshold to identify strong instability wave events. I derive a 2D histogram of the number of events above this threshold for each model layer. This results in the identification of two regions of pronounced subTIW activity in 64 m depths. In the following, I focus on these two regions, one located south of the Equator (1 to 3.5°S and 15 to 28°W) and one located north of the Equator (2.5 to 5°N and 12 to 22°W). Liu et al. (2019a) suggest that when they apply a narrower temporal bandpass filter, which allows for separating subTIWs from TIWs, they find a manifestation of subTIWs, visible as distinct oscillations of the zonal velocity component in the the subsurface. Hence, I conduct a spectral analysis of both velocity components for the previously identified regions to find the specific subTIW periods there. To also consider the periods varying in different years as is the case in Liu et al. (2019a) I also compute wavelets for both regions. Finally, I find that the average subTIW period in the northern region is between 24 and 53 days and in the southern region it is between 25 to 47 days. Similarly, I derive subTIW periods for the mooring at 4°N, 23°W (30 to 45 days) and at 0°N, 23°W (24 to 53 days). These temporal filtering windows are used when applying a 2D Gaussian filter to the model output prior to the analysis to study subTIW characteristics separately from TIWs.

Results

I show that in both ICON-O and the mooring observations along 23°W subTIWs occur between around 30 to 90 m depth, which are visible as subsurface velocity peaks, comparable to the results from Liu et al. (2019a). subTIWs do not occur in the entire tropical Atlantic basin but are centred in two regions, one north and one south of the Equator. In comparison, TIWs mostly exist north of the Equator. In the northern region, subTIWs are mainly manifested in oscillations of the meridional velocity component, while in the southern region subTIWs can be predominantly seen by oscillations of the zonal velocity component. subTIWs most frequently occur between June and December and generally start to develop one to three months later than TIWs. Like TIWs, subTIWs also exhibit pronounced year-to-year variability. As such, both surface and subsurface TIW can also be present at the same time.

Below and above the subsurface velocity maximum associated with subTIWs, vertical shear reaches a maximum, resulting in a multi-layer shear structure. By causing such a subsurface shear pattern, subTIWs can destabilize the mean flow and generate vertical mixing. This finding is supported by positive values of reduced shear squared above the thermocline, which is a proxy for mixing.

Lastly, I assess the influence of subTIWs on mixing and heat fluxes relative to TIWs. While the impact of subTIWs on altering mixing and heat fluxes is generally smaller compared to TIWs, I find the strongest

effect when both TIWs and subTIWs are present simultaneously. I argue that despite the apparent minor importance of subTIWs alone, interactions between the two instability wave modes play an important role for thermocline dynamics and heat budget. This results in the following key findings:

Key findings

1. THE EXISTENCE OF SUBTIWS IN THE TROPICAL ATLANTIC OCEAN IS SHOWN FOR THE FIRST TIME IN SIMULATIONS AND OBSERVATIONS.
2. SUBTIWS IN THE TROPICAL ATLANTIC OCEAN PREDOMINANTLY OCCUR IN TWO SEPARATE REGIONS NORTH AND SOUTH OF THE EQUATOR.
3. SURFACE AND SUBSURFACE TIWS SHARE SIMILAR CHARACTERISTICS BUT CAN NONETHELESS BE CONSIDERED TO BE DISTINCT WAVES, WHICH BOTH IMPACT THERMOCLINE DYNAMICS. THEIR IMPACT IS STRONGEST DURING THE SIMULTANEOUS OCCURRENCE OF TIWS AND SUBTIWS.

Conclusion

Since I find that subTIWs have an effect on vertical mixing and heat flux in the upper ocean, I conclude that future studies of the upper ocean heat budget should consider both TIWs and subTIWs. This is particularly important in the off-equatorial regions, which exhibit strong subTIW activity. The identification and detailed description of subTIW characteristics in the Atlantic Ocean leads to a number of open questions:

Open questions

1. HOW DO SUBTIWS AND TIWS INTERACT?
2. ARE THE EFFECTS OF SUBTIWS LIMITED TO THE SUBSURFACE OR DO THEY ALSO HAVE AN IMPRINT ON THE SST, COMPARABLE TO CHARACTERISTIC TIW PATTERNS?

Finding the answers to those questions in future studies is crucial to properly assess the role and importance of subTIWs for the upper ocean and air-sea interactions.

1.5 DISCUSSION

How important are TIWs for the ocean heat budget?

While the work presented in this thesis delivers an important contribution to a more complete understanding of TIWs in the tropical Atlantic Ocean, particularly concerning the vertical expression and the role of temporal variability in TIW related shear modulation, it also raises the question of how important TIWs in the tropical Atlantic Ocean really are for the upper ocean heat budget.

Overestimation of TIW impact based on observations

It has been discussed extensively in the past that TIWs modulate the mixed layer heat budget and equatorial SST. However, there are discrepancies in previous findings, which make it impossible to draw a final conclusion about the extent of TIW impact. In fact, a recent study based on a number of turbulence measurements in both Pacific and Atlantic Ocean, poses the question if the effect of TIW-induced mixing on the mean state might have previously been overestimated (Moum et al., 2022). Moum et al. (2022) argue that the observations made during 2008 at 0°N, 140°W, which are the basis for several studies on the influence on TIWs (e.g. Inoue et al., 2012; Inoue et al., 2019; Moum et al., 2009), measured the passage of a particularly strong TIW, which is not representative and might thereby have led to the overestimation of the TIW-induced mixing effect. In addition, it is still unclear how much, and in what proportion, advection and vertical mixing contribute to surface cooling or warming and how they interact (Moum et al., 2022). Some studies also suggest that TIW related warming due to vertical heat advection is balanced by TIW related cooling due to horizontal heat advection, leading to a small net effect of TIWs on the mixed layer heat budget and SST (Jochum et al., 2004).

The importance of spatio-temporal variability

Based on the findings of my studies, I argue that the large spatio-temporal variability of TIWs may also substantially contribute to discrepancies between previous studies. While the results published in the literature based on a small number of TIW events might all be true for the specific cases that were considered, I suggest that no overall conclusion may be drawn from such analyses. As pointed out for example by Grodsky et al. (2005), the location of the measurements in regard to the cold tongue location is crucial for the effect of TIWs on SST. The horizontal temperature gradient is significantly smaller close to the Equator, in the centre of the cold tongue, compared to the edge of the cold tongue, with implications for a possible TIW impact through temperature advection and mixing. My finding that deep reaching mixing only seasonally occurs at the TEF of TIWs further supports this argument that the study location strongly influences the results. As such, it can be expected that the effect of TIWs on mixed layer heat budget and SST differs significantly between boreal summer, when frontal mixing is strong, and the rest of the year. Further, differing

results are expected from studies based on observations from ship sections or moorings that do not cover the location of the TEF.

Hence, my findings corroborate that TIWs are likely to be less significant for the mixed layer heat budget than previously anticipated and that the effect of advection outweighs the role of mixing in modulating upper ocean and surface temperatures. I suggest that while TIWs unequivocally have an impact on the SST and the upper ocean heat budget, which can extend down to the thermocline, such effects appear to be only instantaneous. However, when analysing long time series, which cover a large number of TIWs, the impact of TIWs on the temperature mean state is negligible.

Impact of subTIWs on heat budget and SST

Furthermore, the identification and characterisation of subTIWs raises the question if and how these subsurface waves impact the heat budget and ocean surface. However, in comparison to TIWs, subTIWs are not yet well studied. Therefore, it is not yet clear how they may impact the upper ocean heat budget and SST. Due to the similarities of TIW and subTIW characteristics and the extensively discussed effect of TIWs, it stands to reason that subTIWs also contribute to a modulation of ocean heat budget and SST. Since subTIWs frequently occur south of the Equator, also in the absence of TIWs, I analyse the impact of subTIWs on the heat budget in an area between 27.5 to 13°W and 1.25 to 4.65°S in the ICON-O setup with online heat budget calculation, as used for the paper in Appendix A. This is the area in which I find the most pronounced subTIW activity in this simulation. I find that, comparable to TIWs north of the Equator, subTIWs south of the Equator lead to a pattern of alternating warm and cold SST patches, indicating an instantaneous imprint of the wave onto the ocean surface. I further find that during the passage of subTIWs, vertical mixing leads to a temperature increase between mixed layer depth and thermocline. However, within the mixed layer, mixing causes cooling, which is counterbalanced by horizontal and vertical advection. As such, in line with my findings for TIWs, subTIWs only have a very small effect on the total temperature in the mixed layer. This result is also confirmed when looking into the change in SST during an entire subTIW season. Here the SST change is defined as the difference in the SST, averaged over the described area, between the start and the end of the subTIW season. These temperature changes are shown in Figure 1.6b. Positive values indicate warming, negative values indicate cooling. As a reference, the turbulent kinetic energy, which is an indicator for the intensity of subTIW activity, is shown in Figure 1.6a in ascending order, integrated over each subTIW season. The year 2011 is missing as no subTIWs were found that year. It becomes apparent that subTIWs do not cause a clear surface warming or cooling and there is no linear relationship between the intensity of the waves and a change in surface temperature. These results are solely based on the analyses of subTIWs south of the Equator. However, since they

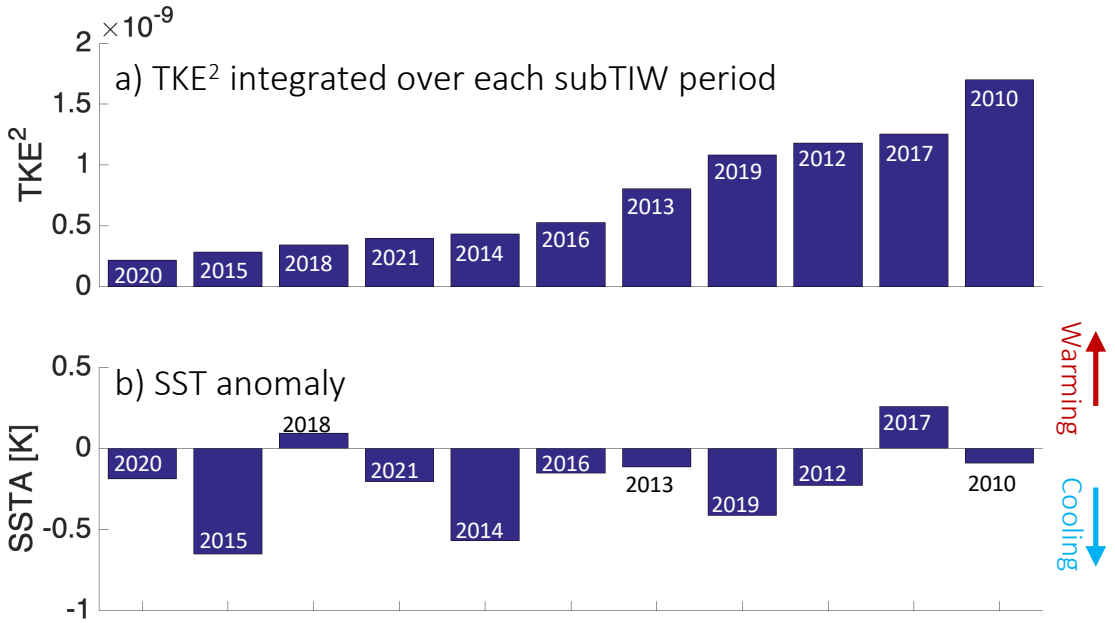

Figure 1.6: Turbulent kinetic energy (TKE) integrated over each subTIW period in ascending order (a) and regional SST anomaly for each subTIW period (b). SST anomalies are calculated as an area mean between 27.5 to 13°W and 1.25 to 4.65°S.

are strongest in this location, it can be assumed that if there was an impact of subTIWs on the upper ocean heat budget and SST, it should be found in this region. Therefore, I conclude that, similar to TIWs, subTIWs also primarily have an instantaneous effect on the ocean surface but are negligible for the temperature mean state.

TIW related air-sea interaction

Although the effect of TIWs on upper ocean temperatures appear to be small, my findings do not imply that TIWs are wholly unimportant, instead suggest to rather focus on the implications of the instantaneous imprint of TIWs. TIWs unarguably have a strong SST expression with sharp lateral fronts, which force enhanced air-sea interaction (Ferrari, 2011). Unfortunately, due to the sparsity of observations and limitations of coupled simulations, which are needed to study the complex interactions of TIWs with the overlying atmosphere, there are only few studies to date on the atmospheric impact of TIWs as well as TIW related ocean-atmosphere interactions.

Impact of TIWs on biological processes

Further, in this dissertation I only investigated the physical oceanographic processes related to TIWs. However, sharp fronts like those caused by TIWs have implications for biological and biogeochemical processes as I have described in Section 1.1.4. As such, despite being a spatially and temporally closely confined feature, the TIW induced deep reaching frontal mixing and enhanced subsurface shear may play

a role in biological processes, such as the exchange of nutrients or CO_2 between atmosphere, surface and subsurface ocean.

1.6 SUMMARY AND CONCLUSION

Summary

In this dissertation I explored the spatio-temporal variability of instability waves in the tropical Atlantic Ocean and their impact on upper ocean mixing using comprehensive, high-resolution ICON-O model simulations. My main focus was on investigating TIWs and SUBTIWs under the explicit consideration of their large spatial extent, horizontally and vertically, and their temporal variability. Due to the sparsity of observations, answering such research goals currently relies on the use of high-resolution models.

RESULTS IN A NUTSHELL

My analyses can be divided into two parts, represented by the attached papers, which I summarized in Section 1.3 and 1.4. In the following, I want to summarize my results by referring to my overarching research questions:

Paper 2

1. WHAT IS THE CHARACTERISTIC SPATIAL STRUCTURE AND TEMPORAL OCCURRENCE OF INSTABILITY WAVES IN THE TROPICAL ATLANTIC OCEAN, IN PARTICULAR IN THE VERTICAL?
   This question is mainly answered in the second part of my dissertation (Section 1.4, Appendix B). Here, I moved away from the surface and investigated the vertical expression of instability waves in the Atlantic Ocean. For the first time, I showed the presence of SUBTIWs in the Atlantic Ocean in simulations and observations. They predominantly occur in two regions, one north and one south of the Equator and are located between mixed layer and thermocline depth in about 30 to 90 m depth. I demonstrated that while similar in characteristics, SUBTIWs and TIWs can be found independently of each other, with SUBTIWs occurring on average 3 months later than TIWs. SUBTIWs induce a vertical multi-layer structure of enhanced shear, centred around the SUBTIWs in the subsurface, which has the potential to impact vertical mixing. Unlike TIWs, SUBTIWs are of comparable strength both north and south of the Equator.

Paper 1

2. HOW IS THE INFLUENCE OF INSTABILITY WAVES ON UPPER OCEAN MIXING IN THE TROPICAL ATLANTIC OCEAN ALTERED BY CHANGES IN THE BACKGROUND CONDITIONS?
   This question I explored in the first part of my dissertation (Section 1.3, Appendix A). More precisely, I posed the questions whether mixing occurs at all TIWs or if TIW related mixing is influenced by processes on other time scales? I find that mixing is sharply confined to the TEF of TIWs and follows a clear seasonal cycle, which can be linked to an increase in vertical shear between zonal background currents. This enhanced background shear is predominantly connected to the seasonality of the SEC.

As such, the SEC can be attributed great importance in modulating TIW related mixing. Further, my results show that while this deep reaching frontal mixing locally increases the temperature tendency between mixed layer depth and thermocline, the overall effect of mixing on the heat budget and SST is small.

Conclusion

I conclude that it is of great importance for the study of TIWs to consider both spatial and temporal variability of the waves as well as temporal variability of the background conditions. In particular, with regard to the vertical structure of TIWs, I suggest that future studies should also consider the presence of subsurface Tropical Instability Wave (subTIW)s and their possible role in modulating the effects of TIWs. Final agreement on the role and importance of TIWs for the upper ocean heat budget and SST in tropical oceans will likely not be found until these vital aspects are widely incorporated.

On the need of further observations

Regardless of the scope of TIW research, a larger network of observations is needed to fully understand TIWs. This is particularly important for studying TIW characteristics in the vertical. While satellite observations offer a great possibility to study TIWs over large time and space scales, they are limited to the surface expressions of TIWs. In comparison, studies on mixing and subsurface processes related to TIWs rely on single spot moorings, sections from research cruises and model simulations. Unless a significantly larger network of observations that cover several years over all seasons at different locations becomes available, high resolution models are needed to study the extent and characteristics of TIWs in the vertical. However, as Holmes and Thomas (2015) point out, results of TIW mixing are sensitive to the applied mixing scheme of the underlying model. Therefore, further validation with observations is required.

Limitations of this thesis

It should be noted that this aspect is a limitation of the work presented in my dissertation. While I use observational data to validate the quality of the simulated background conditions and am therefore confident about the significance of my results, my work still relies on simulations from one single model in a certain configuration. Depending on the choice of e.g. the mixing scheme, parameterization and the vertical grid and resolution, or a different model entirely, findings might differ. Therefore, more robust conclusions could be made by repeating the analyses under varying model configurations or by using output from a different high-resolution model.

Lastly, I would like to point out that all findings and conclusions in this thesis are based on studying TIWs in the Atlantic Ocean. While I expect them to be largely transferable to the Pacific Ocean as well, I can not foreclose that there are differences to the Pacific Ocean. In particular, TIWs are reported to be stronger and more frequent in the

Pacific Ocean, which might affect their contribution to the total equatorial shear and the relative role of TIWs in it. Furthermore, the tropical Pacific Ocean is strongly effected by El Niño/La Niña. TIWs interact with this climate mode and for example are found to be stronger during La Niña events (An, 2008). While TIWs in the Atlantic Ocean are also modulated by interannual variability such as the Atlantic Niño (Tuchen et al., 2022), the connection is less pronounced. It might be worthwhile to repeat the analyses in this dissertation for the Pacific Ocean as well to see if the findings are indeed transferable or if there are unknown differences between TIWs in the Pacific and Atlantic Ocean.

1.7 OUTLOOK

Throughout this thesis I repeatedly draw attention to how important it is to consider the spatio-temporal variability of TIWs to fully understand their characteristics and their relevance for tropical oceans. Maintaining an observational network with a high enough spatial and temporal resolution to cover both the horizontal and vertical extent of TIWs and capture temporal variability across different time scales is simply not feasible. Therefore, I believe that for the foreseeable future studying TIWs will rely on the use of high-resolution simulations. While it would undoubtedly be desirable to depict a conclusive picture of TIWs based on observations alone, complex high-resolution simulations offer great possibilities to shine a light on some of the unanswered questions and discrepancies surrounding TIWs. In particular, the development of high-resolution coupled ocean-atmosphere models allows for gaining new insights into the ocean-atmosphere interaction in the presence of TIWs.

TIWs in coupled models: Air-Sea interactions

As pointed out before, one of the most important characteristics of TIWs is the distinct surface expression with cusps of cold SST and strong lateral temperature fronts. Such fronts disturb the overlying atmosphere and can therefore affect the regional climate. However, to date studies on this topic are limited due to the lack of both observational data and appropriate simulations. There are some studies that investigate the role of TIWs on the overlying atmosphere in atmosphere only simulations with prescribed SST. This however neglects that the interaction between TIWs and the atmosphere goes both ways. Hence, atmosphere only models are not sufficient to describe the role of TIWs in the regional climate. Instead, high-resolution coupled simulations are needed.

State-of-the-art Earth System models typically have a horizontal grid spacing in the order of 100 km (Müller et al., 2018), which is too coarse to resolve the important frontal features of TIWs. However, high-resolution coupled ICON simulations have very recently become available. They range from an ultra high resolution of 2.5 km, which is limited to a simulation period of one year, to a 30 year long simulation with a 10 km spatial resolution. In a recent study, Hohenegger et al. (2022) explore such a new ICON-Sapphire model configuration, which is fully coupled. The simulation was run globally for a full year with a grid spacing of 5 km, and for 2 months with a grid spacing of 2.5 km in both atmosphere and ocean. This makes it very well suited to study the interaction of ocean and atmosphere over TIW fronts. I contributed to the study by Hohenegger et al. (2022) with an analysis of the representation of TIWs in the coupled ICON-Sapphire configuration and some analyses on the atmospheric impact of the waves. I find that the 2.5 km grid spacing even allows for submesoscale frontal

features like the development of secondary TIW fronts to be resolved. These counterclockwise rotating secondary fronts (Figure 1.7a) have a direct imprint on the atmospheric heat fluxes (Figure 1.7b), highlighting the importance of studying air-sea interactions of TIWs in highly resolved simulations. However, these findings are only a first

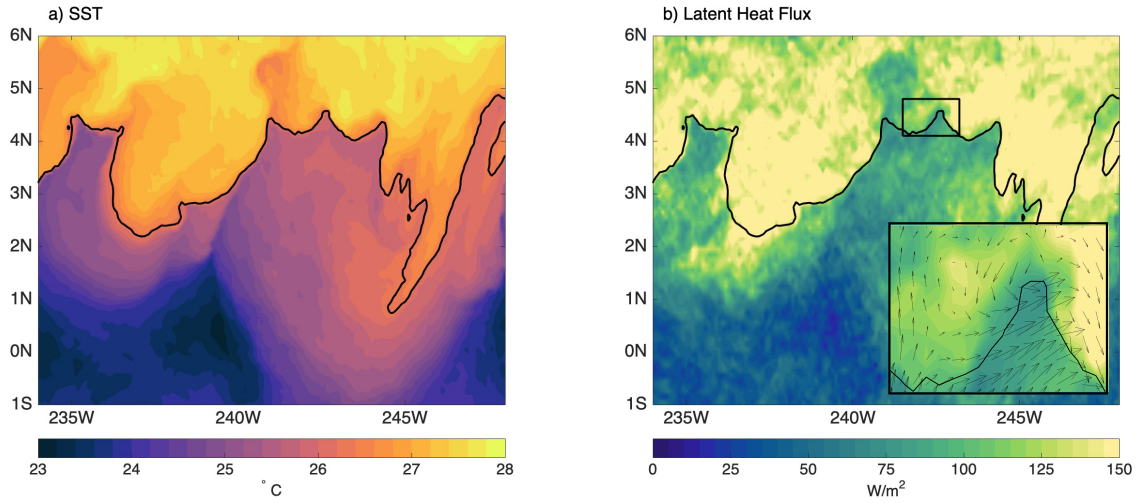

Figure 1.7: Breaking of a TIW in the Pacific Ocean in the ICON-Sapphire setup with a grid spacing of 2.5km used in Hohenegger et al. (2022) with (a) SST and (b) latent heat flux. Black line shows the 26.3°C isotherm. Snapshot for 5 February 2020 23:00.

step to illustrate the potential of such high-resolution, global coupled simulation and more detailed analyses of air-sea interaction in the presence of TIWs should follow. Since I suggest that TIW induced ocean-atmosphere interaction might actually be of greater importance than the impact of TIWs on the upper ocean heat budget and the mean surface state, I think that the development of model configurations like ICON-Sapphire is a necessary advancement to broaden our understanding of the role of TIWs in the climate system. However, despite this new ICON-Sapphire configuration being an important milestone in high-resolution coupled simulations and offering great opportunities for process studies or ocean-atmosphere interactions at TIW fronts, it is currently limited to a short run time. It can therefore not yet be used to draw statistically significant conclusions, nor study the impact of TIWs on rain fall over the adjacent continents or other teleconnections on longer time scales. For this, coupled simulations of at least 10 km spatial resolution and a simulation period of several years are needed, which are also available as of late within the coupled ICON framework. This provides a great chance for future studies that can build on my findings based on the ocean-only setup.

The end

At this point I would like to conclude the unifying essay and direct the reader to the two papers, which have resulted from my work on

this dissertation (Appendix A and B). Although I have answered many questions regarding TIW characteristics and their role in the Atlantic Ocean, new questions have arisen, and some old questions remain. I am reminded of the old scientific adage, best said by Isaac Newton - *if I have seen further, it is by standing on the shoulders of giants*. That is, to complete the work presented herein, I have relied on the countless efforts of others before me. Likewise, I believe that my work builds on prior understanding, and contributes to a solid foundation for others to build upon.

A

SEASONALITY OF MIXING AT TROPICAL INSTABILITY WAVE FRONTS IN THE ATLANTIC OCEAN

The attached article is in preparation for submission in *Journal of Geophysical Research: Oceans*.

Specht, Mia Sophie, Johann Jungclaus, and Jürgen Bader. "Seasonality of Mixing at Tropical Instability Wave Fronts in the Atlantic Ocean." *In preparation*

AUTHOR CONTRIBUTIONS: M.S.S. designed the research question, performed the analysis, created the figures and drafted the manuscript. Throughout the process, J.J. and J.B. provided scientific guidance and feedback. All authors contributed to editing and revising the manuscript.

Seasonality of Mixing at Tropical Instability Wave Fronts in the Atlantic Ocean

Mia Sophie Specht[1,2], Johann Jungclaus[1], Jürgen Bader[1]

[1]Max Planck Institute for Meteorology, Hamburg, Germany
[2]Max Planck Institute for Meteorology, International Max Planck Research School of Earth System Modelling, IMPRS, Hamburg, Germany

ABSTRACT Tropical Instability Waves (TIWs) have been shown to modulate upper ocean mixing. However, previous studies on the modulation of TIW related mixing are based on small numbers of TIWs and have not considered temporal variability, which can lead to discrepancies in the findings. In this study, using a 12-year simulation carried out with a comprehensive, global, high-resolution ocean model, we present for the first time, evidence that deep reaching mixing at TIW fronts in the Atlantic Ocean exhibits a pronounced seasonal cycle. We find that, regardless of whether TIWs are present earlier in the year, mixing primarily occurs in boreal summer, coinciding with a vertical shear maximum between the mean zonal currents. We argue that in the Atlantic Ocean, shear at TIW fronts does usually not suffice to trigger mixing. Instead, the background shear needs to be sufficiently large in addition to TIW shear, to overcome the stability and generate frontal mixing. The background shear in turn varies seasonally and is strongly driven by the variability of the South Equatorial Current (SEC). As such, the variability of the SEC strongly contributes to the generation and modulation of deep reaching mixing at TIW fronts. Our results highlight the importance of seasonal variability when studying TIW impacts and that such variability could be one possible reason for conflicting past findings on the effect of TIWs on mixing.

A.1 INTRODUCTION

Temperature and velocity variability in the tropical Atlantic Ocean are predominantly governed by the seasonal cycle and interannual to decadal variability (e.g. Prodhomme et al., 2019). However, there is also a significant amount of intraseasonal variability, which is largely driven by Tropical Instability Waves (TIWs). TIWs are large-scale westwards propagating waves which occur in both Pacific and Atlantic Ocean. In the Atlantic Ocean, which is the focus of this study, TIWs have typical periods of about 15 to 60 days and wavelengths of 600 to 1200 km (de Decco et al., 2018; Jochum and Murtugudde, 2006).

TIWs are closely connected to the equatorial zonal flow field, as they are generated by instabilities of the mean zonal circulation. The equatorial Atlantic flow field is characterized by opposing zonal currents. At the surface, there are the eastward flowing North Equatorial Countercurrent (NECC), centered around 5°N, and the westward flowing South Equatorial Current (SEC), with two branches centered around 2°N and 4°S. In the subsurface, there is the eastward flowing Equatorial Undercurrent (EUC) with its core located at the Equator (e.g. Brandt et al., 2010; Hummels et al., 2013; Molinari, 1982). Cyclonic shear within the SEC north of the Equator as well as increased shear between the northern SEC branch and the EUC can cause barotropic instabilities, which are one of the main generating mechanisms for TIWs (Grodsky et al., 2005; Jochum et al., 2004; Proehl, 1998; von Schuckmann et al., 2008; Weisberg and Weingartner, 1988).

At the surface, TIWs exhibit a characteristic pattern of alternating patches of cold and warm Sea Surface Temperature (SST). The fronts of the cusp-shaped TIW related cold patches are sharply defined with a strong lateral SST gradient. Such pronounced temperature fronts are important for ocean-atmosphere interactions as well as the interaction and exchange between surface ocean and deeper ocean (Ferrari, 2011), due to increased vertical velocities at the fronts. This in turn has implications for the vertical exchange of heat, carbon and nutrients (Lévy et al., 2012; Sherman et al., 2022). Moreover, TIW fronts are regions of enhanced vertical shear, which is suggested to modulate equatorial turbulence and mixing (Cherian et al., 2021; Holmes and Thomas, 2015; Lien et al., 2008). In fact, several studies find TIWs to modulate the mixed layer heat budget and SST through both increased mixing and advection (e.g. Grodsky et al., 2005; Liu et al., 2019b; Moum et al., 2009; Weisberg and Weingartner, 1988). However, the findings on the effect of TIWs on SST and heat budget are not consistent. For example Grodsky et al. (2005) report that TIWs lead to a moderate mixed layer warming in the tropical Atlantic Ocean of 0.35°C, whereas Hummels et al. (2013) argue that TIWs contribute to mixed layer cooling. Similar discrepencies in the role of TIWs are described in the

literature for the Pacific Ocean as well (e.g. Liu et al., 2019a; Maillard et al., 2022).

We suggest that one possible reason for these discrepancies is the applied methodology. While previous studies have employed both observations and simulations of different resolution and complexity, in each case, only few TIW events were examined. However, TIWs exhibit strong spatio-temporal variability, both intra-annually as well as from year to year (Caltabiano et al., 2005). Hence, several years of data are required to capture the temporal variability of TIWs. To date, there are no observations available with a sufficiently high spatial and temporal resolution to both cover the spatial extent of TIWs and capture their temporal variability, which is needed to study the TIW impact on mixing.

Therefore, in this study we aim to complete a comprehensive analysis of the temporal variability of TIW related mixing in the tropical Atlantic Ocean by examining over a decade of daily output from a simulation of the global, high-resolution, ocean general circulation model ICON-Ocean. This long simulation period allows for the analysis of about 60 TIWs. As such, we can gain novel insights into the temporal, and in particular seasonal, variability of mixing at TIW fronts. While it is not the aim of this study to offer final conclusions about the effect of TIWs on ocean heat budget and SST, we provide a possible explanation for the inconclusive findings in current literature. Although this study aims at the process understanding of TIW frontal mixing, our results also have implications for future studies which aim to further examine the importance of TIWs for the mixed layer heat budget.

A.2 DATA AND METHODS

A.2.1 *ICON-O Simulation*

This study is based on a 12-year long simulation of the ocean-only model ICON-O, which is part of the coupled general circulation model Icosahedral Nonhydrostatic Weather and Climate Model (ICON) of the Max Planck Institute for Meteorology. For the atmosphere component of ICON a nonhydrostatic approach is applied (Giorgetta et al., 2018; Zängl et al., 2015). In contrast, the ocean component of the model framework is following a hydrostatic approach. General information about ICON-O, regarding the underlying icosahedral grid, model equations and the spatial and temporal discretization can be found in Korn (2017) and Korn et al. (2022). We use an ICON-O setup comparable to the uniform grid configuration used in Korn et al. (2022) with a spatial resolution of $\sim$10 km and 128 vertical levels. The simulation has undergone a spin-up period of 25 years, during which it is forced by daily Ocean Model Intercomparison Project (OMIP) data

(Röske, 2006) and which is initialized with temperature and salinity fields from the Polar Science Center Hydrographic Climatology (PHC, Steele et al., 2001). The spin-up is followed by a simulation period from 1948 to 1978, forced by 6-hourly NCEP data (Kalnay et al., 1996). From January 1979 to December 2021, the ocean is forced by hourly ERA5 reanalysis data (Hersbach et al., 2020). Further details about the configuration, such as the applied vertical mixing parametrization are also described in Korn et al. (2022).

A unique characteristic of the configuration used here, is an online calculation of the ocean heat budget. In general, the ocean heat budget can be calculated as (e.g. Menkes et al., 2006):

$$\frac{\partial T}{\partial t} = -u\frac{\partial T}{\partial x} - v\frac{\partial T}{\partial y} - w\frac{\partial T}{\partial z} + D_l(T) + D_v(T) + I(z), \tag{A.1}$$

with $\frac{\partial T}{\partial t}$ being the temperature tendency, $-u\frac{\partial T}{\partial x} - v\frac{\partial T}{\partial y}$ the temperature change due to horizontal advection, $-w\frac{\partial T}{\partial z}$ the temperature change due to vertical advection, $D_l(T)$ the temperature change due to horizontal diffusion and mixing, $D_v(T)$ the temperature change due to vertical diffusion and mixing and $I(z)$ the heating rate due to penetrative solar heat flux. $I(z) = Q_s\frac{\partial f(z)}{\partial z}$ with Q_s being the net surface solar heat flux and $f(z)$ the fraction of solar heat flux that reaches depth z.

The discretization of advection typically leads to numerical inaccuracies. In ICON-O, a combination of a second order centred and a first order upwind scheme is applied and weighted by a flux-limiter algorithm. Such an approach ensures stability but goes along with numerical diffusion. We make no attempt to separate the numerical and physical advection but assume the physical advection to dominate. We do not apply any explicit diffusion, thus $D_l(T) = 0$. Temperature change due to vertical diffusion $D_v(T)$ is represented by implicit diffusion with a turbulent kinetic energy (TKE) diffusion scheme (Gaspar et al., 1990). The single terms of the heat budget are calculated at each model time step and saved as daily means.

Daily mean output used for the analyses was generated over a period from January 2010 to January 2021. The simulation is global; however, we select a region from 15°S to 15°N and 60°W to 20°E to study mixing connected to TIWs in the Atlantic Ocean. A particular focus lies on the area between the Equator and 2°N, where TIW fronts are most pronounced and vertical shear in the upper ocean is enhanced due to the mean zonal currents (Hummels et al., 2013). To simplify the analysis, model output is interpolated from the original icosahedral grid using nearest neighbour interpolation onto a regular lon-lat grid with $0.1° \times 0.1°$ horizontal spacing.

Between 2010 and 2021, around 60 TIWs were simulated. While our results and conclusions are based on examining all simulated TIWs, we choose to illustrate our findings regarding spatial features, based

on TIWs simulated during 2020, which we find to be a representative year. Analogous figures for the entire simulation period can be found in the appendix (Fig. A.14).

A.2.2 *Proxies for Mixing*

Turbulent vertical mixing in ICON-O is parameterized based on a prognostic equation for TKE which is implemented following Gaspar et al. (1990). Details of the implementation and deviations to the original approach can be found in Korn et al. (2022). In this scheme, TKE is produced by shear production, convective mixing in case of unstable stratification and surface wave breaking. Thereby, shear production dominates within the area discussed in this study. In the TKE scheme, larger shear leads to larger turbulence and in turn results in larger parameterized turbulent diffusivities. The shear is therefore related to the turbulent vertical diffusivity, i.e. mixing. However, apart from shear there are also other factors that determine the rate of mixing, the most important of which is the vertical buoyancy gradient, i.e. stability of the water column. Another proxy for mixing instead of the shear is thus the reduced shear squared S_{red}, which takes into account both shear and stability. In this study, we will use both the non-constant turbulent vertical diffusivity from the model and the reduced shear squared as proxies for the strength of turbulent mixing. S_{red} is calculated as $S_{red} = S^2 - 4N^2$ with the vertical shear $S^2 = (\frac{du}{dz})^2 + (\frac{dv}{dz})^2$ and N^2 being the Brunt-Väisala-Frequency $N^2 = -\frac{g}{\rho_0}\frac{d\rho}{dz}$. Here, $g = 9.81 ms^{-2}$ is the gravitational acceleration and ρ is the potential density. $S_{red} > 0$ is equivalent to Richardson Number $Ri < 0.25$, which is a common critical threshold to indicate that the flow is unstable and mixing can occur (Howard, 1961; Miles, 1961). S_{red} is calculated offline, based on daily mean output of the 2D velocity field and the simulated vertical density gradient.

A.3 RESULTS

A.3.1 *Comparison of the Simulated Flow Field to Observations*

We first want to assess how realistically the model can simulate the tropical Atlantic circulation and its variability. A schematic of the mean zonal circulation is shown in Figure A.1. In Specht et al. (2021b), which used a 16-year long ICON-O model run with the same setup as the present study, only without the online calculation of the heat budget components, it was demonstrated that the mean equatorial zonal flow field in such an ICON-O configuration is realistically simulated and that the strength and location of the EUC, NECC and SEC agree well with observational studies (e.g., Brandt et al., 2010; Hummels et al., 2013; Lumpkin and Johnson, 2013; Perez et al., 2019).

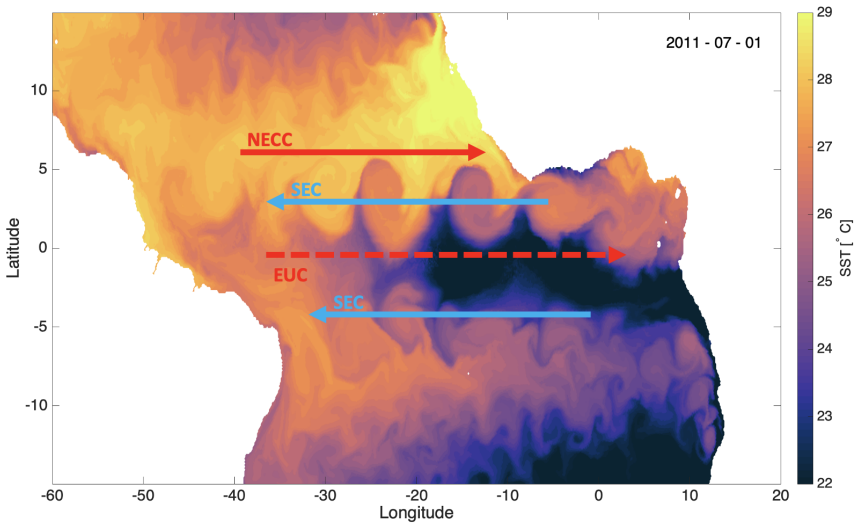

Figure A.1: Schematic of the zonal currents in the Atlantic Ocean, which are relevant for our study, overlayed on a snapshot of simulated SST on 01.07.2011. Blue arrows indicate westward currents, red arrows indicate eastward currents. SEC: South equatorial current, NECC: North equatorial countercurrent, EUC: Equatorial undercurrent. SEC and NECC are located at the surface while the EUC has its core in the subsurface. SST is given in °C.

The SEC exhibits a pronounced semi-annual cycle with its maximum strength in boreal summer and a weaker secondary maximum in boreal winter (Hummels et al., 2013; Richardson and McKee, 1984). The EUC is modulated seasonally both in regard to its depth (Arhan et al., 2006; Brandt et al., 2008; Kolodziejczyk et al., 2009) and its current strength (Johns et al., 2014). However, Specht et al. (2021b) did not validate the temporal variability of the zonal circulation or the shear between them. Thus, to further assess the quality of the background conditions and in particular the seasonal evolution, we compare the simulated zonal flow field and vertical shear to observations from shipboard sections from Hummels et al. (2013) and historical ship drift data from Richardson and McKee (1984). In Figure A.2a, a mean section of the zonal velocity along 10°W is shown for comparison to results from Hummels et al. (2013, Figure 5a therein). Here, both location and strength of the EUC (red shading) and SEC (blue shading) of the simulation agree well with the observations from the ship sections. The temporal evolution of the SEC is only sparsely covered in observations as no long term moorings are available at the location of the SEC core. Richardson and McKee (1984) were the first to document the semi-annual cycle of the SEC with a maximum in boreal summer and weaker second maximum in boreal winter, based on historical ship drift data. The original data from this study is not available. We estimate the observed monthly mean values of zonal velocity between

1 to 3°N and 25 to 30°W based on Figure 6 in Richardson and McKee (1984). While based on the monthly and daily means ICON-O generally overestimates the strength of the SEC, the semi-annual evolution of the SEC is well captured in the simulation. However, the difference in SEC strength between model and observations from Richardson and McKee (1984) is of little concern as the comparison should be assessed with caution due to the different periods of observations (1920 to 1940) and simulation (2010 to 2021) and the high margin of error in the compilation of ship drift data (Richardson and McKee, 1984). Furthermore, the observations all lay within the range of the simulated interannual variability which suggests that the seasonality of the SEC is simulated sufficiently well in ICON-O.

Lastly, we evaluate the seasonal cycle of simulated vertical shear $S^2 = (\frac{du}{dz})^2 + (\frac{dv}{dz})^2$ as this parameter is vital for mixing. Comparing a climatology of simulated S^2 along 10°W between 2°S and 2°N (Fig. A.2c) to a climatology resulting from 13 cruise sections as shown in Hummels et al. (2013, Figure 7 therein) shows that ICON-O is able to realistically reproduce the seasonality of vertical shear between the zonal currents. In particular the two maxima close to the surface in boreal spring and winter are well captured. Hence, we conclude that the background conditions of the Atlantic equatorial flow field and their temporal variability are simulated sufficiently well to study the role of the equatorial flow field in modulating TIW related mixing.

A.3.2 *Mixing at TIW Fronts in ICON-O*

Previous studies by Cherian et al. (2021), Holmes and Thomas (2015) and Lien et al. (2008) find that equatorial turbulence in the Pacific Ocean is modulated by TIWs, in particular at the fronts of the wave. The effect of modulated turbulence can reach below the mixed layer depth (MLD). In the following, we show that such TIW induced mixing with deep reaching effect can be reproduced in ICON-O in the Atlantic Ocean as well. While this is true for many of the simulated TIWs, here we show such mixing in a representative example of only one simulated TIW on the 01.08.2020 (Fig. A.3).

Simulated SST captures the TIW characteristic cold cusps well and is shown in Figure A.3 for TIWs on 01.08.2020. To distinguish between the lead edge front (LEF) and the trail edge front (TEF) of the wave, the zonal SST gradient is shown in Figure A.3b. The LEF is characterized by a negative zonal SST gradient while the TEF is characterized by a positive SST gradient. The terminology of the different TIW fronts is not coherent in literature. Some studies (e.g. Holmes and Thomas, 2015) refer to the leading edge of the TIW warm anomaly as the LEF, while others define this as the TEF (Warner et al., 2018). For clarification of the location of TEF and LEF and the TIW specific cold

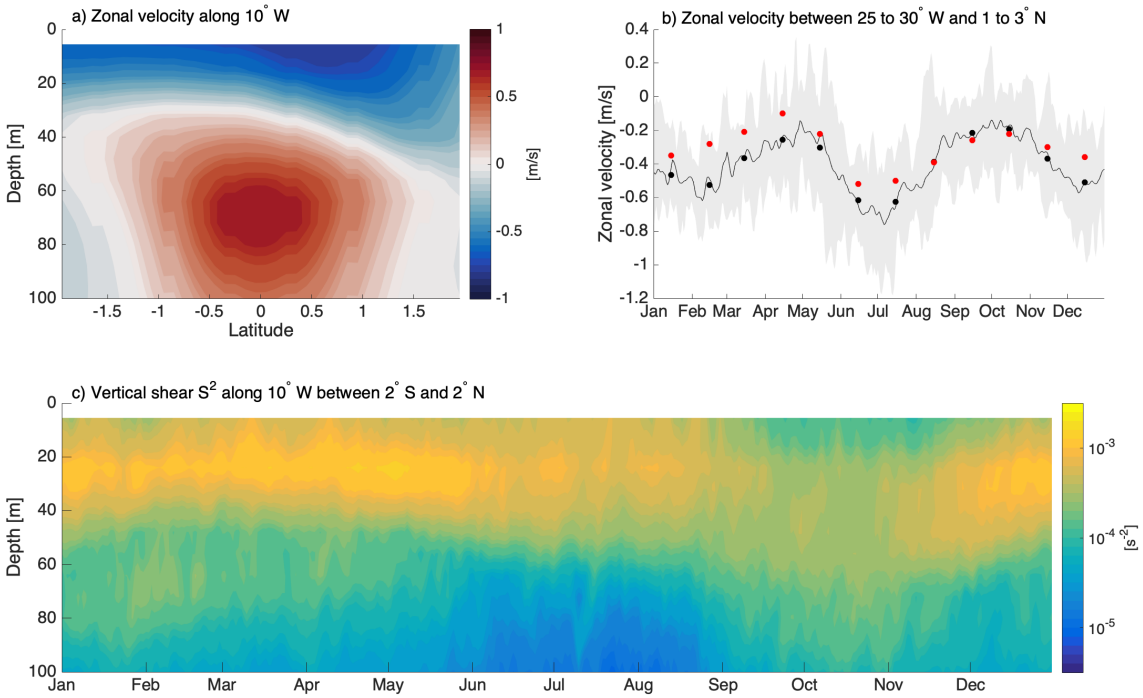

Figure A.2: Background flow conditions in ICON-O. (a) Section of zonal velocities along 10°W as long term June mean. (b) Climatology of the SEC as zonal velocity average between 1 to 3°N and 25 to 30°W. Black solid line indicates the climatology based on simulated daily means. Black dots are the climatology based on simulated monthly means and red dots are monthly means from observations estimated from Richardson and McKee (1984). Grey shading illustrates the range of the climatology simulated in ICON-O. (c) Seasonal evolution of simulated vertical shear S^2 along 10°W, averaged between 2°S and 2°N.

and warm anomalies as used in this study, a schematic can be found in Figure A.4. Figure A.3c shows the simulated vertical shear squared S^2 at the surface and Figure A.3d shows reduced shear squared S_{red}, a proxy for mixing. Positive values of S_{red} refer to a Richardson Number below the critical value of 0.25 and therefore indicate mixing.

Vertical shear S^2 (Fig. A.3c) along the TEF is large enough to overcome the fourfold stability $4N^2$, leading to positive values of S_{red} (Fig. A.3d) and hence mixing can occur at the TEF. In contrast, at the LEF S^2 is close to zero and cannot overcome the stability which prevents mixing at the LEF. These results are in agreement with Lien et al. (2008) and Holmes and Thomas (2015); however, both studies find positive values of S_{red} mainly at the trough of a TIW, i.e. the part of the wave close to the Equator at the equatorward end of the positive SST anomaly (see Holmes and Thomas (2015, Figure 2c therein), and Lien et al. (2008, Figure 4 therein) and Figure A.4 for the location of the trough), while our results indicate mixing along the entire TEF, extending as far as 5°N.

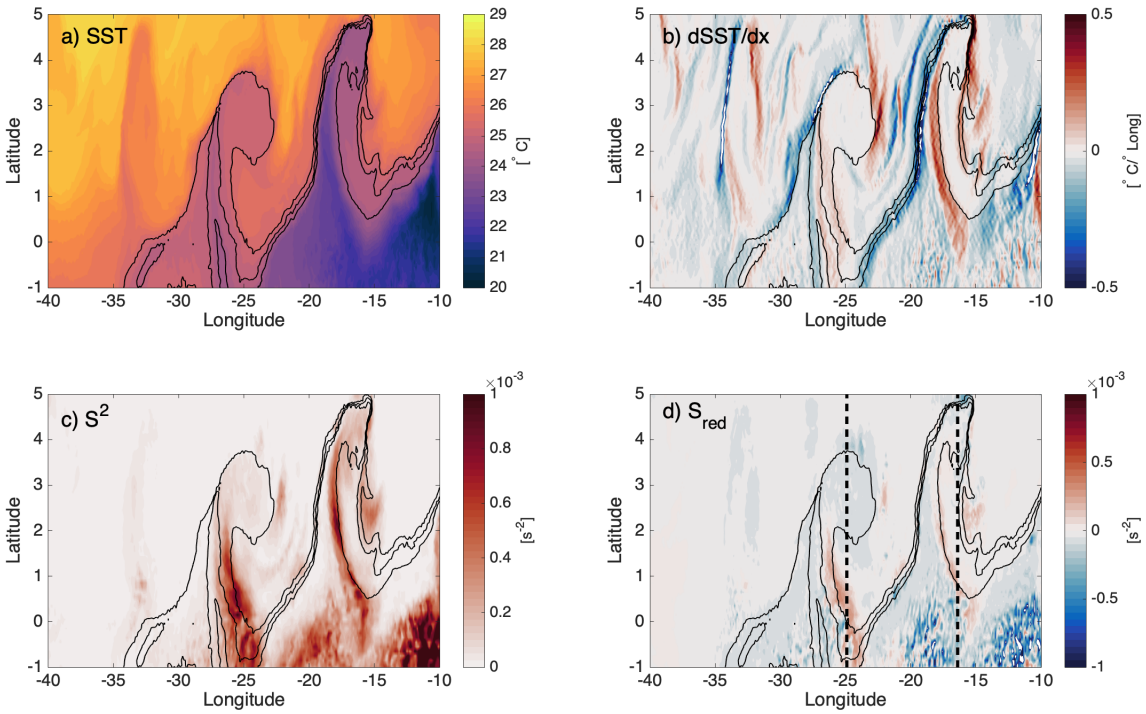

Figure A.3: Snapshot of a simulated TIW on 01.08.2020 showing (a) SST in °C, (b) the zonal SST gradient in °C/Longitude, (c) the vertical shear squared S^2 in s^{-2} between the uppermost model layers and (d) the reduced shear squared S_{red} in s^{-2}. Black contours in all panels are the 24.5 to 25.5°C SST isotherms with an increment of 0.5°C. Dashed lines panel d) indicate the location of the TEF of the displayed TIWs.

However, mixing not only occurs at the surface but reaches down below the mixed layer to the depth of the thermocline as seen in Figure A.5 for the two TEFs highlighted by the black dashed lines in Figure A.3d. The top black line in Figure A.5 shows the MLD, defined as the depth at which the density difference to the surface is 0.125 sigma units (Korn et al., 2022). The bottom black line shows the thermocline depth, defined as the 20°C isotherm. Here, the simulated vertical momentum diffusion is shown as a proxy for mixing. Along both sections, mixing occurs right below the MLD at the location of the fronts and extends to the thermocline depth. The deep reaching mixing is closely confined to the front, highlighting the need for data with high spatial resolution to ensure that the sharp frontal features and related mixing are properly resolved.

The deep reaching mixing at the TEFs leads to a local warming between MLD and thermocline (Fig.A.6b). However, the effect on the total heat budget below the mixed layer (Fig.A.6a) is negligible as the impact of advection (Fig.A.6c) substantially exceeds the mixing induced warming by one order of magnitude. Only in small areas along the TEF where mixing is strong, is temperature tendency due

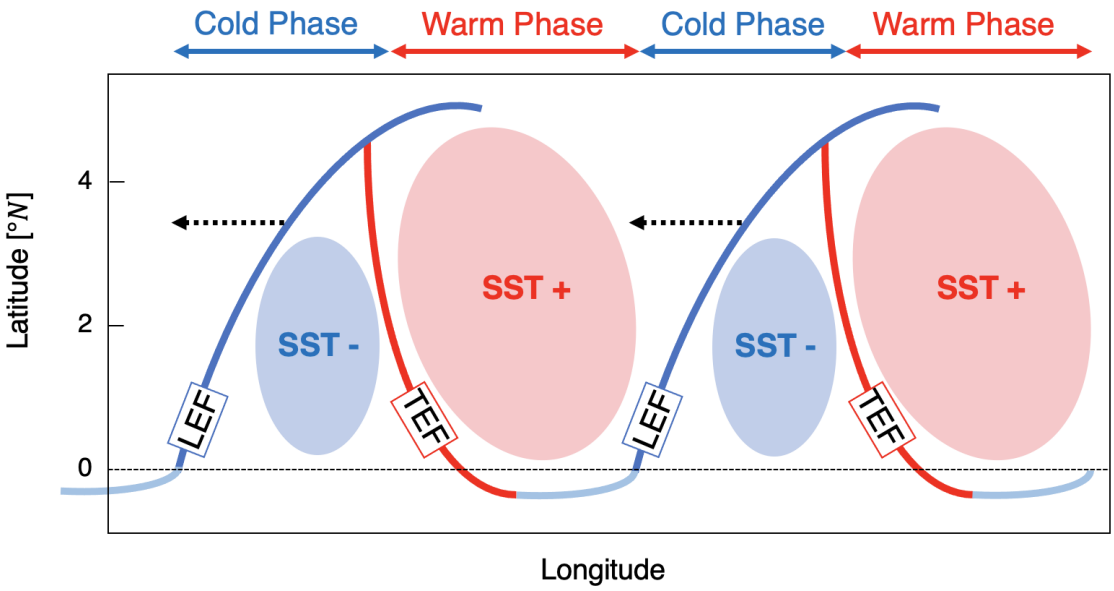

Figure A.4: Schematic of a typical TIW. LEF: Lead edge front, located at the front of the wave, characterized by a negative zonal temperature gradient. TEF: Trail edge front, located at the back of the wave, characterized by a positive zonal temperature gradient. Shaded circles show the temperature signature of the respective part of the wave. The black dotted arrow indicates the propagation direction of the wave.

to mixing of comparable magnitude to the temperature tendency due to advection between MLD and thermocline depth (Fig.A.6d). Hence, despite mixing playing only a minor role in modulating the heat budget below the MLD overall, confined to the TEF, mixing can balance the advection term and thereby contribute to the heat budget between MLD and thermocline.

A.3.3 *Seasonality of Mixing at TIW Fronts*

The deep reaching mixing at TIW fronts described in the previous section occurs at many but not all simulated TIW fronts. Independent of when TIWs are present throughout the year, the mixing predominantly takes place in boreal summer. Holmes and Thomas (2015) argue that mixing at the TEF is driven by an interaction between the EUC and TIWs. They suggest that strain in the horizontal velocity field of TIWs is acting on the already existing shear of the EUC. This causes horizontal vortex stretching which in turn leads to increased zonal EUC shear and causes the frontal mixing (Holmes and Thomas, 2015). From this reasoning it would follow that mixing can occur at the TEF of all TIWs. However, we find that the occurrence of mixing at TEFs of TIWs is determined by a pronounced seasonal cycle.

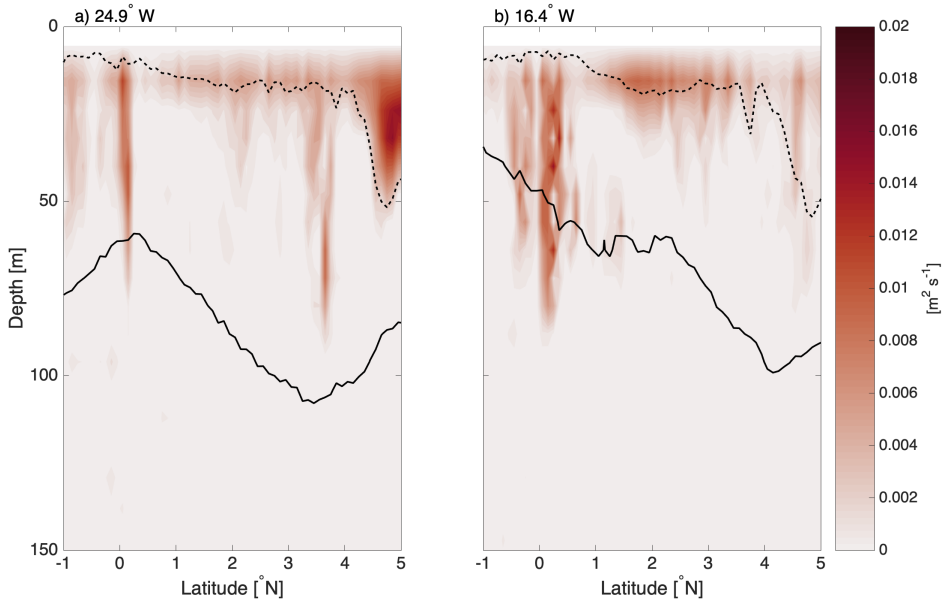

Figure A.5: Snapshot of simulated vertical momentum diffusion along TIW TEFs on 01.08.2020. The locations of the sections are indicated by the dashed lines in Figure A.3d). Solid black lines indicate the thermocline depth, represented by the 20°C isotherm and dashed black lines indicate the mixed layer depth.

A 2D gaussian bandpass filter is applied to SST in space and time to visualize TIW related SST anomalies (Fig. A.7). The filter has a temporal filtering bandwidth of 15 to 60 days and a spatial filtering bandwidth of 4 to 20° longitude (∼ 400 to 2000 km), allowing TIWs to pass. The filtering windows are chosen according to TIW periods and wavelengths defined in a previous study by de Decco et al. (2018). SSTs filtered accordingly can be assumed to represent the TIW related surface pattern. Figure A.7 displays results of the ICON-O simulation for 2020. These results are representative for all simulated years. We chose to show the year 2020 only to better visualize our results. An extension of Figure A.7 for the full 12 years of simulation can be found in the appendix (Fig. A.14).

Despite TIWs being present for most parts of the year in 2020 (Fig. A.7a) with intensity increasing in May, vertical shear S^2 in 64m (Fig. A.7b), indicating potential for subsurface mixing, is enhanced only for a short period from late June until late August. S^2 exhibits a clear TIW related pattern with strong vertical shear along the TEFs. Simulated vertical momentum diffusion is also increased along the fronts while being negligible before June (Fig. A.7c), confirming the suggested subsurface mixing. The depth levels of 64 and 60 m are chosen to ensure a location below the MLD (average depth of ∼20 m in the study area) but above the thermocline depth (average depth of

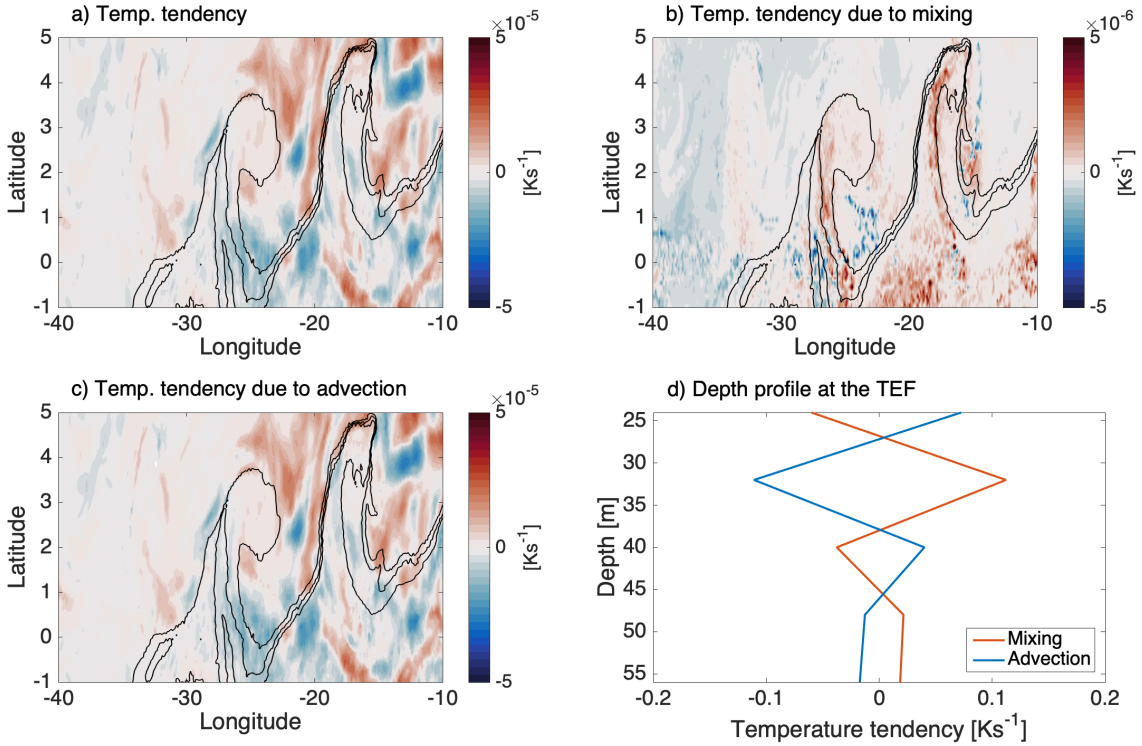

Figure A.6: Snapshot of simulated heat budget terms on 01.08.2020 integrated between 24 and 56 m showing (a) temperature tendency, (b) temperature tendency due to mixing, (c) temperature tendency due to advection. Positive values indicate a warming, negative values a cooling. In (d) depth profiles of the temperature tendency due to mixing (red) and temperature tendency due to advection (blue) between 24 and 56 meters at a single point at the TEF are shown. All temperature tendency terms are given in Ks^{-1}. Note that the color scale in (b) is one order of magnitude less than in (a) and (c).

$\sim$80 m in the study area) to capture frontal mixing that is not limited to the surface but extends below the MLD as described in the previous section. Shear is calculated in the center of the grid cell, while vertical diffusion is calculated on the cell interfaces. Therefore, the two chosen depth levels differ.

Analysing reduced shear S_{red} at the surface in combination with the zonal SST gradient for the period when frontal mixing occurs (Fig. A.8) clearly shows that mixing, i.e. positive values of S_{red}, is organised along the TEF of TIWs. To highlight those results, the start of deep reaching mixing for each wave is highlighted by the thick, solid black lines in Figure A.8a. The same lines are overlaid on the zonal SST gradient in Figure A.8b, where positive values denote the TEF of a TIW and negative values denote the LEF.

Based on the results shown so far, in particular Figure A.7, we argue that the frontal mixing is a seasonal feature and that, while clearly

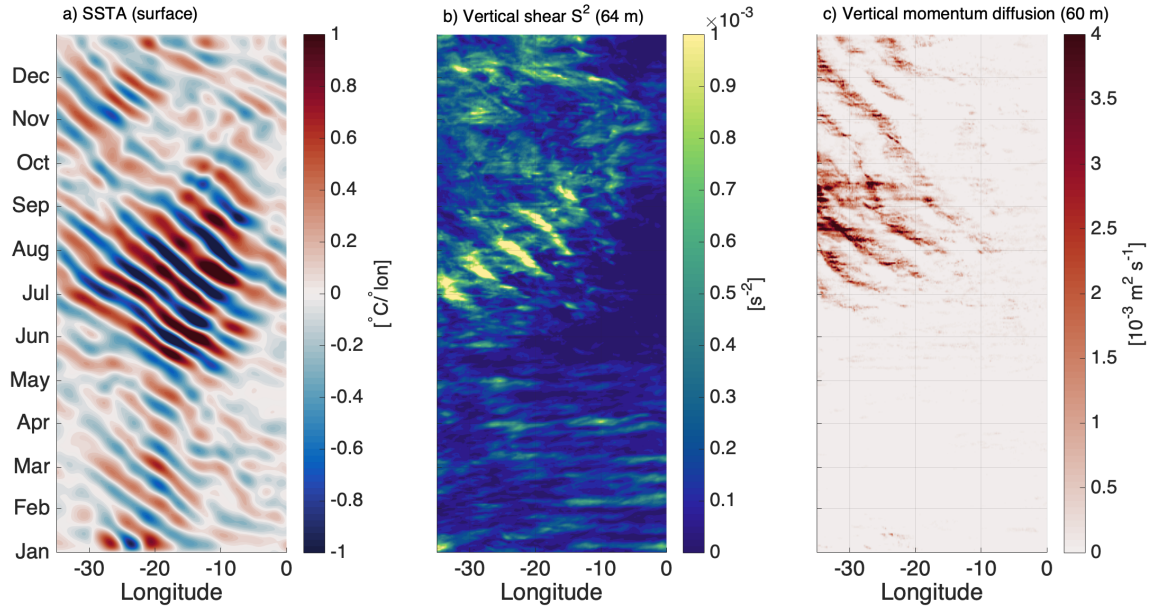

Figure A.7: Hovmoeller diagram of simulated (a) SST anomaly in °C, (b) S^2 in s^{-2} and (c) vertical momentum diffusion in 2020 in $m^2 s^{-1}$. S^2 is shown for 64 m depth, vertical momentum diffusion is shown for 60 m depth.

being closely related to TIWs, the presence of TIWs is not sufficient to initiate mixing at fronts.The results from 2020 are consistent with the rest of the simulated time period: throughout the 12 years of our simulation, deep reaching mixing at TEFs of TIWs consistently starts between June and July and lasts for about 3 month, stopping no later than September. In some years, a second period of weaker and shorter lasting frontal mixing occurs in November and December. From these findings it follows that another process with strong seasonality must be involved, which in connection with the presence of TIWs leads to mixing. Such seasonality of mixing at TIW fronts has not been reported before. It should be noted that TIWs are present in boreal summer for the entire simulation. Hence, we cannot determine if deep reaching mixing between June and September could also occur despite the absence of TIWs and where it would occur in that case. However, the strong resemblance of the spatial pattern of deep reaching mixing between June and September and the TIW pattern itself, suggests the necessity of TIW presence for mixing to occur.

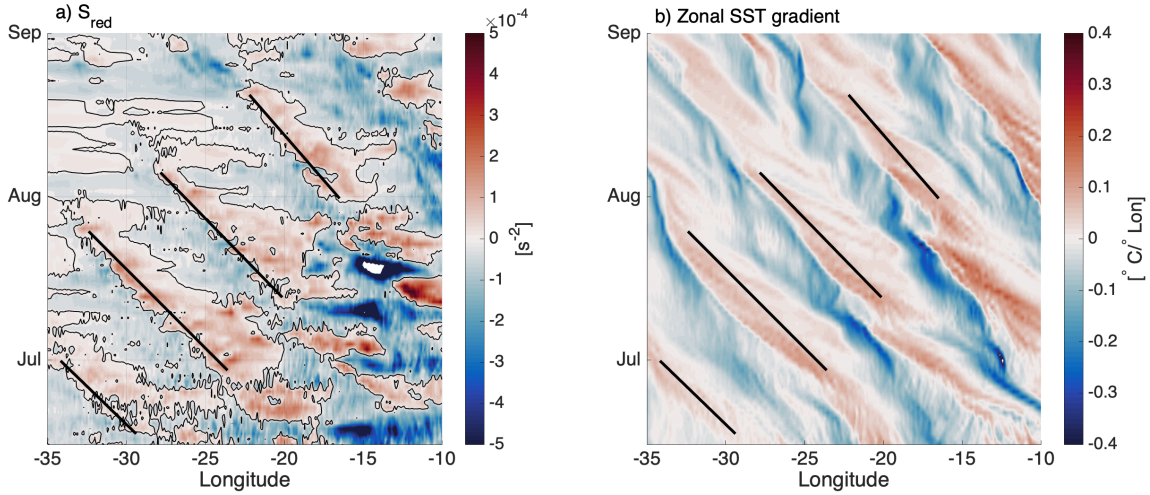

Figure A.8: Hovmoeller diagram of (a) simulated S_{red} and (b) zonal SST gradient from June to September 2020.

A.3.4 *Role of the Equatorial Zonal Flow Field in Modulating the Seasonality of Mixing at TIW Fronts*

A.3.4.1 *Seasonality of vertical shear S^2 between EUC and SEC*

Due to the seasonal characteristics of SEC and EUC and their relevance for shear and TIW generation, we suspect a connection to the seasonality of mixing at TIW fronts. Because mixing at TIW fronts is largely related to strong vertical shear S^2, we investigate the seasonality of shear between EUC and SEC in ICON-O. Vertical current shear in boreal summer is strongest on average at ∼0.65°N and 32 m depth (Fig.A.9). The corresponding vertical shear time series is shown in Figure A.10. Grey dots show daily values of S^2 at 0.65°N and 32 m depth, averaged between 15 and 30°W, where both SEC and TIWs are most pronounced. The black solid line shows the 30-day running mean of S^2 and blue shaded bars indicate the periods when deep reaching mixing at TIW fronts occurs each year.

We find that mixing at TIW fronts begins when the vertical shear between SEC and EUC is strongest and mixing subsides when S^2 is weakest. The shear maximum coincides with the seasonal maximum of the SEC in June/July (Fig. A.2b) while the EUC undergoes a decrease in current strength and deepens at the same time. The secondary shear maximum can occur in December/January when the SEC has its second maximum, highlighting the importance of the SEC in modulating vertical shear between the two currents, compared to the EUC, which does not exhibit semi-annual variability in the area between 15 and 30°W (Johns et al., 2014).

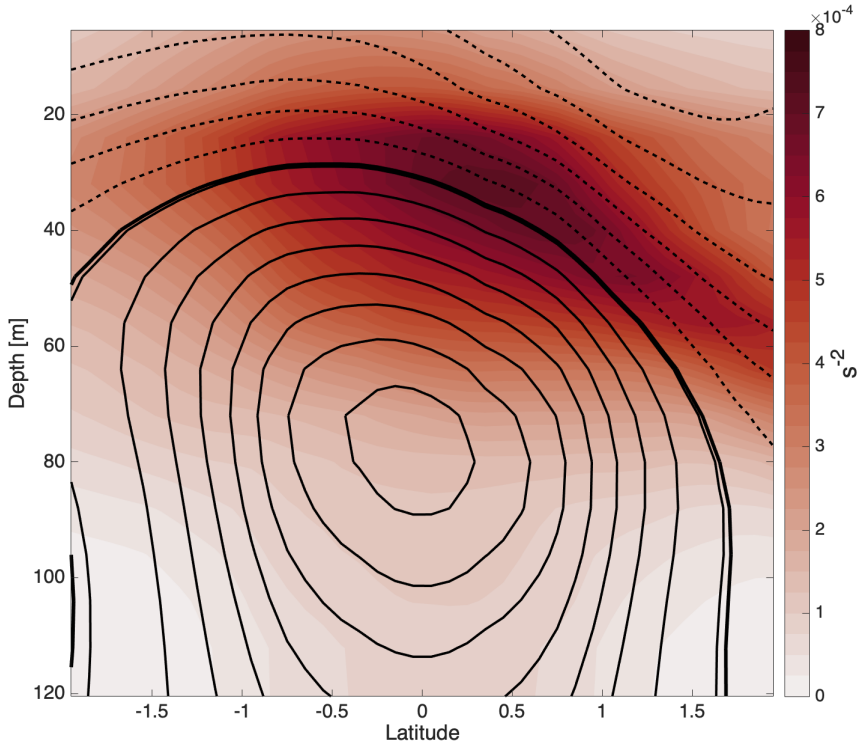

Figure A.9: Simulated mean zonal flow field (contours) in m/s and S^2 (shading) in s^{-2} in July, averaged over 15 to 30°W. Solid contour lines indicate eastward velocities, dashed contour lines indicate westward velocities. The thick contour line represents $0m/s$. The contour interval is $0.1m/s$.

A.3.4.2 *Relative importance of EUC versus SEC for S^2 variability*

While both the EUC and the SEC contribute to the vertical shear between them, we suggest that the strength of the SEC is of greater importance for the shear variability and that therefore the SEC plays the bigger role in modulating TIW frontal mixing. There are two main reasons for this conclusion.

Firstly, SEC and S^2 time series are more strongly correlated than EUC and S^2. However, the differences are too small to be a sole argument for the larger importance of the SEC strength (r = 0.9 vs. r = 0.8).

Secondly, while the EUC exhibits its strongest mode of variability in the seasonal cycle, the SEC follows a semi-annual cycle with its maximum in June/July and a second, weaker maximum in December (Fig. A.2b). This same semi-annual characteristic is also present in the S^2 time series (Fig. A.10). Both SEC and S^2 have their most dominant peak in the power spectral density around 180 days. Furthermore, while in all 12 years of simulation frontal mixing at TIW occurs starting in June/July, in some years when TIWs are also present in boreal winter, despite being weaker compared to summer, mixing

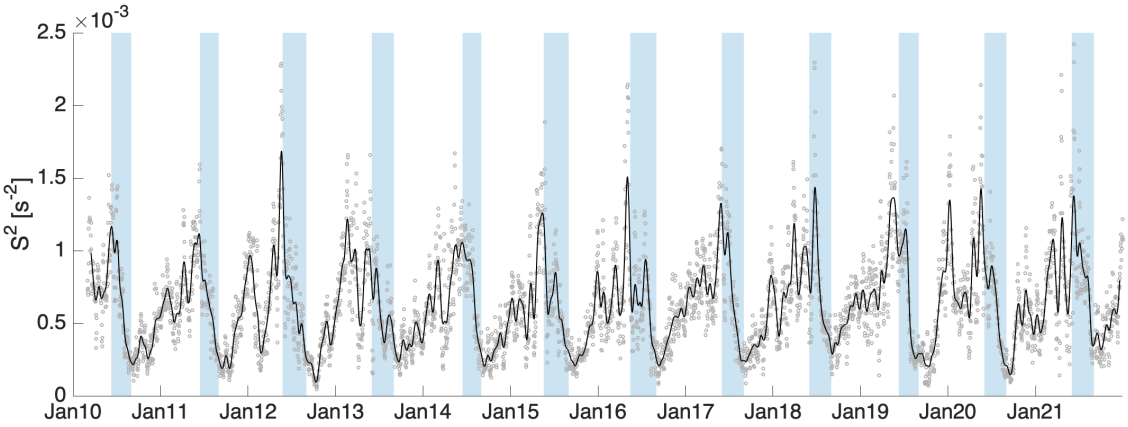

Figure A.10: Time series of simulated S^2 at 0.65°N, 32 m depth, averaged between 15 and 30°W. Grey circles show daily means of S^2, black line shows a 30 day running mean. Values are given in s^{-2}. Shaded blue bars indicate the periods when deep reaching mixing occurs.

along the TIW TEF also occurs at the end of the year, coinciding with the secondary peak in both SEC strength and shear between SEC and EUC. These results corroborate findings by Jouanno et al. (2011) who also highlight that the intensification of the SEC is the main driver of vertical shear of the mean zonal flow field.

The close connection between deep reaching mixing at TIW fronts and the variability of the SEC becomes further apparent when analysing bandpass filtered vertical shear. Figure A.11 displays Hovmoeller diagrams of unfiltered S^2 in 64 m depth (a) as well as bandpassed filtered S^2 in the bandwidth of TIWs (b, shading) and the SEC (b, contour lines) in 2020. To highlight the contribution of TIWs in S^2 variability, a filtering bandwidth of 15 to 60 days is chosen while for the SEC we apply a filtering bandwidth of 150 to 210 days. TIWs and the SEC are the most dominant mode of variability in the respectively chosen filtering window. Hence, applying such bandpass filters allows for a good estimation of the TIW and SEC contribution to shear variability.

The similarity of the pattern of unfiltered (Fig. A.11a) and TIW filtered S^2 (Fig. A.11b) shows that mixing in boreal summer is closely connected to the occurrence of TIWs and is not simply caused by the shear of the mean zonal circulation. Further, subsurface shear maxima coincide with positive TIW filtered shear, which represents the TEF of the wave, hence supporting our results in A.3.2. SEC filtered S^2 is overall about half as strong as TIW filtered S^2. During the entire mixing period, SEC filtered shear is in its positive phase (Fig. A.11b), representing the seasonal SEC maximum. This highlights that while

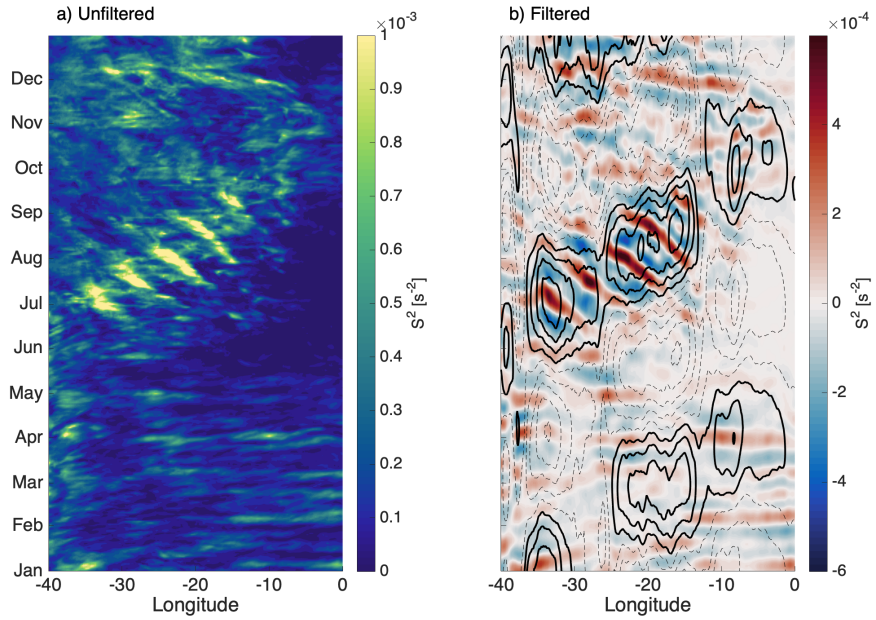

Figure A.11: Hovmoeller diagram of (a) unfiltered and (b) filtered simulated S^2 at 64 m depth in 2020. Panel (b) shows TIW filtered S^2 (bandpass filtered with a filtering window of 15 to 60 days) as shading and SEC filtered S^2 (bandpass filtered with a filtering window of 150 to 210 days) as contour lines. Thick solid lines are positive values, dashed lines are negative values. Contour lines have an interval of $0.2 \times 10^{-4} s^{-2}$. All values are given in in s^{-2}.

TIWs already have a strong contribution to subsurface S^2, an increase in SEC strength is also needed in order for mixing to take place.

A.3.5 *Dynamics of Mixing at TIW Fronts*

Following from the clear link between the S^2 maximum, onset of mixing at TIW fronts, and the seasonal SEC maximum, we argue that while TIWs alone are also leading to elevated shear, this shear is not large enough to trigger deep reaching mixing at the waves' fronts. Instead, additional shear is needed to raise the preexisting TIW shear levels above a certain threshold, e.g. from variability in the background currents.

To further investigate the role of shear from the background currents on frontal mixing, we analyse the relative importance of vertical shear of meridional velocity $\frac{dv}{dz}$ and vertical shear of zonal velocity $\frac{du}{dz}$, separately. The background flow is predominantely zonal, while TIWs also have a pronounced meridional compononent. Hence, separating shear into a zonal and a meridional component allows for assessing the impact of the background currents on shear. Following the approach used by Cherian et al. (2021), we split S_{red} into two parts S_{red_u} and S_{red_v}

to assess where and when $\frac{dv}{dz}$ and $\frac{du}{dz}$ are individually larger than $2N^2$ and cause mixing. For mixing to occur $S_{red} = S^2 - 4N^2 > 0$ which is equivalent to

$$S_{red} = \underbrace{\left(\left(\frac{du}{dz}\right)^2 - 2N^2\right)}_{S_{red_u}} + \underbrace{\left(\left(\frac{dv}{dz}\right)^2 - 2N^2\right)}_{S_{red_v}} > 0. \tag{A.2}$$

While not allowing for a precise distinction of the individual contributions of $\frac{du}{dz}$ and $\frac{dv}{dz}$ to S_{red}, separating S_{red} into S_{red_u} and S_{red_v} offers a valuable approximation. The two terms should only be examined together with the total S_{red}.

In Figure A.12 we show S_{red} and its individual components for one of the TIWs on 01.08.2020 which we previously described in Figure A.3 as an example of the mixing dynamics in boreal summer. In comparison, Figure A.13 displays S_{red} and its individual components for a TIW in mid September 2020, when vertical shear between EUC and SEC is at its minimum (compare Figure A.10).

In boreal summer, both N^2 and S^2 are high at the TEF (Fig. A.12b and d) with S^2 being enhanced strongly enough to overcome the fourfold stability and induce mixing, which suggests that the local increase in shear is more important in driving mixing than the stability. In fact, the high level of stability at the front would suggest that no mixing occurs. Hence, the stability is acting against mixing while shear has the opposing effect. Decomposing S_{red} into its zonal and meridional components corroborates the results by Cherian et al. (2021) who find that between 1°S and 2°N in the Pacific Ocean, mixing is driven by zonal shear while north of 2°N mixing is primarily driven by meridional shear (Fig. A.12e and f). The latitude where $\frac{du}{dz}$ contributes most strongly to S_{red} (Fig. A.12e, $\sim$ 1°N) coincides with the latitude of maximum shear of the background currents. In agreement with Holmes and Thomas (2015) we find meridional diffluence, i.e. positive values of $\frac{dv}{dy}$ in the cold cusp of the TIW (not shown). The meridional diffluence is strongest close to the TEF. Holmes and Thomas (2015) suggest that the resulting horizontal vortex stretching enhances the pre-existing zonal shear $\frac{du}{dz}$ of the EUC. However, we argue that in the Atlantic Ocean the zonal shear does not primarily stem from the EUC. Instead, the shear is generated between EUC and SEC with shear strength being modulated mostly by the intensity of the wind driven SEC.

While our findings based on the ICON-O simulation are in agreement with the results from Holmes and Thomas (2015) and Cherian et al. (2021) during boreal summer when frontal mixing also occurs,

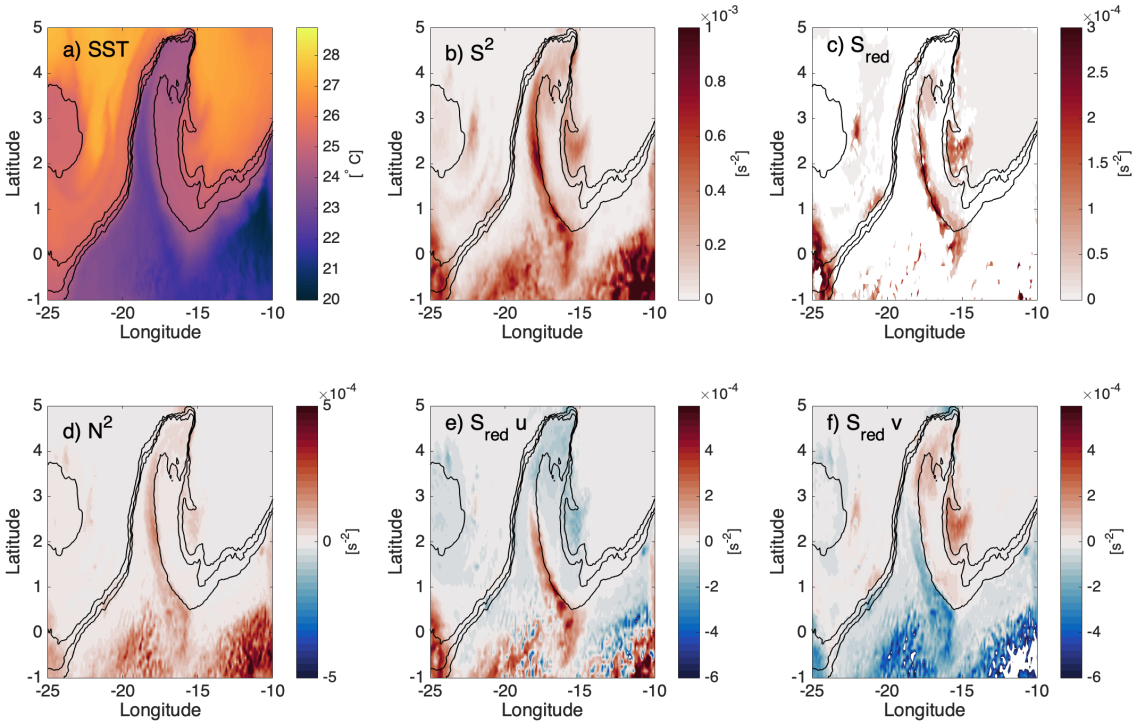

Figure A.12: Snapshot of a simulated TIW on 01.08.2020 showing (a) SST in °C, (b) S^2,(c) S_{red} and its individual components (e) S_{red_u} and (f) S_{red_u} and (d) N^2. Shear and stability values in (b) to (f) are given in s^{-2}.

we depict a different picture outside the summer months. When shear between the SEC and EUC is low in boreal spring and autumn, shear along the TEF is high, comparable to TIW frontal shear in summer (Fig. A.13b). Frontal mixing occurs close to the Equator (Fig. A.13c). However, unlike in summer, mixing is restricted to the mixed layer. Further, mixing is entirely driven by vertical shear of the meridional velocity which can be related to the meridional motion of the TIWs (S_{red_v}, Fig. A.13f), while $\frac{du}{dz}$ does not contribute to mixing. $S_{red_u} < 0$ within the entire TIW (Fig. A.13e). This confirms our previous suggestion that in the equatorial Atlantic Ocean pre-existing shear of the mean zonal flow field $\frac{du}{dz}$ must be sufficiently large for TIWs to be able to modulate turbulence, which here is the case mainly in boreal summer. Thus, TIW frontal mixing is a mainly seasonal feature, strongly modulated by the SEC strength and the resulting shear between SEC and EUC. However, we would like to emphasize that these findings are based on examining TIWs solely in the tropical Atlantic Ocean and that our conclusions may not apply to the Pacific, where TIWs are generally more energetic and occur most of the year.

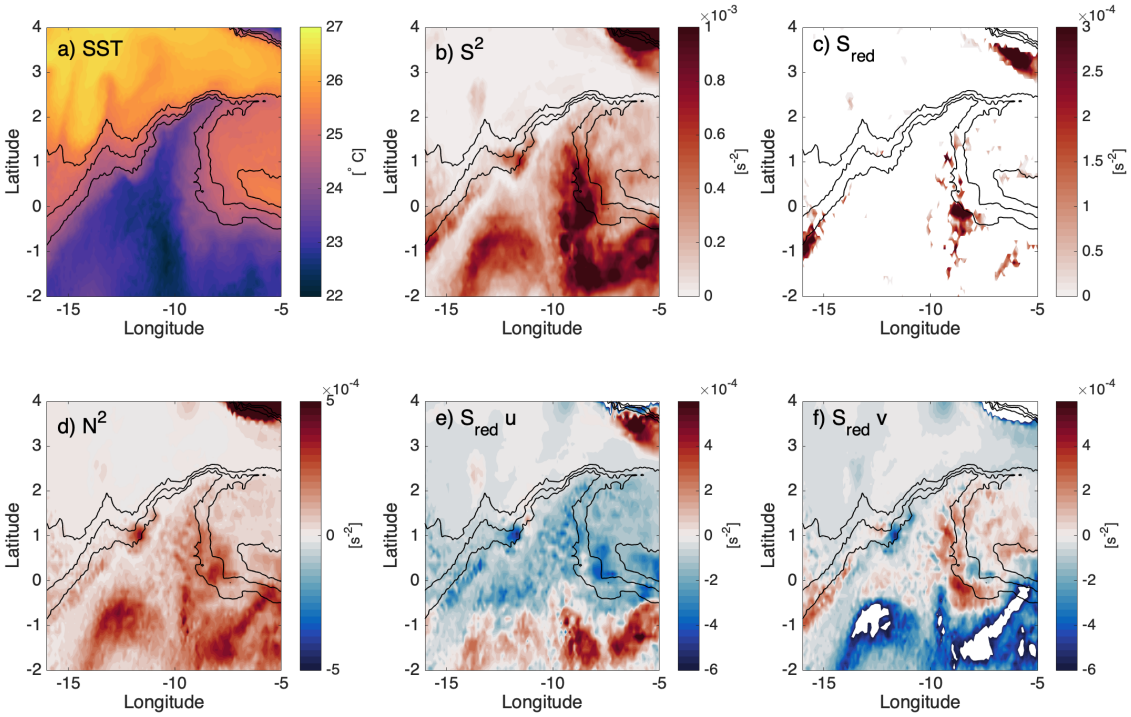

Figure A.13: Same as Figure A.12 but for 13.09.2020. (a) SST in °C, (b) S^2,(c) S_{red} and its individual components (e) S_{red_u} and (f) S_{red_u} and (d) N^2. Shear and stability values in (b) to (f) are given in s^{-2}.

A.4 SUMMARY AND DISCUSSION

We have demonstrated for the first time, using 12 years of a high-resolution ICON-O simulation, that deep reaching mixing at the trail edge front (TEF) of Tropical Instability Waves (TIWs) in the Atlantic Ocean exhibits strong seasonality. Previous studies have investigated the modulation of equatorial turbulence by TIWs (e.g. Cherian et al., 2021; Holmes and Thomas, 2015; Lien et al., 2008), however, these studies did not consider the temporal variability, which may result in an incomplete explanation of the dynamics involved in TIW frontal mixing. TIW frontal mixing in the Atlantic Ocean predominantly starts in June/July and lasts for ∼3 months, ending no later than September. Mixing only occurs at the TEF of the wave. While this is in agreement with previous studies, further research is needed to explain why mixing is restricted to the TEF.

The seasonal mixing coincides with the maximum of vertical shear between the opposing mean zonal currents South Equatorial Current (SEC) and Equatorial Undercurrent (EUC). We argue that in the Atlantic Ocean, vertical shear from TIWs alone is not sufficiently large to generate deep reaching mixing. Therefore, mixing does not occur

at all TIW fronts. Instead, additional shear is needed that elevates the TIW shear enough to overcome the stability and trigger mixing. This additional shear is provided by the seasonally modulated shear between SEC and EUC, which in turn is predominantly driven by the variability of the SEC. Hence, we conclude that seasonal mixing at TIW fronts is the result of a superposition of TIW and background current shear and that the variability of the SEC has a leading role in the generation and modulation of deep reaching mixing at TIW fronts.

The results shown in this study are all based on model simulations. To validate our simulation results with observations, further measurements are needed. Previous observational studies of TIWs are limited to single spot measurements from moorings, mostly along the Equator, and sparse cruise data. While observations from cruises offer the possibility to measure sections along and across TIW fronts, a large number of such sections would be needed at comparable locations and during different seasons to not only deliver observational evidence for deep reaching mixing at TIW fronts but also its seasonality. Alternatively, despite being limited in their spatial resolution, an array of moorings between the Equator and 4°N would offer the possibility to observe seasonality of TIW mixing. However, at the present time, long term moorings in the tropical Atlantic Ocean are limited to the Equator and 4°N without any moorings in between (Bourlès et al., 2019), hence not including the area around 2°N where TIW fronts are strongest. Therefore so far, investigating mixing at TIW fronts and the related temporal variability relies on using model simulations, which have a resolution high enough to resolve the sharp fronts of TIWs, such as the simulation used in this study. However, a previous comparison of the present model configuration with various observations in regard to the mean zonal flow field and the simulation of TIWs in general (Specht et al., 2021b) as well as the agreement of our findings with studies on TIW mixing in the Pacific Ocean, gives us confidence in the significance of our results despite the lack of observational evidence.

Our finding that deep reaching mixing at TIW fronts is a seasonal feature, highlights the importance of taking into account the temporal, in particular seasonal, variability of TIWs and the background state when studying the TIW impact on mixing. However, while previous studies mainly focused on understanding the processes by which TIWs impact mixed layer and SST, the possibility that this TIW impact may be substantially affected by seasonal variability of the background conditions was not considered. We suggest that to fully understand the influence of TIWs on mixing, a sufficiently large number of wave events during different seasons needs to be analysed and that some of the previous disagreements about the effects of TIWs may stem from neglecting temporal variability. Further, as pointed out by Holmes and

Thomas (2015), TIW related mixing is sensitive to the choice of the mixing scheme. Therefore, in addition to a validation of our findings with observations, a sensitivity study using model configurations with different mixing schemes could lead to further insights into the seasonality of mixing at TIW fronts.

ACKNOWLEDGEMENTS ICON-O primary data and scripts used in the analysis and other supplementary information that may be useful in reproducing the author's work will be archived by the Max Planck Institute for Meteorology in the MPG.PuRe repository and can then be obtained. Model output used for the analysis will be archived in the DRKZ long term archive LTA DOKU. We would like to acknowledge Helmuth Haak for his help and technical support in running and providing the ICON-O simulation used in this study and Nils Brüggemann for his efforts to incorporate the heat budget diagnostic into ICON-O. We further thank Swantje Bastin for her feedback and comments which helped improving the original manuscript.

A.5 APPENDIX

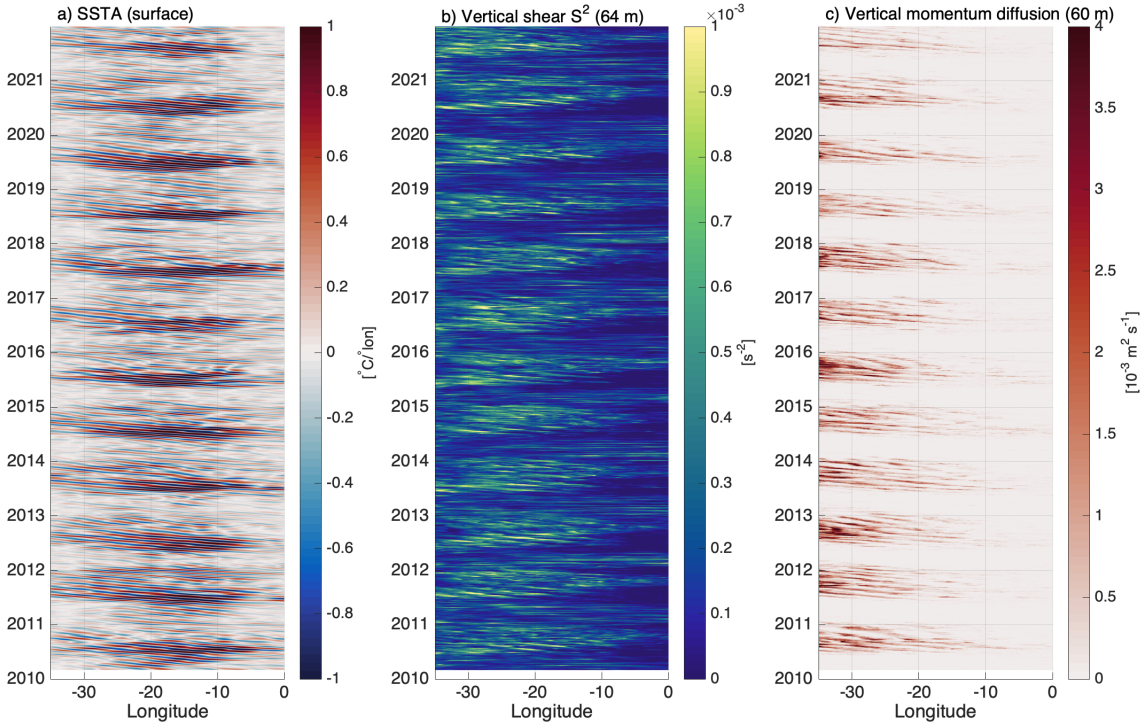

Figure A.14: Hovmoeller diagram of (a) simulated SST anomaly in °C, (b) S^2 in s^{-2} and (c) vertical momentum diffusion for the entire simulation period. S^2 is shown for 64 m depth, vertical momentum diffusion is shown for 60 m depth.

B

IDENTIFYING AND CHARACTERIZING SUBSURFACE TROPICAL INSTABILITY WAVES IN THE ATLANTIC OCEAN

The attached article has been published in *Journal of Geophysical Research: Oceans*.

Specht, Mia Sophie, Johann Jungclaus, and Jürgen Bader. "Identifying and characterizing subsurface tropical instability waves in the Atlantic Ocean in simulations and observations." *Journal of Geophysical Research: Oceans* 126.10 (2021): e2020JC017013.

AUTHOR CONTRIBUTIONS: M.S.S. designed the research question, performed the analysis, created the figures and drafted the manuscript. Throughout the process, J.J. and J.B. provided scientific guidance and feedback. All authors contributed to editing and revising the manuscript.

Identifying and Characterizing Subsurface Tropical Instability Waves in the Atlantic Ocean in Simulations and Observations

Mia Sophie Specht[1,2], Johann Jungclaus[1], Jürgen Bader[1]

[1]Max Planck Institute for Meteorology, Hamburg, Germany
[2]Max Planck Institute for Meteorology, International Max Planck Research School of Earth System Modelling, IMPRS, Hamburg, Germany

Received: 24. November 2020, Accepted: 1. September 2021

ABSTRACT Recent observations in the Pacific Ocean suggest that, apart from Tropical Instability Waves (TIWs) at the surface, there also exist subsurface Tropical Instability Waves (subTIWs), which can alter vertical mixing. However, the extent to which subTIWs impact mixing and heat flux is still unknown. Moreover, studies on subTIWs have been conducted exclusively in the Pacific. Here, we show the presence of subTIWs in the Atlantic for the first time, using mooring observations. Analysing 16 years of simulations of a comprehensive, global, high-resolution ocean model, we characterize subTIWs in the Atlantic with regard to their spatial and temporal variability and investigate their influence on vertical mixing. We find subTIWs in the Atlantic between 40 and 90 m depth in both the model and observations. Further, model results reveal that unlike TIWs, subTIWs frequently occur also south of the Equator in the Atlantic Ocean. We show that subTIWs induce an oscillating multi-layer shear structure, suggesting subTIWs to destabilize the mean flow and thereby induce mixing. This is strongest north of the Equator, where both TIWs and subTIWs act simultaneously. We conclude that despite similar characteristics, TIWs and subTIWs are distinct waves which both impact mixing and heat flux within the thermocline. Therefore, future studies of thermocline dynamics in the tropical oceans should not only consider TIWs but also take into account the effect of subTIWs, particularly in the subTIW dominated region south of the Equator.

B.1 INTRODUCTION

Temperature and velocity variability in the Tropical Atlantic Ocean are dominated by the seasonal cycle and interannual to decadal variability, such as the Atlantic meridional and zonal mode (Busalacchi and Picaut, 1983; Cabos et al., 2019; Carton et al., 1996; Deppenmeier et al., 2016; Lübbecke et al., 2018; Muñoz et al., 2012; Murtugudde et al., 2001; Prodhomme et al., 2019; Tourre et al., 1999; Xie and Carton, 2004). However, the dominant feature of intraseasonal variability, tropical instability waves (TIWs), have been found to be significant for the mixed layer heat budget and air-sea interactions in the tropical Atlantic (Bunge et al., 2007; Grodsky et al., 2005; Jochum and Murtugudde, 2006). A recent study by Liu et al. (2019a) states that TIWs can have complex vertical velocity structures, which interact with the zonal mean flow and thereby impact vertical mixing. In the equatorial Pacific Ocean this is true particularly for the oscillating zonal component of TIWs. Despite large efforts to understand the horizontal structure and generation mechanisms of surface-intensified TIWs, such vertical structures of TIWs and their impact on vertical mixing have been scarcely studied. In a novel approach to study the vertical structure of TIWs, Liu et al. (2019a) used observed temperature and velocity records from a mooring at 0°N, 140°W to show the existence of subsurface mode tropical instability waves (subTIWs) in the tropical Pacific. The vertical shear caused by such subTIWs can interact nonlinearly with the shear of the zonal mean flow and largely change the total shear above the Equatorial Undercurrent (EUC) core, suggesting that subTIWs play an important role in vertical heat transport and mixing (Liu et al., 2019a, 2020). Further, subTIWs may alter the character of TIWs. However, these results are based on a single spot mooring in the equatorial Pacific and therefore, neither horizontal structure nor generation mechanisms of subTIWs have been determined (Liu et al., 2019a). Hence, while TIWs are an extensively studied feature of all tropical oceans, to date little is known about subTIWs and the existence of subTIWs in the Atlantic is yet to be shown.

In this study, we show the existence of subTIWs in the Atlantic for the first time, using observations from two moorings at 4°N, 23°W and 0°N, 23°W and 16 years (2003 to 2019) of daily temperature and velocity output from the global, comprehensive, high resolution (10 km) setup of the ocean model ICON-O (ICOsahedral Non-hydrostatic-Ocean). Spatio-temporal analyses of subTIWs require using model simulations because observations are too sparse, in both spatial and temporal domain. The continuous simulation over almost two decades allows for statistically more robust analyses compared to the few years of available observations. In particular, subTIW year-to-year variability and the relevance of subTIW induced variability relative to variability

on longer time scales, such as the seasonal cycle, can be assessed. We take advantage of the horizontal and vertical high-resolution ICON-O model output to investigate the spatial distribution of subTIWs and their impact on vertical mixing in different regions of the tropical Atlantic. We assess the relative importance of subTIWs compared to TIWs for vertical mixing, and the role of subTIWs in altering vertical and horizontal heat fluxes. Further, we analyse the combined effect of simultaneous occurrence of TIWs and subTIWs on vertical mixing and heat fluxes.

We find that subTIWs are present in the tropical Atlantic with characteristics distinctively different from the ones known for surface-intensified TIWs. In particular, unlike TIWs, subTIWs are most prominent away from the Equator in both northern and southern hemisphere. The main occurrence period of subTIWs is one to three months later than the occurrence of surface-intensified TIWs. In agreement with Liu et al. (2019a) our results suggest that subTIWs can alter vertical mixing above the thermocline. Since subTIWs can occur at different times, in greater depth and in different regions than TIWs, the effect of subTIWs on mixing is not included when only studying TIWs. Further, we show that the impact on vertical mixing and heat flux is largely increased by the simultaneous occurrence of TIWs and subTIWs. Hence, it is important to consider both TIWs and subTIWs when studying upper ocean dynamics in the tropical Atlantic, as well as studying TIW/subTIW interaction.

B.2 DATA

B.2.1 *Observational Data*

B.2.1.1 *Hourly Mooring Data at 4°N, 23°W*

Observations at 4°N, 23°W used in this study are part of the Tropical Atlantic Current Observation Study (TACOS) which measures upper ocean velocity and shear at the 4°N, 23°W Prediction and Research Moored Array in the Tropical Atlantic (PIRATA) mooring (Bourlès et al., 2019; Perez et al., 2019). The TACOS mooring data was first analysed and described in detail in Perez et al. (2019). It provides a unique high-resolution 1-year data set (6 March 2017 to 26 March 2018) which allows for assessing the temporal and vertical current structure at this location (Perez et al., 2019).

In this study, we analyse data from 10 downward facing point acoustic current meters mounted on the mooring, with sample volumes centred at 7, 12, 17, 22, 27, 32, 37, 47, 57, 66.6, and 86.6 m (hereafter, the last two will be referred to as 67 and 87 m, respectively, as done by Perez et al., 2019). Details on the individual lengths of each sensor

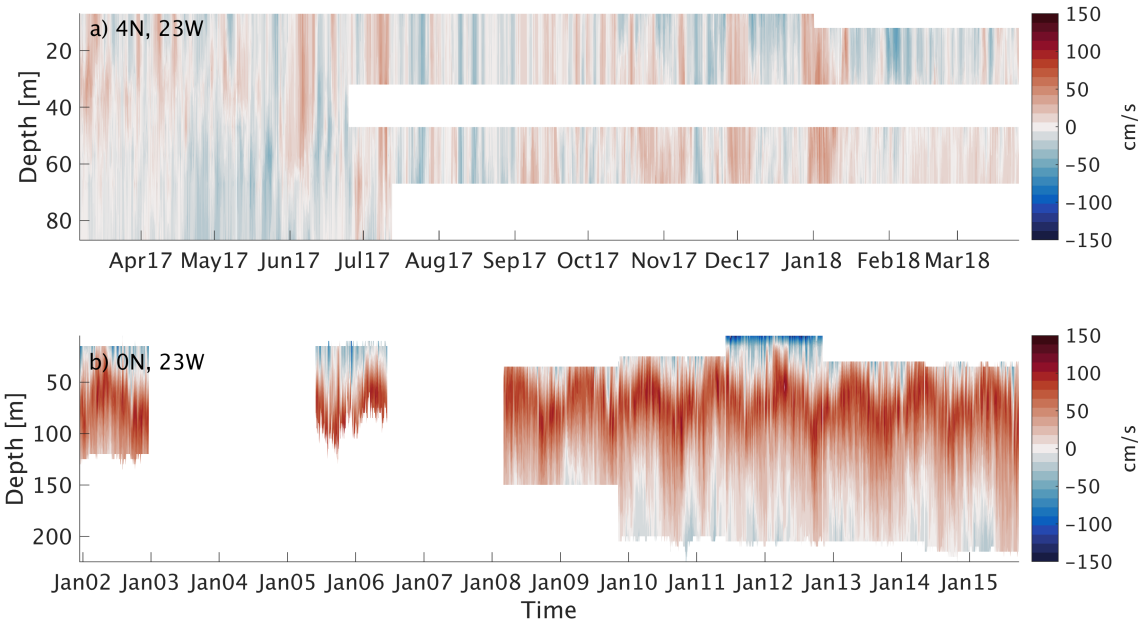

Figure B.1: Available zonal velocity records at 4°N, 23°W (a) and 0°N, 23°W (b) since mooring deployment. Velocities are given in cm/s. Positive values indicate eastward velocities, negative values indicate westward velocities.

record and their mean values can be found in Perez et al. (2019). Data gaps occur at individual sensor depths, as shown in Figure B.1a. Thus, we filled these gaps by interpolating over depth between the sensors directly above and below the errant sensor. Finally, we interpolated all mooring data onto a regular 2 m depth grid for direct comparison with the model data and observations at 0°N, 23°W. We did not extrapolate the missing velocity data at 87 m after July 2017. Instead we focus our analysis on the upper 67 m.

B.2.1.2 *Hourly Mooring Data at 0°N, 23°W*

Hourly velocity records at 0°N, 23°W are available from an acoustic doppler current profiler (ADCP) mooring at the PIRATA mooring site. At this location, subsurface ADCPs were moored since 2001 (Bourlès et al., 2019). Available zonal velocity records are shown in Figure B.1b. Unfortunately, large gaps exist in the velocity records, from December 2002 until June 2005 and from June 2006 until March 2008. Records before March 2008 are only available between 15 to 120 m. From March 2008 until September 2015 velocities were measured between 25 to 210 m. From June 2011 until November 2012 records are also available near the surface between 5 m and 25 m (Figure B.1b). Due to the sparsity of velocity data before 2008, we only use observations from 2008 onwards. Small temporal gaps are filled by linear interpolation.

Further, during periods where velocity records start below 30 m depth, we extrapolate vertically to gain a consistent dataset between 30 to 120 m. This allows us to study both TIWs and subTIWs in a multi-year data set. Further, same as done with the observations at 4°N, 23°W, we interpolated the data onto a regular 2 m vertical grid for comparison.

B.2.2 *ICON-O Model Setup*

We examine the spatial extent of subTIWs and their regional effects on vertical mixing using a high-resolution setup of the global, comprehensive ocean component of the ICON model, ICON-O. ICON-O is part of the ICON framework which has a non-hydrostatic atmosphere (Giorgetta et al., 2018; Zängl et al., 2015). However, despite the name, the non-hydrostatic approach is not realized in the ocean component of the model framework. Instead, ICON-O has a hydrostatic ocean. Details on ICON-O, regarding the underlying icosahedral grid, model equations and the spatial and temporal dicretization can be found in Korn (2017). The particular ICON-O setup used in this study, has a horizontal resolution of 10 km and 128 vertical levels with a high number of layers in the upper ocean (12 layers in the upper 100 m, not equally spaced). Simulation of vertical mixing is based on a prognostic equation for turbulent kinetic energy (TKE, Gaspar et al., 1990). The model has undergone a spin-up period of 25 years, during which it is forced by 24-hourly OMIP (Ocean Model Intercomparison Project) data (Röske, 2006) starting from the Polar Science Center Hydrographic Climatology (PHC, Steele et al., 2001). The spin-up is followed by a simulation period from 1948 to 1978, forced by 6-hourly NCEP data (Kalnay et al., 1996). This part of the model setup is similar to the previous STORM simulations withICON-O's predecessor MPI-OM as described in Storch et al. (2012). From January 1979 until December 2019 the ocean is forced by hourly ERA5 reanalysis data (Hersbach et al., 2020), which by the time of the model simulation was available from 1979 onwards. ERA5 provides hourly output at increased grid spacing of 31 km globally and 137 levels in the vertical, compared to 6-hourly output at 79 km on 60 vertical levels in ERA-Interim (Hersbach et al., 2019, 2020). For the analyses, only output from the period February 2003 until December 2019 is considered. From the global model output of daily and monthly 3D velocity fields, temperature and salinity, we select a region from 10°S to 10°N and 60°W to 20°E to study subTIWs in the Atlantic Ocean. Furthermore, prior to the analyses we interpolate all model output from the original icosahedral grid onto a regular grid with $0.1° \times 0.1°$ horizontal grid spacing using nearest neighbour interpolation.

B.3 METHODS

B.3.1 *Identifying subTIWs*

We identify subTIWs in the equatorial Atlantic in both model and observations, under consideration of the subTIW characteristics found in the equatorial Pacific by Liu et al. (2019a). Following Liu et al. (2019a) velocity anomalies in the TIW period band vary with depth and show distinct peaks in the subsurface layer. When applying a narrower temporal bandpass filter to isolate subTIWs from TIWs, they find oscillating zonal velocities clearly centred in the subsurface, which they suggest to be the manifestation of subTIWs. Unlike the study by Liu et al. (2019a), our analysis is not solely based on mooring data. Hence, we first need to identify the regions in which instability waves are strongest in the Atlantic. Based on these regions, we then define the temporal bandpass filtering window for subTIWs in the tropical Atlantic. To identify subTIW dominated regions, similarly to the methods used by de Decco et al. (2018), we filter the model temperature output using a 2D gaussian filter, which we first apply in time and then in space. The chosen band pass filtering width allows oscillations with a period of 15 to 60 days and wavelengths of 4 to 20° longitude ($\approx$ 400 to 2000 km) to pass. These are the periods and wavelengths of TIWs in the Atlantic, which were found in previous studies (e.g. de Decco et al., 2018). It is reasonable to assume that subTIWs reside within the same period and wavelength window. We compute the standard deviation of the filtered temperature in a 4-month moving average window at each grid point in an area from 10°S to 10°N in the Atlantic, for the entire simulation period and each model layer within the thermocline. This approach for finding strong instability wave events is modified following the method applied in Perez et al. (2019). We combine the resulting time series of temperature standard deviation for each grid point to determine the 90th percentile of temperature standard deviation for the chosen model domain of 10°S to 10°N in the Atlantic. The resulting value for the domain wide 90th percentile, calculated for each model layer, is taken as the threshold value for strong instability wave activity. At each grid point, we count the total number of events above the calculated 90th percentile temperature threshold during the simulation period. As such, we construct a 2D histogram of strong instability wave events in all model layers in the thermocline. In the subsurface, instability waves are most pronounced in 64 m depths. Here, two regions of strong events can be found, which are both characterized by an accumulation of strong events. One of them is located north of the Equator at 2.5 to 5°N, 12 to 22°W (hereafter called Region North), the other one is located south of the Equator at 1 to 3°S, 15 to 28°W (hereafter called Region South). Figure B.2 shows the 2D histogram of strong instability wave

events in 64 m depth and the chosen regions on which our analyses focus in the following. The locations of the two moorings used in this study are shown as dots. Further, the dashed box in Figure B.2 shows the region in which strong TIW activity at the surface can be found, called Region Equator (0 to 2°N, 9 to 19°W). This region is determined using a 2D histograms of strong instability waves at the surface.

Next, we conduct wavelet and spectral analysis of the meridional and zonal velocity time series at 64 m depth to find the individual subTIW periods in each region. Both power spectral density and wavelet transforms are calculated for each grid point and averaged afterwards to gain a box averaged power spectrum and wavelet transform. The averaged wavelet transforms are shown in Figure B.4b and B.4d and will be described in detail in Section B.4.2. Figure B.4a and B.4c show all individual spectra (grey lines) as well as the resulting mean (black line) and the chosen filtering periods (red shading). Unlike Liu et al. (2019a), we use both wavelet analysis and power spectral density analysis to identify subTIW periods to take into account varying periods in the different regions and years. This method results in an average subTIW period of 24 to 53 days in Region North and 25 to 47 days in Region South. For the observational data, resulting subTIW periods are 26 to 30 days at 0°N, 23°W and 30 to 45 days at 4°N, 23°W. Hence, to study pure subTIW dynamics, we apply a 2D gaussian filter in space and time to the model output with a regionally varying temporal filter according to the determined periods, and a spatial filter of 4 to 20° longitude. For the mooring data only temporal filtering is applied.

B.3.2 *Mixing and Heat Flux Calculation*

The potential for mixing is assessed via calculation of vertical shear of horizontal velocity $S^2 = \left(\frac{du}{dz}\right)^2 + \left(\frac{dv}{dz}\right)^2$ and reduced shear squared $S^2_{red} = S^2 - 4N^2$, with N being the Brunt-Väisala-Frequency. Reduced shear squared S^2_{red} relates to the Richardson number Ri which is an indicator for the likelihood of mixing in the ocean. For $S^2_{red} > 0$, Richardson number $Ri < 0.25$ from which follows that the flow is more likely to be unstable and mixing can occur.

SubTIW related vertical heat flux is calculated as $Q_w(z) = c[\overline{w(z)'T(z)'}]$ where primes denote subTIW temperature and velocity anomalies, overbar indicates time averaging and square brackets indicate horizontal averaging over the respective areas through which the flux is directed. $c = c_p \cdot \rho$ is the volumetric heat capacity and assumed to be constant (Cummins et al., 2016), with the specific heat of seawa-

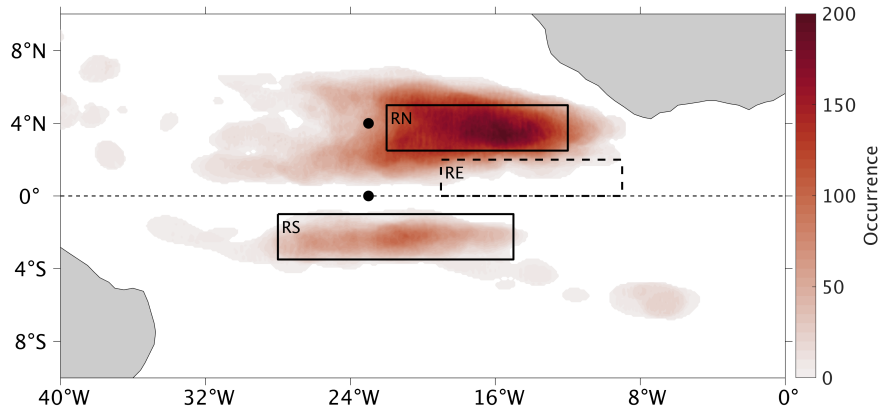

Figure B.2: 2D histogram of strong subTIW occurence in 64 m depth in the study region during the entire 16 year simulation period. Black dots indicate the location of the PIRATA mooring sites (0°N, 23°W and 4°N, 23°W), black solid boxes mark the identified subTIW regions. Region North (RN): 2.5 to 5°N, 12 to 22°W. Region South (RS): 1 to 3.5°S, 15 to 28°W. Black dashed box marks the region of pronounced TIW activity at the surface, Region Equator (RE): 0 to 2°N, 9 to 19°W.

ter $c_p = 3850 \frac{J}{kgK}$ and density of seawater $\rho = 1025 \frac{kg}{m^3}$. To assess the vertical heat flux in each region in the upper and lower thermocline separately, we calculate Q_w across a plane in the middle of the upper and lower thermocline, respectively. Hence, $Q_w(z_{upper}/2)$ describes the heat flux across a plane in the middle of the upper thermocline and $Q_w(z_{lower}/2)$ describes the heat flux across a plane in the middle of the lower thermocline. Equivalently, meridional and zonal heat flux are calculated as $Q_v(lat) = c[\overline{v(lat)'T(lat)'}]$ and $Q_u(lon) = c[\overline{u(lon)'T(lon)'}]$, respectively. We calculate the horizontal heat flux across each region by calculating Q_v and Q_u for a plane in the middle of the region, e.g. $Q_v(lat/2)$ and $Q_u(lon/2)$, for both upper and lower thermocline.

B.3.3 *Calculating TIW and subTIW Composites*

Composite analysis allows for studying the impact of TIWs and subTIWs separately and for quantifying the relative importance of TIWs compared to subTIWs for vertical shear S^2, stratification N^2, horizontal heat flux Q_u, Q_v and vertical heat flux Q_w above the thermocline in all three regions. To calculate the composites, we adapt the approach described by Foltz et al. (2020): For each region we define TIW energy as 15 to 60 day band-pass filtered $u'^2 + v'^2$ at the uppermost model layer, averaged over the respective regions. Consequently, subTIW energy is defined as area averaged $u'^2 + v'^2$ in 64 m depth, band-pass filtered with the periods described in Section B.3.1 for each

Table B.1: Depth averaged mean values of vertical shear S^2, stratification N^2 and horizontal heat flux Q_u, Q_v in Region North and Region South, calculated using the entire time series to normalize the composite means. Mean values are seperated into upper thermocline (7 to 40 m) means and lower thermocline (40 to 80 m) means. Vertical heat flux Q_w in each region is given as the time mean flux across a plane in the middle of the upper and lower thermocline, respectively.

Region		$\mathbf{S^2}$ $[10^{-4}s^{-2}]$	$\mathbf{N^2}$ $[10^{-4}s^{-2}]$	$\mathbf{Q_u}$ $[10^4 Wm^{-2}]$	$\mathbf{Q_v}$ $[10^4 Wm^{-2}]$	$\mathbf{Q_w}$ $[Wm^{-2}]$
North	upper	0.4	3.8	5.7	-31.7	24
	lower	0.1	6.1	-6.3	-32.7	17
South	upper	1.5	1.8	0.9	2.5	3.9
	lower	0.3	4.1	9.0	6.8	3.5

region separately. As such, we gain a TIW and subTIW energy time series for each region. Values greater than one standard deviation above mean are considered high energy periods, values less than mean minus 40% of one standard deviation are considered low energy periods, following the definition by Foltz et al. (2020). All periods with high energy are combined to the composite for strong TIW and subTIW activity, all periods with low energy are combined to the composites for weak or no TIW and subTIW activity. We then compute mean composite values for each variable and region, averaged over the upper (7 to 40) and lower thermocline (40 to 80 m) separately. The composite mean is normalized by dividing the individual composite mean by the respective depth averaged mean over the entire time series. The mean values of vertical shear S^2, stratification N^2, horizontal heat flux Q_u, Q_v and vertical heat flux Q_w in each region that were used to normalize the composite means are listed in Table B.1. Normalized composite means of 1 indicate that the considered wave event does not alter the overall mean. Values larger than 1 indicate an increase in the respective variable due to the wave, while values less than 1 indicate a decrease caused by instability waves. We test for significance of the resulting composite means using bootstrapping methods. All shown values are significant on the 99% significance level.

B.4 RESULTS

B.4.1 *Comparison of Observed and Simulated Zonal Mean Flow Field*

Ocean circulation in the tropical Atlantic Ocean is dominated by zonal currents, namely the South Equatorial Current (SEC) and North Equatorial Countercurrent (NECC) at the surface and the EUC at greater depths (Figure B.3). These currents are of particular interest to our study as increased shear between the opposing currents can create instabilities which generate subTIWs. Hence, the realistic representation of these currents is a prerequisite for studying subTIWs in ICON-O.

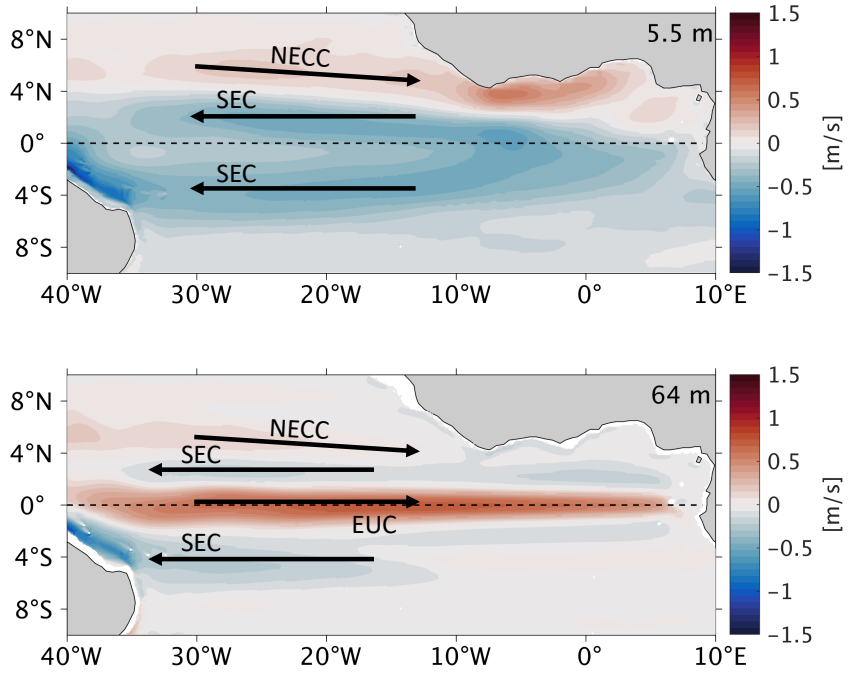

Figure B.3: Simulated long term mean zonal velocity in the surface layer (5.5 m, top panel) and subTIW layer (64 m, bottom panel). Velocities are given in m/s. Positive values indicate eastward velocities, negative values indicate westward velocities. Black arrows show a schematic of the dominant zonal currents in the respective depths. EUC: Equatorial Undercurrent; NECC: North Equatorial Countercurrent; SEC: South Equatorial Current.

Therefore, we compare observations and model output of the equatorial flow field to show that ICON-O resolves the equatorial current system well.

The long term mean zonal flow field over the 16 year simulation is shown in Figure B.3. At the surface (Figure B.3, top panel), the NECC can be seen as a clear eastward current north of approximately 4°N. Between the NECC and the Equator, flow is directed westward by the SEC. The location and strength of both the SEC and NECC agree well with results from previous studies (Brandt et al., 2010; Lumpkin and Johnson, 2013; Perez et al., 2019) and suggest that ICON-O is able to create feasible current shear. At 64 m depth (Figure B.3, bottom panel), the most prominent flow is the eastward EUC, located on the Equator in agreement with observations (Brandt et al., 2010). We further explore the simulation of the EUC by comparison of the simulated long term mean zonal velocity along 23°W with the mean zonal velocity observed during ship sections between 1999 and 2008, presented in Brandt et al. (2010, Figure 2 (a) therein). In these

observations, the EUC extends from just below the surface to 200 m depth at 0°N, 23°W and spans a width from approximately -1.75°S to 1.75°N. The core (defined as the depth of the strongest eastward velocity) is located at the Equator in approximately 80 m depth. Zonal velocity profiles from the PIRATA mooring at 0°N, 23°W, averaged over the observation period (not shown) also show the EUC core depth at the Equator to be 75 m with a maximum zonal velocity of 0.8 m/s. In comparison, the simulated EUC ranges between -1.75°S to 1.5°N with its core depth at the Equator in approximately 70 m depth and a maximum zonal velocity of 1 m/s (not shown), hence of comparable magnitude to the observations.Therefore, we conclude that ICON-O is able to simulate the equatorial zonal currents, in particular the EUC, characteristics sufficiently well to study subTIWs.

B.4.2 *Simulated Velocity Variability in the subTIW Period Band*

We compute power spectral density and wavelet transforms of the simulated, unfiltered meridional velocity in 64 m depth to identify the dominant scales of current variability and their relative strength in the subTIW dominated regions Region North and Region South. In particular, we assess the importance of variability on subTIW time scales.

Spectral energy of meridional velocity in both Region North (Figure B.4a) and Region South (Figure B.4c) is high around periods of one year and 180 days, highlighting the strength of the annual and semi-annual cycle in the tropical Atlantic (Brandt et al., 2016). Further, in both regions spectral energy of meridional velocity peaks in the intraseasonal band (less than approximately 100 days), in particular at periods less than 60 days. This can be explained by the presence of subTIWs and highlights the importance of subTIWs for meridional current variability. The strength of the intraseasonal variability compared to the semi-annual and annual cycle varies within the regions (grey lines in Figure B.4a and B.4c). At individual points intraseasonal variability is the strongest source of variability while others are dominated by the annual or semi-annual cycle. In Region North, the intraseasonal signal can even largely exceed the otherwise strong annual cycle (Figure B.4a). However, when considering the entire regions, indicated by the black lines in Figures B.4a andB.4c, intraseasonal variability is the leading mode of variability. Regionally averaged power spectral density in the intraseasonal period band is about twice as strong as the semi-annual and annual variability in both regions. It should be noted that Region North and Region South were chosen due to high subTIW occurrence and consequently intraseasonal variability in these

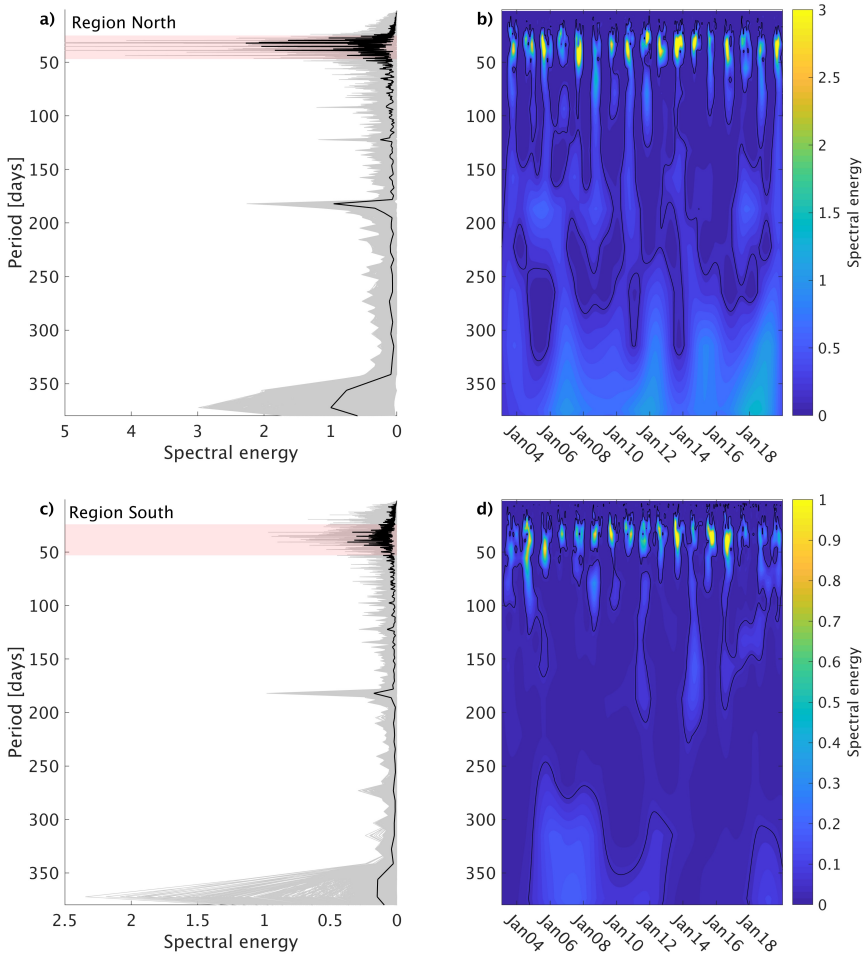

Figure B.4: Power spectral density (a and c and wavelet transforms (b and d) of simulated meridional velocity in 64 m depth in Region North (top panels, a and b) and Region South (bottom panels, c and d). Grey lines in a) and c) show power spectral density for each model grid point in the respective region. Thick black line indicates the box averaged power spectral density. Red shading shows the selected period window for subTIW filtering. The wavelet transforms in b) and d) are calculated by averaging the wavelet transforms computed for each grid point in the respective regions. Black contours in b) and d) are the 95% confidence interval. It should be noted that the axis limits differ between Region North and Region South.

two regions is stronger compared to other regions of the tropical Atlantic. Therefore, this result is not representative for the entire tropical Atlantic, where the semi-annual and annual cycle are the dominant source of variability (Brandt et al., 2016).

Since subTIW occurrence is a seasonal phenomenon, their strength may further be underestimated when only considering power spectral density over the entire simulation period. Therefore, we also com-

pute wavelet transforms of the meridional velocity, which allow for including the seasonal character of subTIWs in the analysis. These are shown in Figures B.4b and B.4d. Here, a clear pattern of high spectral energy in boreal autumn and winter in the subTIW period band can be seen in both regions, which largely exceeds the mean energy in other period bands. This indicates that high energy in the intraseasonal period band is indeed caused by subTIWs.

In conclusion, analysis of power spectral density and wavelet transforms shows that in the identified regions energy in the intraseasonal period band is the leading mode of variability which is further enhanced during boreal autumn and winter when subTIWs typically occur. Hence, subTIWs can be considered an important source of current variability. Lastly, it should be noted that while the relative importance of intraseasonal variability is comparable in both regions, spectral energy is overall higher across all scales of variability in Region North compared to Region South.

B.4.3 *SubTIW Activity in Simulations and Observations at PIRATA Mooring Sites*

In this section, we show that subTIWs can be identified at both PIRATA mooring locations with distinct subsurface velocity maxima in both velocity components. To assess model accuracy in simulating this activity, we compare observed velocities with the corresponding model output.

B.4.3.1 $4^{\circ}N$, $23^{\circ}W$

At 4°N, 23°W, observed subTIW-associated (30 to 45 days bandpass filtered) meridional velocity in 67 m depth shows three subTIWs between June and August 2017 (Figure B.5). Two less pronounced subTIWs can be found in November and December. We do not compare the observations directly to the respective simulation year because we expect the simulation to have its own variability. Therefore, we cannot assume agreement of simulation and observations in a specific year. Looking at all 16 simulation years in Figure B.5 (blue dotted lines) reveals that subTIWs undergo pronounced year-to-year variability. Simulated subTIWs are most pronounced in boreal summer, in agreement with the observations, but can occur until February of the following year with decreasing velocity amplitudes. Throughout the whole simulation period, subTIW amplitudes reach a maximum of about 20 cm/s, compared to the observed maximum velocity amplitude of 24 cm/s. Highlighting the simulated period from March 2004 to March 2005 (solid blue line in Figure B.5) shows that the ICON-O can very well reproduce variability such as the observed subTIWs.

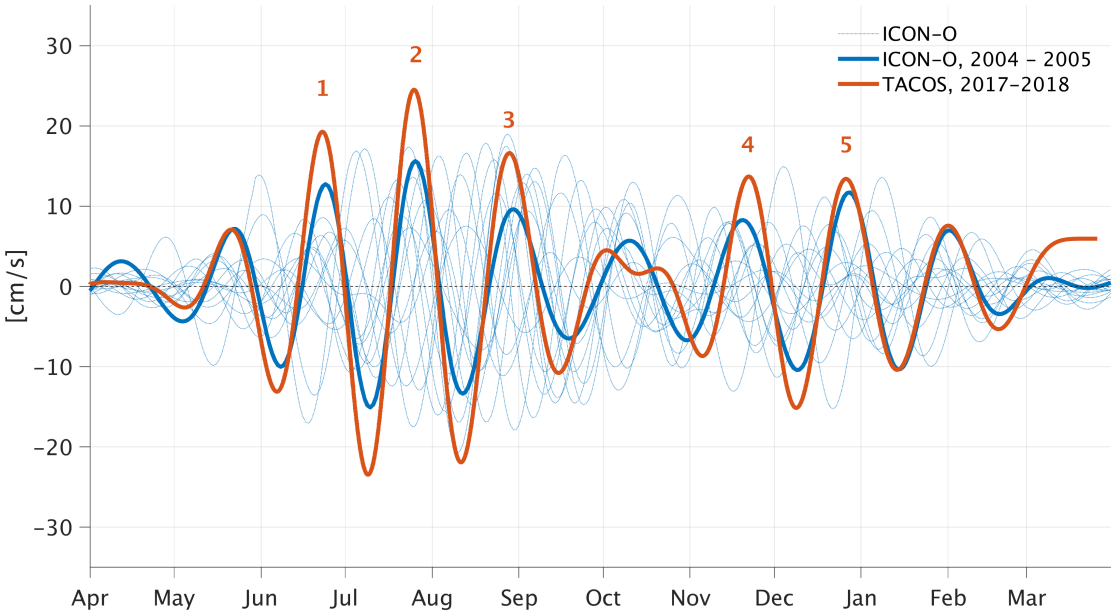

Figure B.5: SubTIW-associated meridional subsurface velocity at 4°N, 23°W in ICON-O for all 16 simulation years (blue dotted lines) and observed subTIW-associated meridional velocities at the TACOS mooring site (orange) from March 2017 until March 2018. The solid blue line shows simulated meridional velocities during March 2004 until March 2005. The temporal filter for both observations and simulation is 30 to 45 days. Orange numbers indicate subTIWs observed at the TACOS mooring site. Observed meridional velocity are shown for 67 m depth, simulated meridional velocity is shown for 64 m depth.

Applying a 30 to 45 day bandpass filter to the observed velocity reveals subsurface velocity maxima at 4°N, 23°W in both horizontal and zonal velocity components (Figure B.6 a and b). Meridional velocity is strongest between 46 to 67 m depth from June to September. A secondary subsurface maximum is located between 32 to 62 m depth from November to January. In comparison, the zonal velocity subsurface maximum is located between 44 and 67 m from June to September and at 30 to 58 m depth from November to January. However, the subsurface velocity maxima in boreal summer are located at the greatest observed depth level. We cannot rule out that velocities are even larger at greater depth.

Both zonal and meridional subsurface velocity anomalies reach amplitudes of about 15 cm/s during November to January. However, in boreal summer, the meridional subsurface velocity anomaly is the dominant component with up to 25 cm/s compared to 10 cm/s for the zonal component. Furthermore, similar to the two-layer shear structure described in Liu et al. (2019a), observed vertical shear ex-

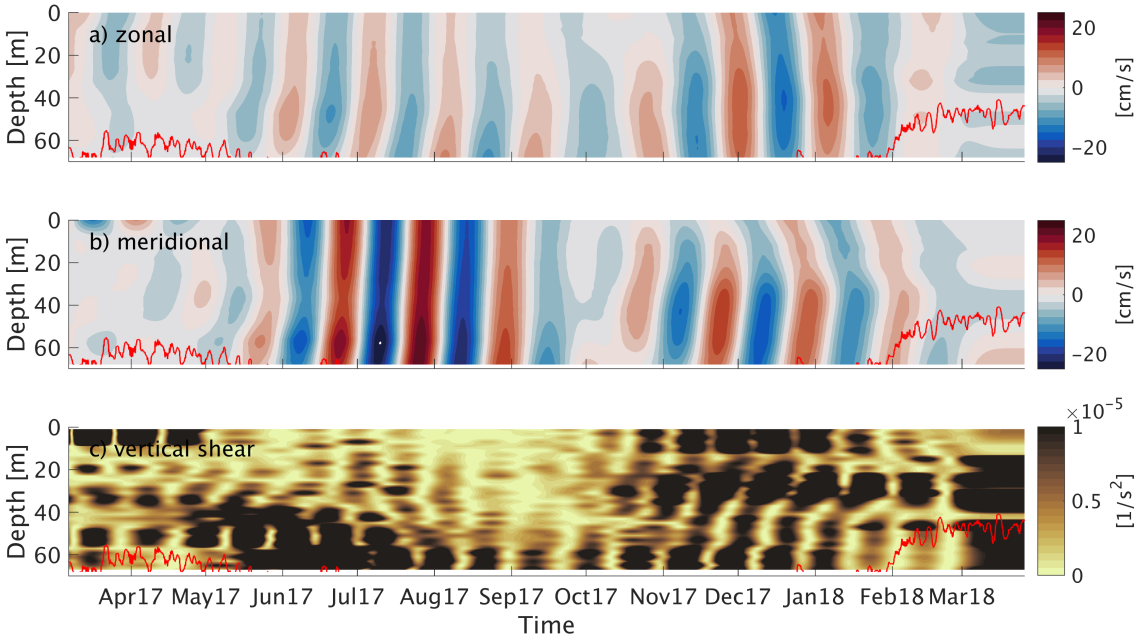

Figure B.6: Observed 30 to 45 day band pass filtered zonal velocity (a, top panel), meridional velocity (b, middle panel) and vertical shear squared $S^2 = \left(\frac{du'}{dz}\right)^2 + \left(\frac{dv'}{dz}\right)^2$ (c, bottom panel) at 4°N, 23°W. Velocities are given in cm/s, vertical shear is given in $1/s^2$. Positive velocities indicate eastward and northward flow. Negative velocities indicate westward and southward flow. The red line represents the thermocline depth (20° isotherm).

hibits a vertically complex multi-layer structure during the times of subTIW occurence, with increased S^2 in the depths of the subsurface velocity maxima. Such vertically complex multi-layer shear structure is not visible when applying a filter of 15 to 60 days, which are the characteristic periods of TIWs.

B.4.3.2 $0°N, 23°W$

At 0°N, 23°W, several years of observations are available in 65 m depth, which allows for a more reliable comparison. Observed subTIW-associated (26 to 30 days bandpass filtered) subsurface meridional velocity oscillations are strongest in August and September with amplitudes of up to 9 cm/s. Simulated subTIW-associated subsurface velocity oscillations are of comparable magnitude. However, strongest oscillations occur in July and August. The observed subTIW-associated zonal subsurface velocity shows strong year-to-year variability. Oscillations with a magnitude of up to 8 cm/s can occur in any month. In comparison, subTIW zonal subsurface velocity oscillations in ICON-O are strongest between August and the following March, with amplitudes of the same magnitude as the observed velocity oscillations.

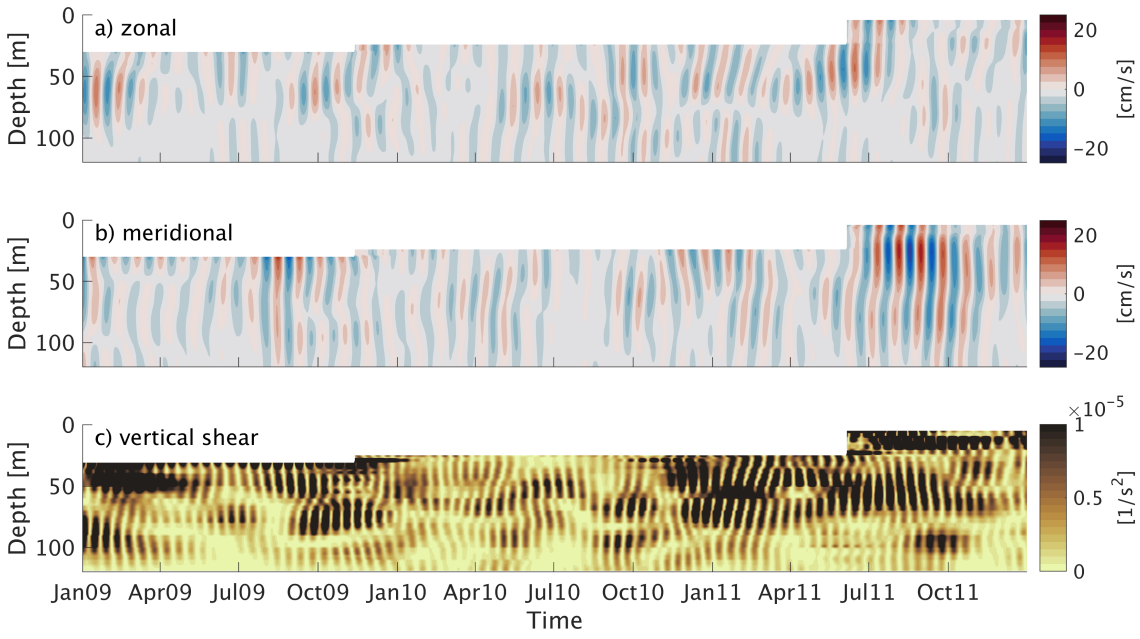

Figure B.7: Observed 24 to 30 day band pass filtered zonal velocity (a, top panel), meridional velocity (b, middle panel) and vertical shear squared $S^2 = \left(\frac{du'}{dz}\right)^2 + \left(\frac{dv'}{dz}\right)^2$ (c, bottom panel) at 0°N, 23°W for January 2009 to January 2012. Velocities are given in cm/s, vertical shear is given in $1/s^2$. Positive velocities indicate eastward and northward flow. Negative velocities indicate westward and southward flow.

Analysis of observed velocities in the subTIW period band (26 to 30 days) shows subsurface zonal velocity anomaly maxima at varying depths between 60 to 100 m depth, with an amplitude of 6 cm/s on average (Figure B.7a). Subsurface meridional velocity anomaly peaks at 66 m depth on average with an amplitude of approximately 9 cm/s (Figure B.7b). Vertical shear features a vertically complex multi-layer structure (Figure B.7c), which resembles the two-layer shear structure described in Liu et al. (2019a), particularly during 2010.

Different from findings in the equatorial Pacific by Liu et al. (2019a), subTIWs in the Atlantic are not solely manifested in subsurface velocity oscillations of the zonal velocity component. Instead, subsurface maxima can be found in both zonal and meridional velocities, with stronger amplitudes found in the meridional component. The latter is particularly true for the mooring north of the Equator, which can be explained by the decreasing strength of the zonal EUC away from the Equator and an increasing role of meridional velocities. When comparing the two mooring locations, subsurface velocity maxima are overall less pronounced at the Equator than to the north, suggesting stronger subTIW activity off the Equator.

B.4.4 *Generation Mechanisms of subTIWs in ICON-O*

Next, we take advantage of the global model domain of ICON-O to investigate the generation mechanisms of subTIWs. Such analyses are not possible with single spot moorings alone. We find that subTIWs are generated both north and south of the Equator through both baroclinic and barotropic conversion, with a larger contribution of baroclinic energy conversion. In particular north of the Equator, baroclinic energy conversion leads to subTIW generation, while barotropic energy conversion feeds energy back into the mean circulation.

To study the generation mechanisms of subTIWs we have a closer look at the eddy kinetic energy. We compute the so called barotropic and baroclinic energy conversion terms. This approach is similar to the one first used by Masina et al. (1999) to investigate the generation of surface-intensified TIWs and which has since been repeatedly used to study the generation of TIWs (e.g. de Decco et al., 2018; Jochum et al., 2004; von Schuckmann et al., 2008). Barotropic energy conversion describes the production and destruction of eddy kinetic energy due to the horizontal shear of the mean flow. Baroclinic energy conversion shows the conversion of eddy available potential energy into eddy kinetic energy and vice versa. Hence, barotropic and baroclinic conversion terms show energy conversion related to horizontal and vertical shear instabilities. Such instabilities can be manifold, in particular in complex flow structures like the equatorial current system, e.g. barotropic and baroclinic instabilities, as well as Kelvin-Helmholtz instabilities and over-reflection (Proehl, 1996). Here, we focus on analysing the generation of subTIWs in terms of energy conversion rates and do not give a detailed description of all possible involved instabilities. As in Jochum et al. (2004) we refer to barotropic and baroclinic instabilities, based on the underlying barotropic and baroclinic energy conversion. Barotropic energy conversion is calculated as $bar_{conv} = -\rho_0 \overline{u'v'} \frac{\partial U}{\partial y}$, with U the annual mean zonal velocity and u', v' the 15 to 60 day filtered velocities. Baroclinic energy is calculated as $barclin_{conv} = -g\overline{\rho' w'}$, with w' the 15 to 60 day filtered vertical velocity and ρ' the 15 to 60 day filtered density. We are aware that our approach shows the energy exchange between the background state and intraseasonal processes in general and may as such also include intraseasonal processes other than subTIWs. However, as previously discussed in Section B.4.2, subTIWs are the main source of intra-seasonal variability in 64 m depth. Hence, it can be assumed that the calculated energy conversion is primarily between the background state and subTIWs and can therefore be used to explain the generation of subTIWs in 64 m depth.

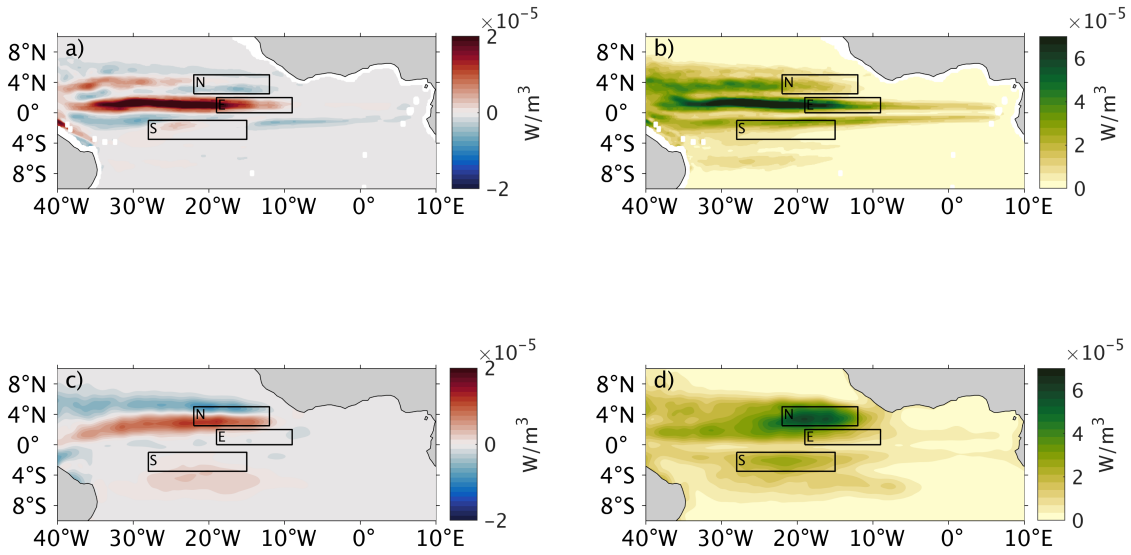

Figure B.8: Barotropic (a and b, upper panels) and baroclinic (c and d, bottom panels) conversion rates in 64 m depth in W/m^3. a) and c) show the mean conversion rates over all simulated subTIW seasons (May to November of each simulation year). Positive values indicate that energy is being fed into the instability. Negative values indicate that energy is being transferred back into the mean circulation. b) and d) show the standard deviation of the conversions rate over all simulated subTIW seasons.

The top panels of Figure B.8 show the mean barotropic conversion rate (a) and its standard deviation (b) in 64 m depth, calculated over all simulated subTIWs periods. The bottom panels of Figure B.8 show the mean baroclinic conversion rate (c) and its standard deviation (d) in 64 m depth, calculated over all simulated subTIWs periods. Both mean baroclinic and barotropic conversion are of comparable magnitude ($O(10^{-5}W/m^3)$, Figure B.8a and c), suggesting that horizontal and vertical shear instabilities play a role in generating subTIWs. The mean barotropic and baroclinic conversion rate south of the Equator is small but positive, meaning that energy is transferred into the instability through both barotropic and baroclinic energy conversion. Despite the small mean conversion rate values, standard deviation of both baroclinic and barotropic conversion is increased south of the Equator. In particular standard deviation of the baroclinic conversion shows a maximum in Region South, which suggest mean values with high variance. Strongest standard deviation of baroclinic conversion can be found in Region North. There, mean baroclinic conversion values are both positive and negative which implies that energy is transferred both into subTIWs as well as back into the mean current. In comparison, barotropic energy conversion is negative in Region North, implying that energy is being transferred from the instability back into the mean circulation. This suggests that in Region North generation of

subTIWs is mainly caused by baroclinic energy conversion. Barotropic energy conversion is high between the Equator and 2°N, west of 10°W. However, in this region subTIWs rarely occur which suggests that the barotropic energy conversion feeds energy into perturbations other than subTIWs. It is unclear, why the baroclinic conversion in the subsurface is high in the western basin, north of 3°N, where subTIWs can not be found. This question needs further investigation, which however is not part of the main scope of this study.

Following from the simulated mean zonal flow field (Figure B.3, bottom panel), we suggest that shear instabilities related to subTIW generation in the southern hemisphere, stem from shear between the southern flank of the EUC and the mean westward current south of it. The EUC intensifies in boreal summer and autumn with an observed maximum in July to September (Hormann and Brandt, 2007) which leads to increased shear between the EUC and the SEC, as such providing forcing for subTIWs. On the other hand, in the northern hemisphere, instabilities are most likely generated by shear between the SEC and NECC.

B.4.5 *Spatial Extent of Simulated subTIWs*

We conduct an Empirical Orthogonal Function (EOF) analysis to study the dominant subTIW spatial pattern. Our results suggest that, unlike known from TIWs, subTIWs are frequently present on both sides of the Equator.

Since subTIWs are propagating waves, the wave pattern is characterized by pairs of EOFs (Wang et al., 2020). The first four EOF modes of the 15 to 60 day filtered simulated temperature in 64 m depth, which only differ in their sign and are shifted by $\pi/2$, respectively, together explain about 85% of the total variance. To focus on the spatial pattern, rather than the propagation of the wave, Figure B.9 shows the first EOF mode, which explains about 38% of the total variance. The EOF in Figure B.9 is presented as a regression map, using the normalized first principal component (PC) time series. The PC1 time series is normalized to unit variance. Hence, the pattern illustrates the change of temperature in °C per standard deviation of the normalized PC time series.

An oscillating temperature pattern is apparent in both hemispheres, mirrored around the core of the EUC on the Equator. This confirms the existence of subTIWs both north and south of the Equator. However, the pattern is not symmetric around the Equator. In the northern hemisphere, the subTIW related temperature pattern expands as far as 8°N, while in the southern hemisphere it limited to 5°S, suggesting

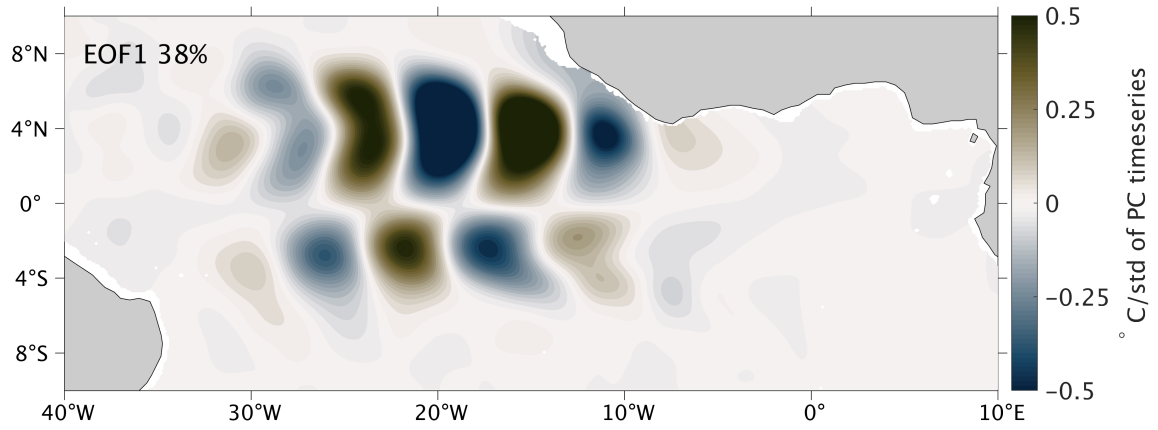

Figure B.9: First EOF mode of 15 to 60 day filtered simulated temperature in 64 m depth and the explained variance. The pattern is shown as a regression map, using the PC1 time series. The time series was normalized to unit variance prior to the regression. The EOF1 regression map shows values as °C/standard deviation of PC1 timeseries.

a larger region of subTIW influence in the northern hemisphere. Such pattern is distinctively different from the characteristic temperature pattern caused by surface-intensified TIWs, which is concentrated exclusively north of the Equator as shown for example in de Decco et al. (2018, Figure 4 therein).

B.4.6 *Regional Differences in subTIWs Characteristics in ICON-O*

In the following, we investigate the spatial differences of subTIWs by focusing on the wave characteristics in Region North and Region South. In both regions, we find subTIWs to be strongest between approximately 30 m and 90 m depth with an average occurrence time approximately three months later than surface-intensified TIWs in Region South and one month later in Region North.

B.4.6.1 *Region North*

In Region North, subTIWs occur between June and January of the following year. Most pronounced subTIW activity is found in July and August (Figure B.10c). During these months, subTIWs and surface-intensified TIWs can also frequently occur simultaneously (Figure B.10e). Figure B.11 illustrates simulated horizontal velocities, vertical shear and reduced shear squared in 2013. Despite showing results for only one year, our analyses consider the entire simulation period. Thus, the mentioned values in the following refer to the full simulation period and may differ from the values seen in Figure B.11.

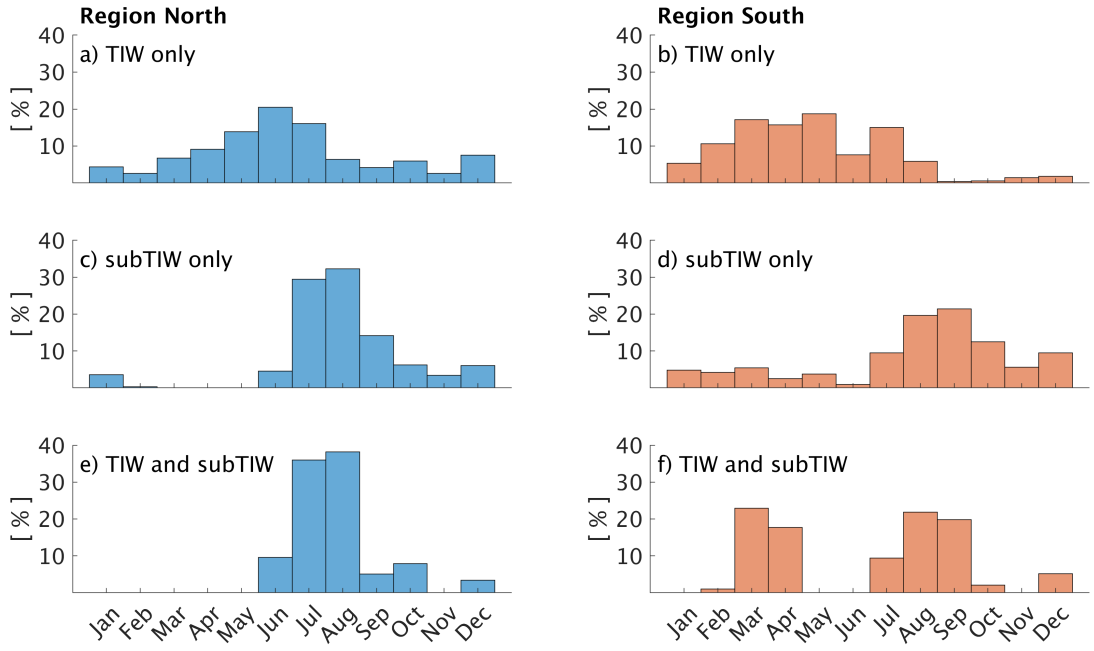

Figure B.10: Histograms of TIW and subTIW occurence in Region North (left) and Region South (right), based on daily model output and calculated for the entire simulation period. TIW and subTIW occurrences in the respective months are shown as percentage of the total amount of occurrencces. a) and b) show the occurrence of only TIWs. c) and d) show the occurrence of only subTIWs. e) and f) show the simultanious occurrence of TIWs and subTIWs.

SubTIWs occur between 32 and 75 m depth, visible as subsurface velocity maxima. Meridional velocities peak at approximately 61 m depth with an average velocity amplitude of about 4.1 cm/s. The velocity magnitudes are likely to be smaller than the observed velocities at the mooring site because we consider box averaged simulated velocities for the regional analysis. S^2 and N^2 were calculated for each grid point before calculating the regional average. Zonal velocities exhibit less frequent subsurface maxima at an average depth of 59 m depth. However, the amplitude of the zonal subsurface velocity maxima is about 2.6 cm/s on average and thus two thirds as strong as the meridional maxima. This points to the importance of the meridional velocity component for subTIWs north of the Equator. Shear squared S^2 exhibits a vertical two-layer structure during periods of subTIW activity with alternating shear maxima below and above the subsurface velocity peaks. This is a feature which cannot be found when applying a wider temporal bandpass filter, such as filtering for TIWs. Thus the two-layer shear structure appears to be a unique feature of subTIWs. Liu et al. (2019a) state that such vertical shear structure caused by subTIWs to be responsible for altered vertical mixing compared the mixing occurring during TIW only periods or times of absence of

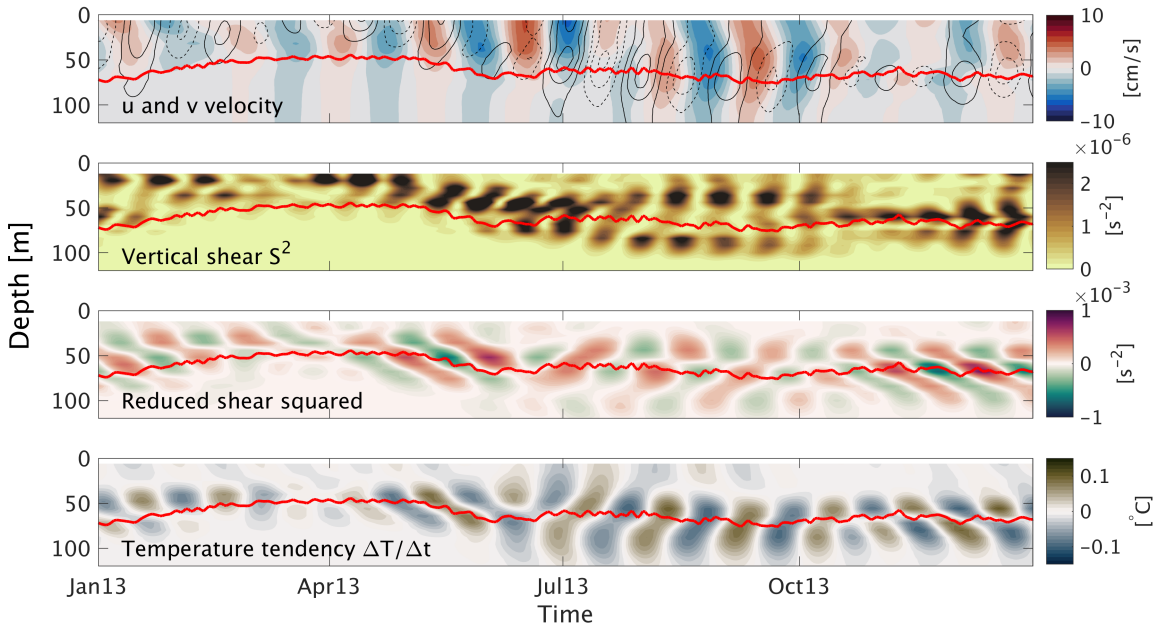

Figure B.11: Simulated 24 to 53 day filtered horizontal velocity, vertical shear S^2, reduced shear squared and temperature tendency $\Delta T/\Delta t$ in year 2013 in Region North. Vertical shear S^2 and reduced shear squared S^2_{red} are calculated using subTIW velocity anomalies u' and v'. Top panel: Zonal velocity u shown in shading in cm/s. Positive values indicate eastward flow, negative values indicate westward flow. Meridional velocity v is shown in contours with contour spacing of 2 cm/s. Dashed lines indicate southward velocities, solid lines northward velocities. Second panel: Vertical shear S^2. Third panel: Reduced shear squared S^2_{red}. Positive values indicate unstable flow conditions. Bottom panel: Temperature tendency $\Delta T/\Delta t$, with T being temperature in $^\circ C$ and t being time in days. Red line in all plots shows the thermocline depth (20°C isotherm).

instability waves. Reduced shear squared $S^2_{red} = S^2 - 4N^2$, which is a measure for vertical flow stability, exhibits an oscillating pattern similar to the vertical shear pattern. During the first half of the year, S^2_{red} is enhanced close to the surface, indicating the effect of surface intensified TIWs. However, from May onward S^2_{red} is stronger below 40 m. In particular, after June S^2_{red} exhibits an oscillating pattern just below and above the thermocline, coinciding with the surface velocity maxima, while close to the surface S^2_{red} vanishes. This supports the idea that the specific vertical shear structure caused by subTIWs, which differs from the periods when subTIWs are absent, destabilizes the flow in the subsurface and thereby may enhance vertical mixing.

B.4.6.2 *Region South*

In Region South, subTIWs can occur all year round. However, they are most frequently present in August and September (Figure B.10d). During this period, the can also occur simultaneously with TIWs

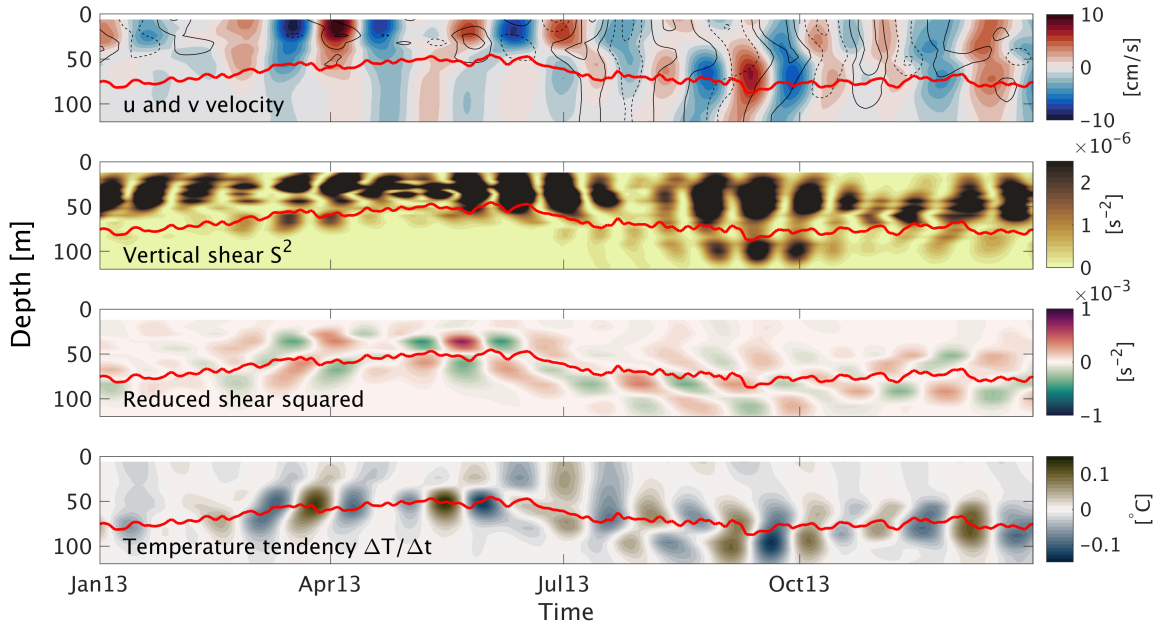

Figure B.12: Simulated 25 to 47 day filtered horizontal velocity, vertical shear S^2, reduced shear squared and temperature tendency $\Delta T/\Delta t$ in year 2013 in Region South. Vertical shear S^2 and reduced shear squared S^2_{red} are calculated using subTIW velocity anomalies u' and v'. Top panel: Zonal velocity u shown in shading in cm/s. Positive values indicate eastward flow, negative values indicate westward flow. Meridional velocity v is shown in contours with contour spacing of 2 cm/s. Dashed lines indicate southward velocities, solid lines northward velocities. Second panel: Vertical shear S^2. Third panel: Reduced shear squared S^2_{red}. Positive values indicate unstable flow conditions. Bottom panel: Temperature tendency $\Delta T/\Delta t$, with T being temperature in °C and t being time in days. Red line in all plots shows the thermocline depth (20°C isotherm).

(Figure B.10f). Again, we only show results for 2013 in Figure B.12, despite considering the entire simulation period for the analysis.

In Region South, subTIWs occur between 29 and 94 m depth. However, unlike in Region North in Region South subsurface velocity maxima most often occur in the zonal velocity component. Zonal velocity peaks in an average depth of 67 m with a velocity amplitude of 4 m/s. In comparison, meridional velocity peaks in 50 m depth with an average amplitude of 4.1 m/s. Hence, meridional velocity subsurface maxima are of comparable magnitude to Region North, while zonal velocity subsurface maxima are about 50% stronger in Region South. Comparable to Region North, a two-layer vertical shear structure is apparent. It is particularly pronounced from August onward, with maxima below and above the subsurface zonal velocity maxima, suggesting that subTIWs cause the vertical shear pattern. In comparison, S^2_{red} is smaller than in Region North. Strongest oscillations can be found in boreal spring, coinciding with near surface velocity maxima.

In contrast, during periods of subTIW occurrence S^2_{red} amplitudes are smaller. Nonetheless, values of S^2_{red} become positive when subTIWs are present. This indicates the potential of subTIWs to destabilize the mean flow in Region South, despite this effect being weaker than north of the Equator.

B.4.7 *Regional Differences in subTIW Impact on Vertical Mixing and Heat Flux in ICON-O*

To assess the regional differences in subTIW impact on vertical mixing and heat flux we conduct a composite analysis for each region separately. Results of the composite analysis are shown in Figure B.13. We also include TIWs in the composite analysis to evaluate the impact of subTIWs relative to the impact of TIWs. We find that in both Region North and Region South subTIWs impact vertical mixing and heat flux. Despite the relative influence of subTIWs often being smaller than the changes caused by TIWs, subTIWs lead to a significant contribution in altering mixing and heat fluxes in the thermocline. Further, we find that heat flux is affected most strongly when both TIWs and subTIWs occur simultaneously, which suggests that the interaction of the two waves is of major importance for the thermocline dynamics.

In Region North, both TIWs and subTIWs increase vertical shear S^2 throughout the entire thermocline. TIWs lead to a shear increase of approximately 40% while subTIWs increase shear by 20% (Figure B.13a and c). The combined effect on shear is of comparable magnitude to the one from TIWs alone. In Region South, in the upper thermocline (Figure B.13a), TIWs and subTIWs have an opposing effect on vertical shear. While TIWs increase shear by 20%, subTIWs deacrease shear by the same amount. However, in the lower thermocline (Figure B.13c), TIWs do not impact vertical shear, while subTIWs cause a shear increase of 10%.

In the lower thermocline, stratification N^2 is only marginally altered by either of the wave types by approximately $\pm$10% (Figure B.13c). On the other hand, in the upper thermocline (Figure B.13a) subTIWs decrease stratification in Region North and Region South by 60% and 20%, respectively. In Region North, TIWs lead to a smaller stratification decrease of 30%, while in Region South TIWs increase stratification by 40%, again opposing the effect of subTIWs in this region.

In the upper thermocline, strongest effects on horizontal and vertical heat fluxes occur when TIWs and subTIWs are present simultaneously (Figure B.13a). In Region South, zonal heat flux is strongly increased by TIWs, while subTIWs lead to a decrease. In Region North, both

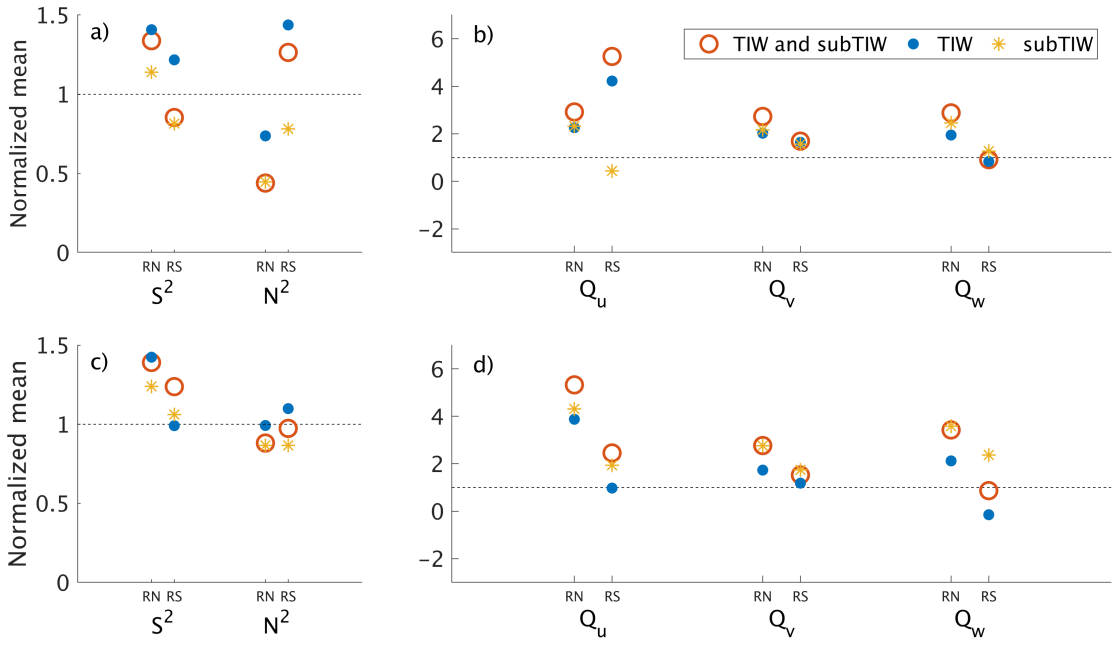

Figure B.13: Composite analysis for strong TIW (blue dot) and subTIW (yellow cross) events and simultaneous occurrence of both (red cirle) in the upper (a and b) and lower thermocline (c and d). Analysis is based on the model output. Upper thermocline includes the upper 40 m, lower thermocline includes 40 to 80 m. RN and RS indicate values for Region North and Region South. S^2 : vertical shear; N^2 : static stability; Q_u : zonal heat flux; Q_v : meridional heat flux; Q_w : vertical heat flux. All values are depth averaged means for the respective composites, normalized by the depth averaged mean of the full time series. The means are listed in Table B.1.

TIWs and subTIWs lead to a doubling in zonal heat flux. Meridional heat flux is increased by the same amount by both TIWs and subTIWs. Vertical heat flux is affected more strongly by subTIWs than TIWs. In fact, in Region South no impact of TIWs alone on vertical heat flux in the upper thermocline can be found. Also in the lower thermocline the combined effect of TIWs and subTIWs generally has the largest effect on all heat flux components (Figure B.13d). Further, heat flux increase caused by subTIWs is stronger than the increase caused by TIWs, which was expected since subTIWs occur below 40 m.

We can relate subTIWs to temperature changes above the thermocline by analysing the temperature tendency $\Delta T/\Delta t$ of the subTIW filtered temperature, shown in the bottom panels of Figure B.11 and Figure B.12. In both Region North and Region South the temperature tendency is strong around the thermocline depth. Temperature tendency is further increased during times of subTIW occurrence and generally coincides with increased vertical shear, suggesting an effect of subTIW and the induced changes in vertical shear on the thermo-

cline temperature. Further, temperature tendency is strongest below approximately 50 m depth, which highlights the importance of subsurface dynamics compared to surface intensified TIWs. To quantitatively assess what the TIW and subTIW induced changes in vertical shear, stratification and heat fluxes imply for the temperature above the thermocline, a detailed heat budget analysis would be necessary. However, such analysis is beyond the scope of the present work.

B.5 DISTINCTION BETWEEN TIWS AND SUBTIWS

Previous studies (e.g. Perez et al., 2019) investigated TIWs in the tropical Atlantic and also considered the vertical extent of TIWs. In particular, Perez et al. (2019) find subsurface maxima of both mean zonal and meridional velocity in 32 to 47 m depth and 57 m depth, respectively, at the TACOS mooring site at 4°N, 23°W in the observational data used in our study as well. Further, they find meridional velocities with amplitudes > 60 cm/s reaching down to 67 m depth and perturbations with velocity amplitudes as large as 40 cm/s reaching down to 87 m depth. However, these studies do not distinguish between waves with different frequencies in the subsurface and consider velocity perturbations at depth to be a signal of TIW downward energy propagation. In the present study we show that there are velocity oscillations in the subsurface with shorter periods compared to TIWs which, when taken into account in the choice of temporal band pass filter, reveal impact on vertical shear which differs from the one associated with TIWs. We argue, that such subTIWs are a feature of the equatorial Atlantic, independent of and distinguishable from TIWs, rather then a depth expression of downward propagating surface-intensified TIWs. We base this conclusion on several findings from this study, namely the differences in occurrence time, spatial distribution and share of baroclinic and barotropic energy conversion in the wave generation. While TIWs develop mainly from May onwards (Figure B.10a and b) in response to an intensification of the surface currents, development of subTIWs is strongest in July to September (Figure B.10c and d), likely due to an intensification of the EUC between July and September (Hormann and Brandt, 2007) which increases the shear between EUC and SEC in the subsurface. SubTIWs can also occur in years when TIWs are absent. Further, TIWs are predominantly located north of the Equator, whereas subTIWs are present away from the Equator in both hemispheres. The region of strongest TIW activity at the surface in ICON-O is highlighted in Figure B.2, called Region Equator. The region is obtained by applying the methods described in Section B.3.1 to simulated surface temperature. In addition, the TIW spatial pattern can clearly be seen in the results from an EOF analysis of surface temperature. Such analysis reveals an oscillating temperature pattern north of the Equator, comparable to the results from de Decco et al.

(2018, Figure 4 therein). Such pattern is contrasting the spatial pattern of subTIWs that we found in our study (Figure B.9). Lastly, previous studies argue that TIWs north of the Equator are mainly generated by barotropic energy conversion due to instabilities of the mean zonal surface currents. In contrast, our results suggest that subTIWs are generated by both barotropic and baroclinic energy conversion in Region South and mainly by baroclinic energy conversion in Region North. However, it should be noted that our analysis does not allow for conclusions regarding the types of instabilities involved in the energy conversion.

B.6 SUMMARY AND CONCLUSION

The presence of subTIWs and their influence on vertical mixing in the tropical Atlantic were investigated using observation data from two PIRATA moorings and high-resolution model output from the comprehensive, global, ocean model ICON-O. We identified subTIWs in observations in the Atlantic Ocean for the first time and studied their spatial distribution and regionally differing effect on mixing and heat flux using a high-resolution ICON-O simulation.

SubTIWs in both model and observations occur between approximately 30 and 90 m depth and manifest themselves as subsurface velocity peaks. SubTIWs north of the Equator are predominately expressed by oscillations of the meridional velocity component, to the south the zonal velocity component is of greater relevance. SubTIWs mostly occur from June to December, with a maximum in July to September. In general, subTIWs begin to form approximately one to three months later than TIWs in response to EUC intensification, however due to the strong year-to-year variability of both TIWs and subTIWs, they can also occur simultaneously. One of the most distinct differences between TIWs and subTIWs is the spatial extent. While TIWs primarily exist north of the Equator, subTIWs exhibit a mirrored pattern around the Equator with centres of high subTIW activity to both the north and south.
SubTIWs induce a multi-layer shear structure with shear maxima below and above the subsurface velocity maximum in both model and observations, which agrees with observations in the tropical Pacific Ocean from Liu et al. (2019a). This oscillating shear pattern in the subsurface ocean shows the potential of subTIWs to destabilize the mean flow and thereby inducing mixing, shown by positive values of reduced shear squared above the thermocline.
We show the relevance of subTIWs in relation to TIWs using a composite analysis of strong TIW and subTIW events. The results suggest great importance of simultaneous occurrence of both TIWs and

subTIWs for vertical mixing and heat fluxes in the thermocline.

We conclude that subTIWs are a feature of the tropical Atlantic which impact vertical mixing and heat flux in the thermocline in two regions north and south of the Equator. Despite sharing similar characteristics and time of occurrence, subTIWs appear to be independent of TIWs. Most evidently, subTIWs occur in different regions than TIWs. Due to the influence of subTIWs on upper ocean mixing and heat flux, future assessment of upper ocean heat budget and regional air-sea interactions should not be limited to the effect of TIWs alone. Instead, the impact of subTIWs should also be taken into account, particularly in the regions north and south of the Equator which are strongly affected by subTIWs. To date, it is not clear how subTIWs and TIWs interact, and it is unclear whether subTIWs only act in the subsurface or if they also have an impact on Sea Surface Temperature (SST) patterns, comparable to TIWs. However, these questions are crucial to fully understand the role and importance of subTIWs for the upper ocean and air-sea interactions and should therefore be addressed in future research.

ACKNOWLEDGEMENTS This study has been conducted using mooring data from the PIRATA project provided by the GTMBA Project Office of NOAA/PMEL. PIRATA and TACOS data can be obtained at the NOAA Pacific Marine Environmental Laboratory (PMEL) website (https://www.pmel.noaa.gov/gtmba/pirata). The research leading to these results has received funding from the German Federal Ministry of Education and Research (BMBF) through the JPI Climate/JPI Oceans NextG-Climate Science-ROADMAP (FKZ: 01LP2002A). ICON-O primary data and scripts used in the analysis and other supplementary information that may be useful in reproducing the author's work is archived by the Max Planck Institute for Meteorology in the MPG.PuRe repository and can be obtained at http://hdl.handle.net/21.11116/0000-0007-7887-A. Model output used for the analysis is archived in the DRKZ long term archive LTA DOKU and can be obtained (http://cera-www.dkrz.de/WDCC/ui/Compact.jsp?acronym=DKRZ_LTA_033_ds00009, (Specht et al., 2021a)). We would like to acknowledge Helmuth Haak for his help and technical support in running and providing the ICON-O simulation used in this study. We further thank Jochem Marotzke and Stefan Bühler for their comments and advise on the study and Armin Köhl for the internal review which helped improving the original manuscript.

BIBLIOGRAPHY

An, S.-I. (2008). Interannual variations of the tropical ocean instability wave and ENSO. *Journal of Climate*, *21*(15), 3680–3686.

Arhan, M., Tréguier, A.-M., Bourlès, B., & Michel, S. (2006). Diagnosing the annual cycle of the Equatorial Undercurrent in the Atlantic Ocean from a general circulation model. *Journal of Physical Oceanography*, *36*(8), 1502–1522.

Ascani, F., Firing, E., Dutrieux, P., McCreary, J. P., & Ishida, A. (2010). Deep equatorial ocean circulation induced by a forced–dissipated Yanai beam. *Journal of Physical Oceanography*, *40*(5), 1118–1142.

Ascani, F., Firing, E., McCreary, J. P., Brandt, P., & Greatbatch, R. J. (2015). The deep equatorial ocean circulation in wind-forced numerical solutions. *Journal of Physical Oceanography*, *45*(6), 1709–1734.

Bastin, S., Claus, M., Brandt, P., & Greatbatch, R. J. (2020). Equatorial deep jets and their influence on the mean equatorial circulation in an idealized ocean model forced by intraseasonal momentum flux convergence. *Geophysical Research Letters*, *47*(10), e2020GL087808.

Bjerknes, J. (1969). Atmospheric teleconnections from the equatorial Pacific. *Monthly Weather Review*, *97*(3), 163–172.

Boebel, O., Schmid, C., & Zenk, W. (1999). Kinematic elements of Antarctic intermediate water in the western south Atlantic. *Deep Sea Research Part II: Topical Studies in Oceanography*, *46*(1-2), 355–392.

Bourlès, B., Araujo, M., Mcphaden, M. J., Brandt, P., Foltz, G. R., Lumpkin, R., ... Nobre, P. et al. (2019). PIRATA: A sustained observing system for tropical Atlantic climate research and forecasting. *Earth and Space Science*, *6*(4), 577–616.

Brandt, P., Hormann, V., Bourlès, B., Fischer, J., Schott, F. A., Stramma, L., & Dengler, M. (2008). Oxygen tongues and zonal currents in the equatorial Atlantic. *Journal of Geophysical Research: Oceans*, *113*(C4).

Brandt, P., Hormann, V., Körtzinger, A., Visbeck, M., Krahmann, G., Stramma, L., ... Schmid, C. (2010). Changes in the ventilation of the oxygen minimum zone of the tropical North Atlantic. *Journal of Physical Oceanography*, *40*(8), 1784–1801.

Brandt, P., Caniaux, G., Bourles, B., Lazar, A., Dengler, M., Funk, A., ... Marin, F. (2011). Equatorial upper-ocean dynamics and their interaction with the West African monsoon. *Atmospheric Science Letters*, *12*(1), 24–30.

Brandt, P., Claus, M., Greatbatch, R. J., Kopte, R., Toole, J. M., Johns, W. E., & Böning, C. W. (2016). Annual and semiannual cycle of equatorial Atlantic circulation associated with basin-mode resonance. *Journal of Physical Oceanography*, *46*(10), 3011–3029.

Bunge, L., Provost, C., & Kartavtseff, A. (2007). Variability in horizontal current velocities in the central and eastern equatorial Atlantic in 2002. *Journal of Geophysical Research: Oceans*, *112*(C2).

Busalacchi, A. J., & Picaut, J. (1983). Seasonal variability from a model of the tropical Atlantic Ocean. *Journal of Physical Oceanography*, *13*(9), 1564–1588.

Cabos, W., de la Vara, A., & Koseki, S. (2019). Tropical Atlantic variability: Observations and modeling. *Atmosphere*, *10*(9), 502.

Caltabiano, A., Robinson, I., & Pezzi, L. (2005). Multi-year satellite observations of instability waves in the Tropical Atlantic Ocean. *Ocean Science*, *1*(2), 97–112.

Carton, J. A., Cao, X., Giese, B. S., & Da Silva, A. M. (1996). Decadal and interannual SST variability in the tropical Atlantic Ocean. *Journal of Physical Oceanography*, *26*(7), 1165–1175.

Chang, P, Yamagata, T, Schopf, P, Behera, S., Carton, J, Kessler, W., ... Shetye, S et al. (2006). Climate fluctuations of tropical coupled systems—the role of ocean dynamics. *Journal of Climate*, *19*(20), 5122–5174.

Cherian, D., Whitt, D., Holmes, R., Lien, R.-C., Bachman, S., & Large, W. (2021). Off-equatorial deep-cycle turbulence forced by tropical instability waves in the equatorial Pacific. *Journal of Physical Oceanography*, *51*(5), 1575–1593.

Chiang, J. C., & Vimont, D. J. (2004). Analogous Pacific and Atlantic meridional modes of tropical atmosphere–ocean variability. *Journal of Climate*, *17*(21), 4143–4158.

Cummins, P. F., Masson, D., & Saenko, O. A. (2016). Vertical heat flux in the ocean: Estimates from observations and from a coupled general circulation model. *Journal of Geophysical Research: Oceans*, *121*(6), 3790–3802.

de Decco, H. T., Junior, A. R. T., Pezzi, L. P., & Landau, L. (2018). Revisiting tropical instability wave variability in the Atlantic ocean using SODA reanalysis. *Ocean Dynamics*, *68*(3), 327–345.

Deppenmeier, A.-L., Haarsma, R. J., & Hazeleger, W. (2016). The Bjerknes feedback in the tropical Atlantic in CMIP5 models. *Climate Dynamics*, *47*(7-8), 2691–2707.

Ding, H., Keenlyside, N. S., & Latif, M. (2009). Seasonal cycle in the upper equatorial Atlantic Ocean. *Journal of Geophysical Research: Oceans*, *114*(C9).

Ding, H., Keenlyside, N. S., & Latif, M. (2012). Impact of the equatorial Atlantic on the El Niño southern oscillation. *Climate dynamics*, *38*(9), 1965–1972.

Düing, W, Hisard, P., Katz, E, Meincke, J, Miller, L, Moroshkin, K., ... Weisberg, R. (1975). Meanders and long waves in the equatorial Atlantic. *Nature*, *257*(5524), 280–284.

Eddebbar, Y., Subramanian, A., Whitt, D., Long, M., Verdy, A., Mazloff, M., & Merrifield, M. (2021). Seasonal Modulation of Dissolved Oxygen in the Equatorial Pacific by Tropical Instability Vortices. *Journal of Geophysical Research: Oceans*, *126*(11), e2021JC017567.

Evans, W., Strutton, P. G., & Chavez, F. P. (2009). Impact of tropical instability waves on nutrient and chlorophyll distributions in the equatorial Pacific. *Deep Sea Research Part I: Oceanographic Research Papers*, *56*(2), 178–188.

Ferrari, R. (2011). A frontal challenge for climate models. *Science*, *332*(6027), 316–317.

Flament, P. J., Kennan, S. C., Knox, R. A., Niiler, P. P., & Bernstein, R. L. (1996). The three-dimensional structure of an upper ocean vortex in the tropical Pacific Ocean. *Nature*, *383*(6601), 610–613.

Foltz, G. R., Hummels, R., Dengler, R. C., Marcus and, & Araujo, M. (2020). Vertical turbulent cooling of the mixed layer in the Atlantic ITCZ and trade wind regions. *Journal of Geophysical Research: Oceans*, e2019JC015529.

Gaspar, P., Grégoris, Y., & Lefevre, J.-M. (1990). A simple eddy kinetic energy model for simulations of the oceanic vertical mixing: Tests at station Papa and Long-Term Upper Ocean Study site. *Journal of Geophysical Research: Oceans*, *95*(C9), 16179–16193.

Giorgetta, M. A., Brokopf, R., Crueger, T., Esch, M., Fiedler, S., Helmert, J, ... Manzini, E. et al. (2018). ICON-A, the atmosphere component of the ICON Earth System Model: I. Model description. *Journal of Advances in Modeling Earth Systems*, *10*(7), 1613–1637.

Godfrey, J., Johnson, G., McPhaden, M., Reverdin, G, & Wijffels, S. E. (2001). The tropical ocean circulation. In *International geophysics* (Vol. 77, pp. 215–246). Elsevier.

Greatbatch, R. J., Claus, M., Brandt, P., Matthießen, J.-D., Tuchen, F. P., Ascani, F., ... Farrar, J. T. (2018). Evidence for the maintenance of slowly varying equatorial currents by intraseasonal variability. *Geophysical Research Letters*, *45*(4), 1923–1929.

Grodsky, S. A., Carton, J. A., Provost, C., Servain, J., Lorenzzetti, J. A., & McPhaden, M. J. (2005). Tropical instability waves at 0 ○ N, 23 ○ W in the Atlantic: A case study using Pilot Research Moored Array in the Tropical Atlantic (PIRATA) mooring data. *Journal of Geophysical Research: Oceans*, *110*(C8).

Hashizume, H., Xie, S.-P., Fujiwara, M., Shiotani, M., Watanabe, T., Tanimoto, Y., ... Takeuchi, K. (2002). Direct observations of atmospheric boundary layer response to SST variations associated with tropical instability waves over the eastern equatorial Pacific. *Journal of Climate*, *15*(23), 3379–3393.

Hastenrath, S. (1978). On modes of tropical circulation and climate anomalies. *Journal of the Atmospheric Sciences*, *35*(12), 2222–2231.

Hersbach, H., Bell, B, Berrisford, P, Horányi, A, Sabater, J. M., Nicolas, J, ... Soci, C et al. (2019). Global reanalysis: Goodbye ERA-interim, hello ERA5. *ECMWF Newsletter*, *159*, 17–24.

Hersbach, H., Bell, B., Berrisford, P., Hirahara, S., Horányi, A., Muñoz-Sabater, J., ... Schepers, D. et al. (2020). The ERA5 global reanalysis. *Quarterly Journal of the Royal Meteorological Society*.

Hohenegger, C., Korn, P., Linardakis, L., Redler, R., Schnur, R., Adamidis, P., ... Bergemann, M. et al. (2022). ICON-Sapphire: Simulating the components of the Earth System and their interactions at kilometer and subkilometer scales. *Geoscientific Model Development Discussions*, 1–42.

Holmes, R., & Thomas, L. (2015). The modulation of equatorial turbulence by tropical instability waves in a regional ocean model. *Journal of Physical Oceanography*, *45*(4), 1155–1173.

Hormann, V., & Brandt, P. (2007). Atlantic Equatorial Undercurrent and associated cold tongue variability. *Journal of Geophysical Research: Oceans*, *112*(C6).

Howard, L. N. (1961). Note on a paper of John W. Miles. *Journal of Fluid Mechanics*, *10*(4), 509–512.

Hummels, R., Dengler, M., & Bourlès, B. (2013). Seasonal and regional variability of upper ocean diapycnal heat flux in the Atlantic cold tongue. *Progress in Oceanography*, *111*, 52–74.

Inoue, R, Lien, R.-C., & Moum, J. (2012). Modulation of equatorial turbulence by a tropical instability wave. *Journal of Geophysical Research: Oceans*, *117*(C10).

Inoue, R., Lien, R.-C., Moum, J. N., Perez, R. C., & Gregg, M. C. (2019). Variations of equatorial shear, stratification, and turbulence within a tropical instability wave cycle. *Journal of Geophysical Research: Oceans*, *124*(3), 1858–1875.

Jochum, M., & Malanotte-Rizzoli, P. (2004). A new theory for the generation of the equatorial subsurface countercurrents. *Journal of Physical Oceanography*, *34*(4), 755–771.

Jochum, M., & Murtugudde, R. (2006). Temperature advection by tropical instability waves. *Journal of Physical Oceanography*, *36*(4), 592–605.

Jochum, M., Malanotte-Rizzoli, P., & Busalacchi, A. (2004). Tropical instability waves in the Atlantic Ocean. *Ocean Modelling*, *7*(1-2), 145–163.

Johns, W. E., Brandt, P., Bourlès, B., Tantet, A., Papapostolou, A, & Houk, A. (2014). Zonal structure and seasonal variability of the Atlantic Equatorial Undercurrent. *Climate Dynamics*, *43*(11), 3047–3069.

Jouanno, J., Marin, F., Du Penhoat, Y., Molines, J. M., & Sheinbaum, J. (2011). Seasonal modes of surface cooling in the Gulf of Guinea. *Journal of Physical Oceanography*, *41*(7), 1408–1416.

Kalnay, E., Kanamitsu, M., Kistler, R., Collins, W., Deaven, D., Gandin, L., ... Woollen, J. et al. (1996). The NCEP/NCAR 40-year reanalysis project. *Bulletin of the American Meteorological Society*, *77*(3), 437–472.

Kennan, S. C., & Flament, P. J. (2000). Observations of a tropical instability vortex. *Journal of Physical Oceanography*, *30*(9), 2277–2301.

Kolodziejczyk, N., Bourlès, B., Marin, F., Grelet, J., & Chuchla, R. (2009). Seasonal variability of the Equatorial Undercurrent at 10 ◦ w as inferred from recent in situ observations. *Journal of Geophysical Research: Oceans*, *114*(C6).

Korn, P. (2017). Formulation of an unstructured grid model for global ocean dynamics. *Journal of Computational Physics*, *339*, 525–552.

Korn, P., Brüggemann, N., Jungclaus, J. H., Lorenz, S., Gutjahr, O., Haak, H., ... Notz, D. et al. (2022). ICON-O: The Ocean Component of the ICON Earth System Model-Global Simulation Characteristics and Local Telescoping Capability. *Journal of Advances in Modeling Earth Systems*, e2021MS002952.

Körner, M., Claus, M., Brandt, P., & Tuchen, F. P. (2022). Sources and pathways of intraseasonal meridional kinetic energy in the equatorial Atlantic Ocean. *Journal of Physical Oceanography*, *52*(10), 2445–2462.

Kucharski, F, Bracco, A, Yoo, J., Tompkins, A., Feudale, L, Ruti, P, & Dell'Aquila, A. (2009). A Gill–Matsuno-type mechanism explains the tropical Atlantic influence on African and Indian monsoon rainfall. *Quarterly Journal of the Royal Meteorological Society: A journal of the Atmospheric Sciences, applied Meteorology and Physical Oceanography*, *135*(640), 569–579.

Legeckis, R., Brown, C. W., Bonjean, F., & Johnson, E. S. (2004). The influence of tropical instability waves on phytoplankton blooms in the wake of the Marquesas Islands during 1998 and on the currents observed during the drift of the Kon-Tiki in 1947. *Geophysical Research Letters*, *31*(23).

Lévy, M., Ferrari, R., Franks, P. J., Martin, A. P., & Rivière, P. (2012). Bringing physics to life at the submesoscale. *Geophysical Research Letters*, *39*(14).

Lien, R.-C., d'Asaro, E. A., & Menkes, C. E. (2008). Modulation of equatorial turbulence by tropical instability waves. *Geophysical Research Letters*, *35*(24).

Liu, C., Fang, L., Köhl, A., Liu, Z., Smyth, W. D., & Wang, F. (2019a). The Subsurface Mode Tropical Instability Waves in the Equatorial Pacific Ocean and Their Impacts on Shear and Mixing. *Geophysical Research Letters*.

Liu, C., Wang, X., Köhl, A., Wang, F., & Liu, Z. (2019b). The northeast-southwest oscillating equatorial mode of the tropical instability wave and its impact on equatorial mixing. *Geophysical Research Letters*, *46*(1), 218–225.

Liu, C., Wang, X., Liu, Z., Köhl, A., Smyth, W. D., & Wang, F. (2020). On the Formation of a Subsurface Weakly Sheared Laminar Layer and an Upper Thermocline Strongly Sheared Turbulent Layer in the Eastern Equatorial Pacific: Interplays of Multiple-Time-Scale Equatorial Waves. *Journal of Physical Oceanography*, *50*(10), 2907–2930.

Lübbecke, J. F., Rodríguez-Fonseca, B., Richter, I., Martín-Rey, M., Losada, T., Polo, I., & Keenlyside, N. S. (2018). Equatorial Atlantic variability—Modes, mechanisms, and global teleconnections. *Wiley Interdisciplinary Reviews: Climate Change*, *9*(4), e527.

Lumpkin, R., & Johnson, G. C. (2013). Global ocean surface velocities from drifters: Mean, variance, El Niño–Southern Oscillation response, and seasonal cycle. *Journal of Geophysical Research: Oceans*, *118*(6), 2992–3006.

Maillard, L, Boucharel, J, Stuecker, M., Jin, F.-F., & Renault, L. (2022). Modulation of the Eastern Equatorial Pacific seasonal cycle by Tropical Instability Waves. *Geophysical Research Letters*, e2022GL100991.

Marshall, J., Kushnir, Y., Battisti, D., Chang, P., Czaja, A., Dickson, R., … Visbeck, M. (2001). North Atlantic climate variability: Phenomena, impacts and mechanisms. *International Journal of Climatology: A Journal of the Royal Meteorological Society*, *21*(15), 1863–1898.

Masina, S, Philander, S., & Bush, A. (1999). An analysis of tropical instability waves in a numerical model of the Pacific Ocean: 2. Generation and energetics of the waves. *Journal of Geophysical Research: Oceans*, *104*(C12), 29637–29661.

McPhaden, M. J., Zebiak, S. E., & Glantz, M. H. (2006). ENSO as an integrating concept in earth science. *Science*, *314*(5806), 1740–1745.

Menkes, C. E., Kennan, S. C., Flament, P., Dandonneau, Y., Masson, S., Biessy, B., … Montel, Y. et al. (2002). A whirling ecosystem in the equatorial Atlantic. *Geophysical Research Letters*, *29*(11), 48–1.

Menkes, C. E., Vialard, J. G., Kennan, S. C., Boulanger, J.-P., & Madec, G. V. (2006). A modeling study of the impact of tropical instability waves on the heat budget of the eastern equatorial Pacific. *Journal of Physical Oceanography*, *36*(5), 847–865.

Miles, J. W. (1961). On the stability of heterogeneous shear flows. *Journal of Fluid Mechanics*, *10*(4), 496–508.

Molinari, R. L. (1982). Observations of eastward currents in the tropical South Atlantic Ocean: 1978–1980. *Journal of Geophysical Research: Oceans*, *87*(C12), 9707–9714.

Moore, D. W., & Philander, S. G. H. (1977). Modeling of the tropical oceanic circulation. *The Sea*, *6*, 319–361.

Moum, J., Lien, R.-C., Perlin, A, Nash, J., Gregg, M., & Wiles, P. (2009). Sea surface cooling at the equator by subsurface mixing in tropical instability waves. *Nature Geoscience*, *2*(11), 761–765.

Moum, J. N., Hughes, K. G., Shroyer, E. L., Smyth, W. D., Cherian, D., Warner, S. J., ... Dengler, M. (2022). Deep cycle turbulence in Atlantic and Pacific cold tongues. *Geophysical Research Letters*, *49*(8), e2021GL097345.

Müller, W. A., Jungclaus, J. H., Mauritsen, T., Baehr, J., Bittner, M., Budich, R, ... Haak, H. et al. (2018). A Higher-resolution Version of the Max Planck Institute Earth System Model (MPI-ESM1. 2-HR). *Journal of Advances in Modeling Earth Systems*, *10*(7), 1383–1413.

Muñoz, E., Weijer, W., Grodsky, S. A., Bates, S. C., & Wainer, I. (2012). Mean and variability of the tropical Atlantic Ocean in the CCSM4. *Journal of Climate*, *25*(14), 4860–4882.

Murtugudde, R. G., Ballabrera-Poy, J., Beauchamp, J., & Busalacchi, A. J. (2001). Relationship between zonal and meridional modes in the tropical Atlantic. *Geophysical Research Letters*, *28*(23), 4463–4466.

Perez, R. C., Lumpkin, R., Johns, W. E., Foltz, G. R., & Hormann, V. (2012). Interannual variations of Atlantic tropical instability waves. *Journal of Geophysical Research: Oceans*, *117*(C3).

Perez, R. C., Foltz, G. R., Lumpkin, R., & Schmid, C. (2019). Direct measurements of upper ocean horizontal velocity and vertical shear in the tropical North Atlantic at 4 ◦ N, 23 ◦ W. *Journal of Geophysical Research: Oceans*, *124*(6), 4133–4151.

Philander, S. (2001). *Atlantic Ocean equatorial currents*. Elsevier: London, UK.

Prodhomme, C, Voldoire, A, Exarchou, E, Deppenmeier, A.-L., García-Serrano, J, & Guemas, V. (2019). How does the seasonal cycle control equatorial Atlantic interannual variability? *Geophysical Research Letters*, *46*(2), 916–922.

Proehl, J. A. (1996). Linear stability of equatorial zonal flows. *Journal of Physical Oceanography*, *26*(4), 601–621.

Proehl, J. A. (1998). The role of meridional flow asymmetry in the dynamics of tropical instability. *Journal of Geophysical Research: Oceans*, *103*(C11), 24597–24618.

Richardson, P. L., & McKee, T. (1984). Average seasonal variation of the Atlantic equatorial currents from historical ship drifts. *Journal of Physical Oceanography*, *14*(7), 1226–1238.

Rodríguez-Fonseca, B., Mohino, E., Mechoso, C. R., Caminade, C., Biasutti, M., Gaetani, M., ... Xue, Y. et al. (2015). Variability and predictability of West African droughts: A review on the role

of sea surface temperature anomalies. *Journal of Climate*, *28*(10), 4034–4060.

Röske, F. (2006). A global heat and freshwater forcing dataset for ocean models. *Ocean Modelling*, *11*(3-4), 235–297.

Ruiz-Barradas, A., Carton, J. A., & Nigam, S. (2000). Structure of interannual-to-decadal climate variability in the tropical Atlantic sector. *Journal of Climate*, *13*(18), 3285–3297.

Seo, H., Jochum, M., Murtugudde, R., Miller, A. J., & Roads, J. O. (2007). Feedback of tropical instability-wave-induced atmospheric variability onto the ocean. *Journal of Climate*, *20*(23), 5842–5855.

Servain, J., Wainer, I., Ludos Ayina, H., & Roquet, H. (2000). The relationship between the simulated climatic variability modes of the tropical Atlantic. *International Journal of Climatology: A Journal of the Royal Meteorological Society*, *20*(9), 939–953.

Sherman, J., Subramaniam, A., Gorbunov, M. Y., Fernández-Carrera, A., Kiko, R., Brandt, P., & Falkowski, P. G. (2022). The Photophysiological Response of Nitrogen-Limited Phytoplankton to Episodic Nitrogen Supply Associated With Tropical Instability Waves in the Equatorial Atlantic. *Frontiers in Marine Science*, 2053.

Shi, W., & Wang, M. (2021). Tropical instability wave modulation of chlorophyll-a in the Equatorial Pacific. *Scientific Reports*, *11*(1), 1–11.

Specht, Jungclaus, M. S., Bader, J., & Jürgen. (2021a). Characterizing Subsurface Tropical Instability Waves in the Atlantic Ocean in Simulations and Observations. World Data Center for Climate (WDCC) at DKRZ. Retrieved from http://cera-www.dkrz.de/WDCC/ui/Compact.jsp?acronym=DKRZ_LTA_033_ds00009

Specht, M. S., Jungclaus, J., & Bader, J. (2021b). Identifying and characterizing subsurface tropical instability waves in the Atlantic Ocean in simulations and observations. *Journal of Geophysical Research: Oceans*, *126*(10), e2020JC017013.

Specht, M. S., Jungclaus, J., & Bader, J. (2023). Seasonality of mixing at TIW fronts in the Atlantic Ocean. *Manuscript in preperation*.

Steele, M., Morley, R., & Ermold, W. (2001). PHC: A global ocean hydrography with a high-quality Arctic Ocean. *Journal of Climate*, *14*(9), 2079–2087.

Storch, J.-S. v., Eden, C., Fast, I., Haak, H., Hernández-Deckers, D., Maier-Reimer, E., … Stammer, D. (2012). An estimate of the Lorenz energy cycle for the world ocean based on the STORM/NCEP simulation. *Journal of Physical Oceanography*, *42*(12), 2185–2205.

Strutton, P. G., Ryan, J. P., & Chavez, F. P. (2001). Enhanced chlorophyll associated with tropical instability waves in the equatorial Pacific. *Geophysical Research Letters*, *28*(10), 2005–2008.

Sun, Z., Liu, H., Lin, P., Tseng, Y.-h., Small, J., & Bryan, F. (2019). The modeling of the North Equatorial Countercurrent in the

Community Earth System Model and its oceanic component. *Journal of Advances in Modeling Earth Systems*, *11*(2), 531–544.

Talley, L. D. (2011). *Descriptive physical oceanography: An introduction*. Academic press.

Thomas, L. N., Tandon, A., & Mahadevan, A. (2008). Submesoscale processes and dynamics.

Tourre, Y. M., Rajagopalan, B., & Kushnir, Y. (1999). Dominant patterns of climate variability in the Atlantic Ocean during the last 136 years. *Journal of Climate*, *12*(8), 2285–2299.

Trenberth, K. E., & Caron, J. M. (2001). Estimates of meridional atmosphere and ocean heat transports. *Journal of Climate*, *14*(16), 3433–3443.

Trenberth, K. E., Branstator, G. W., Karoly, D., Kumar, A., Lau, N.-C., & Ropelewski, C. (1998). Progress during TOGA in understanding and modeling global teleconnections associated with tropical sea surface temperatures. *Journal of Geophysical Research: Oceans*, *103*(C7), 14291–14324.

Tuchen, F. P., Brandt, P., Claus, M., & Hummels, R. (2018). Deep intraseasonal variability in the central equatorial Atlantic. *Journal of Physical Oceanography*, *48*(12), 2851–2865.

Tuchen, F. P., Perez, R. C., Foltz, G. R., Brandt, P., & Lumpkin, R. (2022). Multidecadal intensification of Atlantic tropical instability Waves. *Geophysical Research Letters*, e2022GL101073.

von Schuckmann, K, Brandt, P., & Eden, C. (2008). Generation of tropical instability waves in the Atlantic Ocean. *Journal of Geophysical Research: Oceans*, *113*(C8).

Wallace, J., Rasmusson, E., Mitchell, T., Kousky, V., Sarachik, E., & Von Storch, H. (1998). On the structure and evolution of ENSO-related climate variability in the tropical Pacific: Lessons from TOGA. *Journal of Geophysical Research: Oceans*, *103*(C7), 14241–14259.

Wang, M., Xie, S.-P., Shen, S. S., & Du, Y. (2020). Rossby and Yanai modes of tropical instability waves in the equatorial Pacific Ocean and a diagnostic model for surface currents. *Journal of Physical Oceanography*, *50*(10), 3009–3024.

Warner, S. J., Holmes, R. M., Hawkins, E. H., Hoecker-Martinez, M. S., Savage, A. C., & Moum, J. N. (2018). Buoyant gravity currents released from tropical instability waves. *Journal of Physical Oceanography*, *48*(2), 361–382.

Weisberg, R. H., & Weingartner, T. J. (1988). Instability waves in the equatorial Atlantic Ocean. *Journal of Physical Oceanography*, *18*(11), 1641–1657.

Wu, Q., & Bowman, K. P. (2007). Interannual variations of tropical instability waves observed by the Tropical Rainfall Measuring Mission. *Geophysical Research Letters*, *34*(9).

Xie, S.-P., & Carton, J. A. (2004). Tropical Atlantic variability: Patterns, mechanisms, and impacts. *Earth Climate: The Ocean-Atmosphere Interaction, Geophys. Monogr*, *147*, 121–142.

Zängl, G., Reinert, D., Rípodas, P., & Baldauf, M. (2015). The ICON (ICOsahedral Non-hydrostatic) modelling framework of DWD and MPI-M: Description of the non-hydrostatic dynamical core. *Quarterly Journal of the Royal Meteorological Society*, *141*(687), 563–579.

Zebiak, S. E. (1993). Air–sea interaction in the equatorial Atlantic region. *Journal of Climate*, *6*(8), 1567–1586.

ACKNOWLEDGMENTS

I want to thank my supervisors Johann Jungclaus and Jürgen Bader for their guidance and advice during my PhD. Thank you for our almost weekly meetings, providing feedback, giving me the freedom to explore what I want to do and supporting my ideas. I also want to thank Jochem Marotzke for his regular input and discussions and my panel chair Stefan Bühler for keeping an eye on my progress. The four of you were a great panel to be supervised by. I am particularly thankful to all of you that you never once doubted that I would manage to finish my PhD despite having a baby along the way. Instead, you supported me and allowed me all the flexibility I needed.

I also want to thank the IMPRS office team, Antje, Connie, and Michaela who always had an open ear and helped me out with my seemingly one trillion bureaucratic questions, especially towards the end.

Those past four years have been quite the journey for me. Doing a PhD during a global pandemic, stuck in home office for a lot of it, while also having and raising a baby at the same time was not an easy task and I could not have done this alone. I am very grateful to my parents who might have never fully understood what I am doing and why I want to do it but have always supported me and helped out in every way they can. I also want to thank Anna, who is truly the best friend I could wish for. Thanks for being by my side through all the highs and lows in the past years and every step along the way. More thankful than I can express here I am for Leigh. I could not have done this without him. Thank you for always having my back, supporting me, believing in me, putting up with me when I get unreasonably stressed out, cheering me up and just being awesome. And of course also thank you for answering even my most stupid Matlab questions and giving me feedback on pretty much everything I have written over the last years.

Last but not least, I want to thank my children: my daughter Lily who always helped me to take my mind of off things and reminded me what really matters in the end, and her little brother, whose impending birth was a better reminder to finally finish up this thesis than any deadline ever could have been.

EIDESSTATTLICHE VERSICHERUNG - DECLARATION OF OATH

Hiermit erkläre ich an Eides statt, dass ich die vorliegende Dissertationsschrift selbst verfasst und keine anderen als die angegebenen Quellen und Hilfsmittel benutzt habe.

I hereby declare upon oath that I have written the present dissertation independently and have not used further resources and aids than those stated.

Hamburg, den 19.01.2023

Mia Sophie Specht

ERKLÄRUNG - DECLARATION

Ich versichere, dass dieses gebundene Exemplar der Dissertation und das in elektronischer Form eingereichte Dissertationsexemplar (über den Docata-Upload) und das bei der Fakultät (zuständiges Studienbüro bzw. Promotionsbüro Physik) zur Archivierung eingereichte gedruckte gebundene Exemplar der Dissertationsschrift identisch sind.

I, the undersigned, declare that this bound copy of the dissertation and the dissertation submitted in electronic form (via the Docata upload) and the printed bound copy of the dissertation submitted to the faculty (responsible Academic Office or the Doctoral Office Physics) for archiving are identical.

Hamburg, den 19.01.2023

Mia Sophie Specht

Hinweis / Reference

Die gesamten Veröffentlichungen in der Publikationsreihe des MPI-M
„Berichte zur Erdsystemforschung / Reports on Earth System Science“,
ISSN 1614-1199

sind über die Internetseiten des Max-Planck-Instituts für Meteorologie erhältlich:
https://mpimet.mpg.de/forschung/publikationen

All the publications in the series of the MPI -M
„Berichte zur Erdsystemforschung / Reports on Earth System Science“,
ISSN 1614-1199

are available on the website of the Max Planck Institute for Meteorology:
https://mpimet.mpg.de/en/research/publications